

LIBRARY

JAN 2 1958

NAVPERLANT

294 - v

JOURNAL OF THE

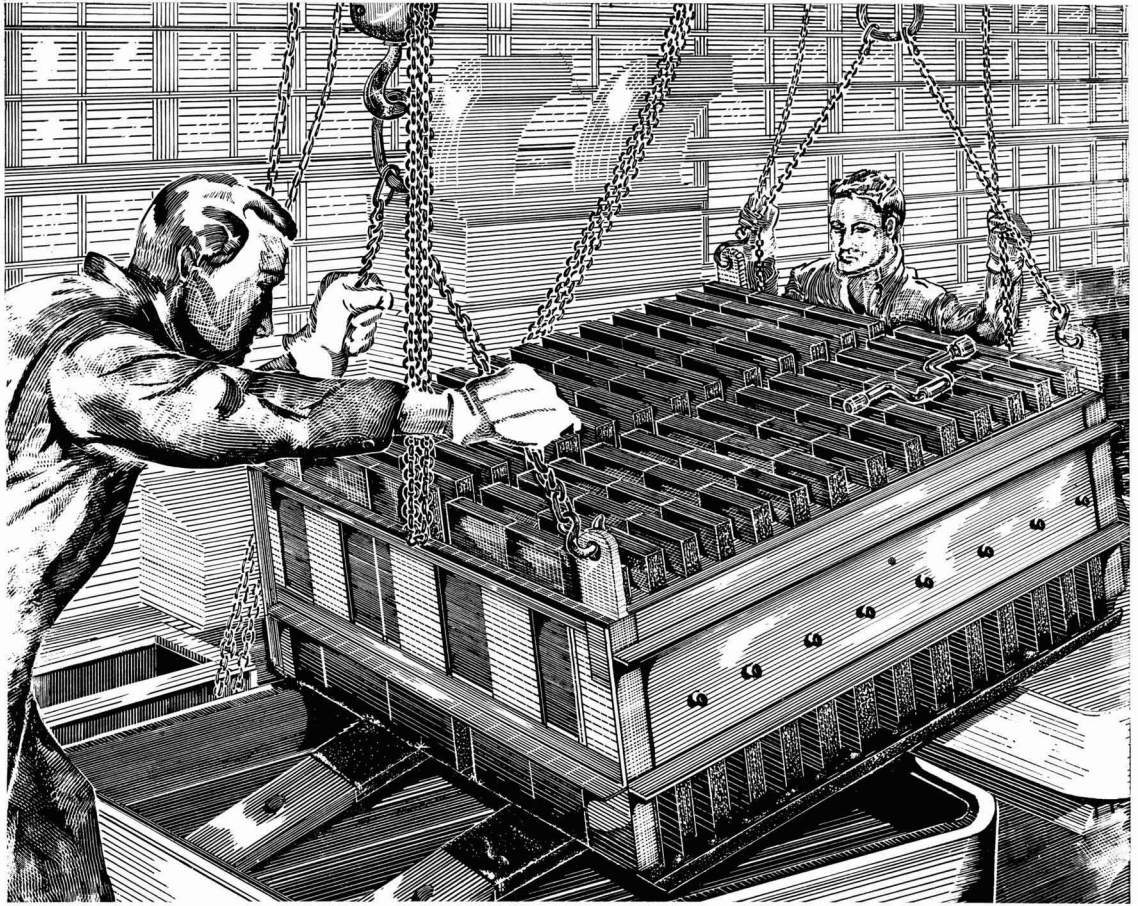
Electrochemical Society

Vol. 105, No. 1

January 1958

แผนกเคมี คณะวิทยาศาสตร์
มหาวิทยาลัยศรีนครินทรวิโรฒ





Making better cells

The skills and experience of the men who renew electrolytic cells are a major factor in their economical performance.

Other significant factors include the quality, design and machining of

GLC anodes, which are carefully "custom made" to the requirements of individual cells.

FREE — This illustration of cell building has been handsomely reproduced with no advertising text. We will be pleased to send you one of these reproductions with our compliments. Simply write to Dept. J-1.

ELECTRODE
GLC[®]
DIVISION

GREAT LAKES CARBON CORPORATION

18 EAST 48TH STREET, NEW YORK 17, N.Y. OFFICES IN PRINCIPAL CITIES

EDITORIAL STAFF

R. J. McKay, Chairman, Publication Committee
Cecil V. King, Editor
Norman Hackerman, Technical Editor
Ruth G. Sterns, Managing Editor
U. B. Thomas, News Editor
H. W. Salzberg, Book Review Editor
Natalie Michalski, Assistant Editor

DIVISIONAL EDITORS

W. C. Vosburgh, Battery
J. E. Draley, Corrosion, I
R. T. Foley, Corrosion, II
John J. Chapman, Electric Insulation
Abner Brenner, Electrodeposition
H. C. Froelich, Electronics
D. H. Baird, Electronics—Semiconductors
Sherlock Swann, Jr., Electro-Organic
John M. Blocher, Jr., Electrothermics and Metallurgy, I
A. U. Seybolt, Electrothermics and Metallurgy, II
W. C. Gardiner, Industrial Electrolytic
C. W. Tobias, Theoretical Electrochemistry, I
A. J. de Bethune, Theoretical Electrochemistry, II

REGIONAL EDITORS

Howard T. Francis, Chicago
Joseph Schulein, Pacific Northwest
J. C. Schumacher, Los Angeles
G. W. Heise, Cleveland
G. H. Fetterley, Niagara Falls
Oliver Osborn, Houston
Earl A. Gulbransen, Pittsburgh
A. C. Holm, Canada
J. W. Cuthbertson, Great Britain
T. L. Rama Char, India

ADVERTISING OFFICE

ECS

1860 Broadway, New York 23, N. Y.

ECS OFFICERS

Norman Hackerman, President
University of Texas, Austin, Texas
Sherlock Swann, Jr., Vice-President
University of Illinois, Urbana, Ill.
W. C. Gardiner, Vice-President
Olin Mathieson Chemical Corp., Niagara Falls, N. Y.
R. A. Schaefer, Vice-President
Cleveland Graphite Bronze Div., Clevite Corp., Cleveland, Ohio
Lyle I. Gilbertson, Treasurer
Air Reduction Co., Murray Hill, N. J.
Henry B. Linford, Secretary
Columbia University, New York, N. Y.
Robert K. Shannon, Assistant Secretary
National Headquarters, The ECS, 1860 Broadway, New York 23, N. Y.

Journal of the Electrochemical Society

JANUARY 1958

VOL. 105 • NO. 1

CONTENTS

Editorial

Of Satellites and of Men..... 4C

Technical Papers

- Formation of Manganese(II) Ion in the Discharge of the Manganese Dioxide Electrode, II. Effect of Volume and pH of Electrolyte. W. C. Vosburgh, M. J. Pribble, A. Kozawa, and A. Sam 1 ✓
- Oxidation of Niobium between 375°C and 700°C.
E. A. Gulbransen and K. F. Andrew..... 4
- The Action of Lead Pigments and Lead Soaps on Aluminum.
M. J. Pryor, R. J. Hogan, and F. B. Patten..... 9
- Analysis of Films on Copper by Coulometric Reduction.
R. H. Lambert and D. J. Trevooy..... 18
- Acid Copper Plating on Aluminum. J. T. N. Atkinson..... 24
- Energy Transfer and Sensitization in Single Crystal Phosphors.
R. Leach 27
- The Calcium-Silicate-Tungstate Phosphor; Phase Relationships and Fluorescent Properties. D. E. Harrison and F. A. Hummel 34
- The Calcium-Silicate-Tungstate Phosphor; Preparation and Physical Properties. S. Jones..... 37
- Heat of Formation of Titanium Tribromide by the Mercury Reduction of Titanium Tetrabromide. E. H. Hall and J. M. Blocher, Jr. 40
- Pressure Distribution within a Vacuum Arc Furnace.
J. W. Suiter 44
- The Anodic Oxidation of Zinc and Zinc-Tin Alloys at Very Low Current Density. S. E. S. El Wakkad, A. M. Shams El Din, and H. Kotb 47
- The Anodic Oxidation of Cadmium, I. Mechanism of Film Formation. P. E. Lake and E. J. Casey..... 52 ✓

Technical Note

Sedimentation Volumes of a Phosphor Powder in Potassium Silicate and Potassium Silicate-Barium Acetate Settling Media. J. F. Hazel and L. Fiorito..... 57

Current Affairs

- Carl Wagner to Become Head of Max Planck Institute at Goettingen 7C
- New York Meeting, April 27 to May 1, 1958..... 7C
- Highlights of the October 6 Board of Directors' Meeting..... 8C
- Future Meeting Dates of the Society..... 2C
- Division News 9C Announcement from
Section News 10C Publisher 12C
- Personals 11C Book Reviews 12C
- News Items 11C

Published monthly by The Electrochemical Society, Inc., from Manchester, N. H., Executive Offices, Editorial Office and Circulation Dept., and Advertising Office at 1860 Broadway, New York 23, N. Y., combining the JOURNAL and TRANSACTIONS OF THE ELECTROCHEMICAL SOCIETY. Statements and opinions given in articles and papers in the JOURNAL OF THE ELECTROCHEMICAL SOCIETY are those of the contributors, and The Electrochemical Society assumes no responsibility for them. Nondeductible subscription to members \$5.00; subscription to nonmembers \$4.00. Single copies \$1.25 to members, \$1.75 to nonmembers. Copyright 1958 by The Electrochemical Society, Inc. Entered as second-class matter at the Post Office at Manchester, N. H., under the act of August 3, 1879.

FUTURE MEETINGS OF The Electrochemical Society



New York, N. Y., April 27, 28, 29, 30, and May 1, 1958

Headquarters at the Statler Hotel

Sessions will be scheduled on
Electric Insulation, Electronics,
Electrothermics and Metallurgy, Industrial Electrolytics,
and Theoretical Electrochemistry (including a symposium
on "Electrokinetic and Membrane Phenomena")

★ ★ ★

Ottawa, Canada, September 28, 29, 30, October 1, and 2, 1958

Headquarters at the Chateau Laurier

Sessions probably will be scheduled on
Batteries, Corrosion, Electrodeposition (including symposia on "Electrodeposition
on Uncommon Metals" and "Chemical and Electropolishing"),
Electronics (Semiconductors), Electro-Organics,
and Electrothermics and Metallurgy

★ ★ ★

Philadelphia, Pa., May 3, 4, 5, 6, and 7, 1959

Headquarters at the Sheraton Hotel

★ ★ ★

Columbus, Ohio, October 18, 19, 20, 21, and 22, 1959

Headquarters at the Deshler-Hilton Hotel

★ ★ ★

Chicago, Ill., May 1, 2, 3, 4, and 5, 1960

Headquarters at the Lasalle Hotel

★ ★ ★

Houston, Texas, October 9, 10, 11, 12, and 13, 1960

Headquarters at the Shamrock Hotel

★ ★ ★

Papers are now being solicited for the meeting to be held in Ottawa, Canada, September 28-October 2, 1958. Triplicate copies of each abstract (*not exceeding 75 words in length*) are due at the Secretary's Office, 1860 Broadway, New York 23, N. Y., *not later than June 1, 1958* in order to be included in the program. *Please indicate on abstract for which Division's symposium the paper is to be scheduled.* Complete manuscripts should be sent in triplicate to the Managing Editor of the JOURNAL at 1860 Broadway, New York 23, N. Y.

BELL TELEPHONE LABORATORIES DEVELOPS NEW COMPACT COMPUTER FOR U. S. AIR FORCE



J. A. Githens, B.S. in E.E., Drexel Institute of Technology, and J. A. Baird, Ph.D. in E.E., Texas A. & M., check the control panel of Leprechaun, a new high-speed computer which solves extremely complex problems in one-tenth of a second. Small size and low power are made possible by new design principles and Bell Laboratories' invention of the transistor.

The United States Air Force assigned Bell Labs an interesting assignment: develop a new kind of electronic computer. The major requirement was greater simplicity. Of course, no computer is simple, but this one (known as "Leprechaun" to its designers) is much smaller and simpler than most of the computers currently in use.

It has only some 9000 electrical components; 5000 of them are transistors. As a result, Lepre-

chaun has less than one-third the components of conventional computers. This facilitates testing, experimentation, assembly and service.

Even in its experimental state, Leprechaun is a stimulating example of great strides in the simplification and miniaturization of circuitry . . . a problem of profound interest to all Bell Laboratories researchers as they develop radically new equipment for your future telephone service.

BELL TELEPHONE LABORATORIES



WORLD CENTER OF COMMUNICATIONS RESEARCH AND DEVELOPMENT



Of Satellites and of Men

THE successful Soviet launching of an earth satellite on October 4, 1957 launched also a host of editorials, columns, and articles expressing surprise, confusion, and almost consternation. Why, it is difficult to understand. The U. S. S. R. had announced, several months in advance, that it expected to launch a satellite "during the fall." The United States had stated that it expected to put up a small experimental ball, probably in December 1957, and a fully instrumented, 22-lb sphere in March 1958. Both countries expect to launch several more satellites during the IGY. The comparatively large weight of Sputnik I, and especially of Sputnik II, indicates a much more ambitious Russian effort in this field than our own, and possibly a somewhat different approach to the rocket problem.

The ascent of the sputniks may also result in a full-scale Congressional investigation of our entire missile and rocket program. The U. S. long ago made it plain that priority was given to missiles rather than to satellites. Whether "top priority" has meant "all-out effort" is another matter. The intelligent American would like to know whether the military, the Administration, the scientists, and the manufacturers are pushing research and development efficiently and to an extent which the experts can consider really satisfactory. Efforts to find out have been negated by official policies of secrecy, which sometimes are justified, but sometimes are quite fantastic. The sudden release of news in late October after the first wave of surprise about Sputnik I had subsided, the meetings of high officials, the announcements that certain programs would be stepped up at considerably more cost, all suggest sudden realization that not only the satellite but the whole weapons program could not bear public scrutiny. Sputnik II has probably started another round of high-level meetings and reappraisals.

Part of the official secrecy seems to have been aimed at warding off hordes of reporters, columnists, and newswriters, all clamoring for stories. To get all stories straight without violating really proper security could take much of the time of trained men who know the facts, but who have other duties, too. Some of the news which is released gets strangely garbled. For instance, when the Air Force successfully fired a rocket from a balloon at 100,000 ft, it was variously called a 4-stage rocket, and "a cluster of rockets."

In spite of the difficulties, some way must be found to allow a certain amount of open inspection. The public must have assurance that pleas of secrecy are not invoked to cover up inefficiency and complacency.

The Russians were well aware of the psychological and propaganda value of "being first." We must assume that the responsible men in our Government were equally aware of this value and discounted its importance. The alternatives are that this aspect was forgotten or ignored, or that Russian announcements were dismissed as idle boasts. We trust that no one in high position will declare Sputnik II another "silly bauble."

—CVK



NOW!

... Greatly Reduced Clogging
of Diaphragms

... Lower
Cell Maintenance Costs

... Longer Anode Life

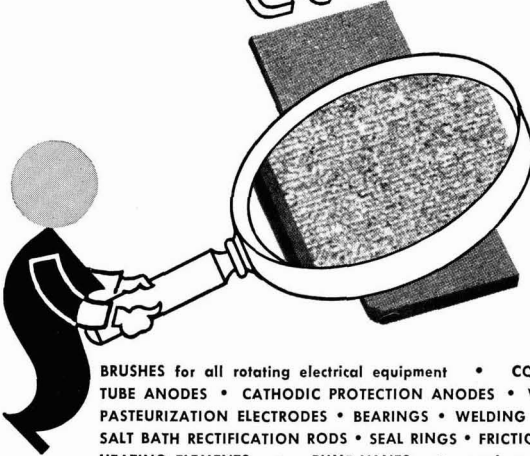
Costly, troublesome clogging of diaphragms due to the oil impregnant in conventional anodes, is materially lessened by the new Stackpole "GraphAnodes." Cell maintenance costs are reduced accordingly.

Better results are achieved because Stackpole GraphAnodes present a uniform, low-porosity surface to the electrolyte. The graphite is consumed slowly and evenly. It does not slough off to clog the diaphragm or contaminate the cell.

Let Stackpole arrange for a convincing demonstration of these new anodes on your own equipment. You be the judge—and, by way of convincing proof we suggest that you pay particular attention to the reduced frequency of diaphragm renewals.

STACKPOLE CARBON COMPANY
St. Marys, Pa.

STACKPOLE GraphAnodes

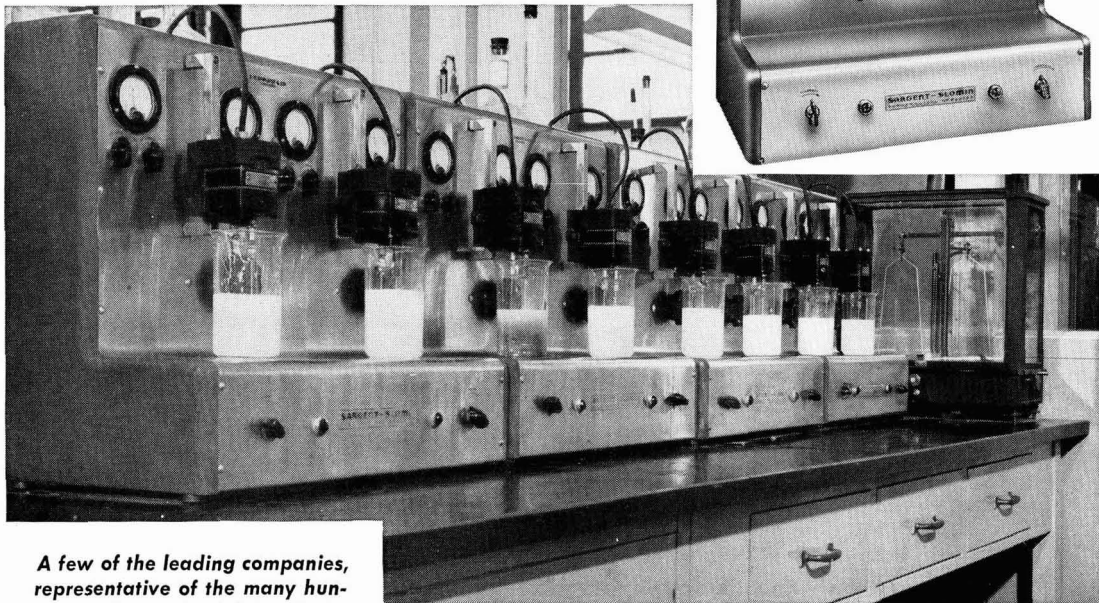
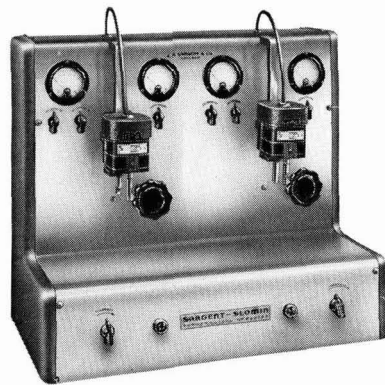


MAGNIFIED, UNRETOUCHED PHOTO... shows uniform structure of Stackpole GraphAnodes. The low-porosity surface assures that electrolyte will act on the surface, not below to cause premature anode deterioration and cell contamination by droppings of unconsumed graphite particles.

BRUSHES for all rotating electrical equipment • CONTACTS (carbon-graphite and metal powder types)
TUBE ANODES • CATHODIC PROTECTION ANODES • VOLTAGE REGULATOR DISCS • WATER HEATER and
PASTEURIZATION ELECTRODES • BEARINGS • WELDING CARBONS • MOLDS AND DIES • POROUS CARBON
SALT BATH RECTIFICATION RODS • SEAL RINGS • FRICTION SEGMENTS • CLUTCH RINGS • ELECTRIC FURNACE
HEATING ELEMENTS • PUMP VANES • and many other carbon, graphite, and electronic components.

SARGENT-SLOMIN ANALYZERS

*are standard equipment
in prominent laboratories*



A few of the leading companies, representative of the many hundreds of industrial laboratories using the Sargent - Slomin and Heavy Duty Analyzers for control analyses . . .

- AMPCO METAL, Inc.
- ANDERSON LABORATORIES
- CALERA MINING COMPANY
- EUREKA WILLIAMS COMPANY
- THE FEDERAL METAL CO.
- FORD MOTOR COMPANY
- THE GLIDDEN COMPANY—Chemical, Metal and Pigment Division
- HOT POINT CO.
- HOWARD FOUNDRY COMPANY
- INTERNATIONAL HARVESTER COMPANY
- KENNAMETAL Inc.
- McQUAY - NORRIS MANUFACTURING CO.
- NATIONAL LEAD COMPANY,
Fredericktown, Missouri
- PIASECKI HELICOPTER CORPORATION
- REVERE COPPER & BRASS INCORPORATED
- THE RIVER SMELTING & REFINING COMPANY
- SILAS MASON COMPANY
- THE STUDEBAKER CORPORATION
- THOMPSON PRODUCTS, INC.

Photo Courtesy INTERNATIONAL HARVESTER COMPANY, Melrose Park, Illinois

Sargent-Slomin Electrolytic Analyzers are recommended for such electro analytical determinations as: Copper in—ores, brass, iron, aluminum and its alloys, magnesium and its alloys, bronze, white metals, silver solders, nickel and zinc die castings. Lead in—brass, aluminum and its alloys, bronze, zinc and zinc die castings. Assay of electrolytical copper, nickel and other metals.

Sargent analyzers are completely line operated, employing self-contained rectifying and filter circuits. Deposition voltage is adjusted by means of autotransformers, with meters indicating volts and amperes and controls on the panel. An easily replaceable fuse guards against circuit overload. Maximum D.C. current capacity is 5 to 15 amperes; maximum D.C. voltage available, 10 volts.

Sargent-Slomin Analyzers stir through a rotating chuck operated from a capacitor type induction motor, having a fixed speed of 550 r.p.m. with 60 cycle A.C. current or 460 r.p.m. with 50 cycle A.C. current. Motors are sealed against corrosive fumes and are mounted on cast metal brackets, sliding on 1/2" square stainless steel rods, permitting vertical adjustment of electrode position over a distance of 4". Pre-lubricated ball-bearings support the rotating shaft. All analyzers accommodate electrodes having shaft diameters no greater than 0.059 inch. Stainless steel spring tension chucks permit quick, easy insertion of electrodes and maintain proper electrical contact. Special Sargent high efficiency electrodes are available for these analyzers. Illustrated above is one model of the five types of Sargent-Slomin and Heavy Duty Analyzers.

S-29465 ELECTROLYTIC ANALYZER—Motor stirred, Two Position, 5 Ampere. With two adjustable heaters, pilot lights and control knobs. For operation from 115 volt, 50 or 60 cycle A.C. circuits.....**\$530.00**

SARGENT

SCIENTIFIC LABORATORY INSTRUMENTS • APPARATUS • SUPPLIES • CHEMICALS

E. H. SARGENT & COMPANY, 4647 W. FOSTER AVE., CHICAGO 30, ILLINOIS
 MICHIGAN DIVISION, 8560 WEST CHICAGO AVENUE, DETROIT 4, MICHIGAN
 SOUTHWESTERN DIVISION, 5915 PEELER STREET, DALLAS 35, TEXAS
 SOUTHEASTERN DIVISION, 3125 SEVENTH AVE., N., BIRMINGHAM 4, ALA.

Formation of Manganese(II) Ion in the Discharge of the Manganese Dioxide Electrode

II. Effect of Volume and pH of Electrolyte

W. C. Vosburgh, Mary Jo Pribble, Akiya Kozawa, and Ahmad Sam

Department of Chemistry, Duke University, Durham, North Carolina

ABSTRACT

Discharge of the MnO_2 electrode at pH 5 to 8 is known to give Mn^{++} in solution as well as a lower oxide. When the volume of electrolyte is varied the amount of Mn^{++} formed in constant time and at constant current density is practically independent of volume. It decreases as the pH increases, becoming small at pH 8. The reaction of lower Mn oxides with electrolytes shows a similar relation to volume and pH. In the early part of a discharge the electrode surface resembles MnOOH in its reaction with the electrolyte. Later, at high pH, the surface seems to be at a lower state of oxidation than Mn_2O_3 .

Under certain conditions Mn^{++} in the electrolyte is a product of the discharge of the MnO_2 electrode (1,2). In a sufficiently acid electrolyte of relatively large volume it is the only product (3), but at pH 5 and pH 7.5 a lower oxide is left on the electrode in addition to Mn^{++} in solution.

In all of these experiments the ratio of electrolyte volume to the amount of MnO_2 was large and much different from that in the Leclanche dry cell. One object of the present investigation was to find the relation of the amount of Mn^{++} formed in a discharge to the volume of the electrolyte. A second object was a further investigation of the relation to pH. The results have added to the understanding of the electrode mechanism.

Experimental

Procedure

Electrodes were prepared by electrodeposition of MnO_2 on graphite rods from an electrolyte of 50 g/l of MnSO_4 and 65 g/l of H_2SO_4 at 90°C (except as otherwise noted) with a current of 25 ma for 30 min, the electrode area being 8 cm^2 . The total Mn was about 0.2 mmole/electrode. They were discharged with a current of 2 ma in electrolytes of varying volume and composition, the apparatus and procedure being essentially as described previously (4). With $(\text{NH}_4)_2\text{SO}_4$ electrolytes a well cleaned lead anode was used. With NH_4Cl electrolytes the anode was either a silver electrode well covered with AgCl (5) or several graphite rods placed around the central MnO_2 electrode.

Most of the discharges were terminated after either 100 or 150 min. Some were carried to completion for the study of the last part of the discharge.

At the termination of a discharge the cathode was removed from the cell either immediately or after 35 min on open circuit and the Mn^{++} concentration of the solution determined colorimetrically. When

graphite anodes were used the solution contained little Mn^{++} , but most of what had been dissolved from the cathode during the discharge was found in oxidized form on the anode rods. This was dissolved by H_2SO_4 and H_2O_2 and determined colorimetrically.

Relation of Mn^{++} in the electrolyte to the volume.—Table I shows the results of a number of experiments with electrolytes of 1M $(\text{NH}_4)_2\text{SO}_4$ buffered at pH 5.2 by 0.2M pyridine and 0.07M H_2SO_4 . Discharges were terminated after 150 min, during which no appreciable change in pH took place. Electrolyte volumes of 33-825 ml were used and a number of discharges made in each. The variation among experiments under the same conditions was large, as shown by the standard deviations. It is nevertheless clear that the total amount of Mn(II) ion produced is independent of the volume, within the limits of these experiments, whereas the concentration clearly varies with the volume.

Table I. Mn(II) ion in the electrolyte after discharge for 150 min at 2 ma in electrolytes of different volumes; pH 5.2

Vol, ml	No. discharges	Mn ⁺⁺ in electrolyte	
		Conc, M x 10 ⁴	Total, mmoles x 10 ²
33	3	24 ± 1.2	7.9 ± 0.37
110	5	5.7 ± 1.0	6.3 ± 1.3
190	7	3.0 ± 0.7	5.6 ± 1.7
240	6	1.9 ± 0.5	4.5 ± 1.2
825	4	0.8 ± 0.08	6.2 ± 0.8

Table II. Mn(II) ion in the electrolyte after discharge for 150 min at 2 ma in electrolytes of different volumes; pH 7.5

Vol, ml	No. discharges	Charge of pH	Total Mn ⁺⁺
			mmoles x 10 ²
33	1	7.5-8.1	2.0
110	1	7.5-7.7	1.6
240	2	7.5-7.9	1.7
825	2	7.5-7.6	2.6

Table II shows that the same relationship holds at pH 7.5. The experiments were the same as before except that the $1M (NH_4)_2SO_4$ electrolyte was buffered with NH_3 . A small increase in pH took place during the discharge, as shown in Table II. At pH 5.2 the average total Mn^{++} was 0.061 mmole, with a standard deviation of 0.011, while at pH 7.5 the average total Mn^{++} was 0.020 mmole, with a standard deviation of 0.005. A decrease with increasing pH is expected since it has been shown previously that very little Mn^{++} is formed in the first 100 ma-min of discharge at pH 7 while its formation starts at or near the beginning at pH 5 (2).

A few additional experiments at pH 5.2 were made with electrodes prepared at $80^\circ C$ instead of $90^\circ C$ and volumes of 110 and 240 ml. The results were not significantly different from those of Table II. The temperature of plating the electrodes has an effect on the overpotential (4), but too little to detect on the formation of Mn^{++} .

Relation to pH.—The results of experiments undertaken to find in more detail the relation between Mn^{++} dissolved and pH are shown in Fig. 1. The circles represent discharges in about 240 ml of solution of $2M NH_4Cl$ and NH_3 with graphite anodes. Discharges lasted 100 min at 2 ma and the cathode remained in the electrolyte after discharge for 35 min on open circuit during which time a small further increase in the Mn^{++} content of the solution took place. The values given are the sums of the Mn in the solution and that dissolved from the anodes. The line shows the general trend of these experiments, but has no theoretical significance.

The squares in Fig. 1 represent discharges in 240 ml of $2M NH_4Cl$ and either NH_3 or pyridine with Ag anodes. An atmosphere of nitrogen was maintained. The greater scattering of the points was probably the result of making the electrodes at different times rather than as a group. The electrodes for the more concordant experiments represented by the circles were all made on the same day and washed and stored in the same way and for about the same time before use. The nature of the MnO_2 is prob-

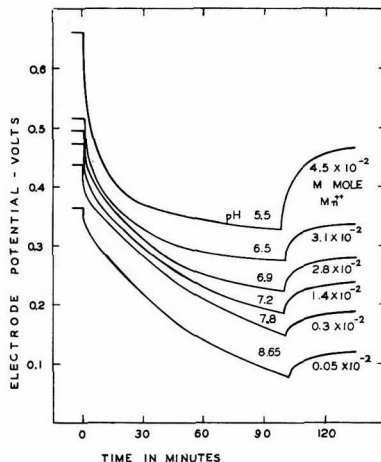


Fig. 2. Discharge curves in $2M NH_4Cl$ with different pH values and with different amounts of Mn^{++} produced.

ably the uncontrolled variable leading to the scattering. However, it is clear that the Mn^{++} dissolved decreases with increase in pH and becomes very small above pH 8; two experiments above this pH with negligible dissolved Mn^{++} are not shown.

The triangles in Fig. 1 represent similar experiments in $1M (NH_4)_2SO_4$ electrolyte and an atmosphere of nitrogen, with discharges lasting 150 min. In the longer time somewhat more Mn^{++} was dissolved. The solid circles represent experiments like those of the open circles, but with $0.1M ZnSO_4$ in the electrolyte. The single solid triangle likewise stands for the conditions of the open triangles, but with $0.1M ZnSO_4$. Two experiments with $ZnSO_4$, like the latter but at pH 7.2 gave no measurable Mn^{++} , in good agreement with the solid circle shown at that pH. The presence of Zn^{++} reduces the amount of Mn^{++} formed.

The larger amounts of Mn^{++} are considerable fractions of the total Mn on the electrode. In some of the discharges over a third of the Mn reduced was found in solution. If all of the reduced Mn after initial drop in potential should go into solution and not change the Mn^{++} concentration appreciably, a flat portion of the discharge curve would be expected, as in acid discharges (3). When all of the reduced Mn remains on the electrode, the closed-circuit potential should decrease throughout the discharge. Figure 2 shows that discharge curves at different pH values vary in shape in the expected manner. These discharges are the ones from which the data for the open circles of Fig. 1 were obtained.

Mn^{++} near the end of the discharge.—In explaining why Mn^{++} is not formed appreciably in the early part of a discharge at pH 7, it was pointed out previously (2) that $MnOOH$ is not dissolved appreciably in a short time by $2M NH_4Cl$ and NH_3 at pH 7 while Mn_2O_3 is dissolved. As a discharge proceeds the closed-circuit electrode potential decreases continuously (Fig. 2) indicating a lower and lower state of oxidation of the electrode surface (2,6). At pH 8 little Mn^{++} is formed in the first 200 ma-min, and it was of interest to see whether more would

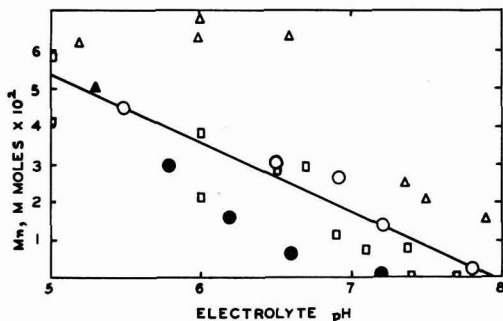


Fig. 1. The relation of the total Mn^{++} dissolved from a discharging electrode to the pH of the electrolyte. Open circle and solid circle represent discharges in $2M NH_4Cl$ and NH_3 without and with $0.1M ZnSO_4$, respectively (by A. Kozawa). Open square represents discharges in $2M NH_4Cl$ and NH_3 or pyridine, and open triangle and solid triangle represent discharges in $1M (NH_4)_2SO_4$ and NH_3 or pyridine for 300 instead of 200 ma-min, without and with $0.1M ZnSO_4$ (by M. J. Pribble).

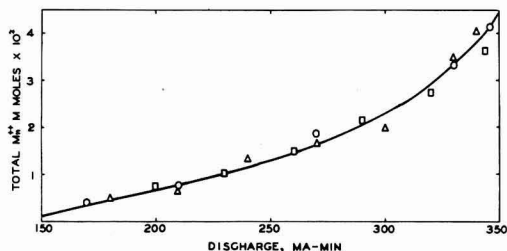


Fig. 3. Mn^{++} formed in the latter part of a discharge in 1M $(NH_4)_2SO_4$ at pH 8. The 3 symbols represent 3 different electrodes.

be formed in the later portion of the discharge, at lower potentials.

Three electrodes plated at 80°C were discharged at 2 ma to a cut-off of zero against the saturated calomel electrode in a cell containing 240 ml of 1M $(NH_4)_2SO_4$ and about 0.07M NH_3 with pH 8. Samples of the electrolyte were taken periodically after 90 min of discharge for determination of Mn^{++} . The results are shown in Fig. 3, in which the total Mn^{++} is plotted against the amount of discharge in ma-min. It is shown that Mn^{++} is formed at an increasing rate between 180 ma-min and the end of the discharge. The total Mn^{++} at the end of the discharge at pH 8 is about equal to that after 200 ma-min at pH 7.5 (Table II) and is about 10% of the total Mn on the electrode.

Reaction of Mn oxides with electrolytes.—If the surface of a discharging electrode is considered to resemble a lower oxide, it is of interest to know in more detail how some of the Mn oxides react with an ammonium salt solution.

Five different oxides were prepared by oxidation of 0.1M $MnSO_4$ in a solution of 1M NH_4Cl and NH_3 with $K_2S_2O_8$ at 70°C. The composition of the product depended primarily on the pH, but the amount of oxidant and the time allowed were of some importance. The reaction was slow and the rate of addition of the oxidant was unimportant. In all cases the reaction was allowed to proceed until its rate became very small. The amount of oxidant was usually about 10% less than theoretical for the formation of $MnOOH$. It was added slowly in 0.1M solution. Since acid is formed in the reaction, it was necessary to add NH_3 frequently to hold the pH approximately constant.

In one preparation no attempt was made to control the pH, which was 8 at the beginning and fell to 1.5 at the end. Analysis showed the product to be $MnO_{1.88}$. The pH is much more important in determining the product than the proportions of the reactants. When the pH was kept at 8 throughout the oxidation, the product was Mn_2O_4 , and when kept at either 6 or 7 the product was $MnO_{1.65}$ or $MnOOH$. When the pH was kept at 8 and a 20% excess of persulfate was used (calculated for $MnOOH$), the composition of the product in two trials was $MnO_{1.4}$. When the theoretical amount of persulfate was used at pH 7 instead of a deficiency the product was $MnO_{1.6}$. Each preparation was washed repeatedly with a very dilute slightly alkali-

line $(NH_4)_2SO_4$ solution until the wash solution gave no test for Mn^{++} .

These oxides react slowly in slightly acid solutions. For example, 50-mg portions of an oxide of the composition $MnO_{1.78}$ were stirred at 25°C with 50-ml portions of $(NH_4)_2SO_4$ solution of pH 4.7 (buffered with pyridine and pyridinium sulfate) for different periods of time. Samples were filtered and the Mn^{++} determined colorimetrically. After 3, 5, and 15 hr and 2, 3, and 7 days the Mn^{++} found was 25, 28, 31, 40, 50, and 55 mg/liter. Equilibrium evidently would require considerably more than a week by this procedure.

However, in a discharge only a limited time is available for the reaction of any lower oxide on the electrode surface with the solution. Therefore, for comparison with discharge data the oxide reacting in a limited time is of more interest than equilibrium data. A 3-hr reaction period was chosen as being of the order of magnitude of the duration of the discharge experiments and long enough for a considerable amount of reaction.

Table III shows the reaction in 3 hr of the above described oxides with 8 different solutions. The solutions were 2M $(NH_4)_2SO_4$ and 0.01M H_2SO_4 to which was added enough pyridine to give the desired pH. For each measurement 50 mg of the oxide was stirred with 50 ml of solution for 3 hr and 25° and the Mn^{++} concentration in the solution determined.

At lower pH values a considerable fraction of the total Mn of each of the oxides goes into solution, the maximum being about 13% of the sample by weight. At pH 7 the 2 highest oxides gave too little Mn^{++} to measure, and the others about 0.2% of the sample. It may be concluded that the surface of a discharging electrode is something like these oxides in the early part of the discharge, since very little Mn^{++} is dissolved up to 100 ma-min by an electrolyte of pH 7.5. Since Mn^{++} is dissolved in larger quantity in the latter part of a discharge, even at pH 8, the electrode surface must eventually be reduced to something considerably more reactive than Mn_2O_4 , which reacts only to a small extent at pH 7.

If the logarithm of the Mn^{++} concentration is plotted against the pH for any one oxide, the points fall fairly well along a straight line. This may be compared with Fig. 1 in which the line expresses a rough relation between the pH and the Mn^{++} concentration rather than the logarithm of the latter. This apparent disagreement is probably not real because the relationship in Fig. 1 is a more complicated one than the reaction of a definite solid

Table III. Mn^{++} dissolved in 3 hr by 2M $(NH_4)_2SO_4$ buffered with 0.01M H_2SO_4 and pyridine at different pH values from different oxides at 25°C

Oxide	Mn^{++} dissolved, M $\times 10^4$							
	pH 4.7	5.0	5.3	5.6	5.9	6.2	6.5	7.0
$MnO_{1.88}$	24	13	7.8	5.1	2.2	1.8	1.2	0.4
$MnO_{1.71}$	18	8.3	5.5	4.0	1.8	1.1	0.7	0.4
$MnO_{1.65}$	12	6.3	4.4	3.1	1.6	1.3	0.6	0.3
$MnO_{1.59}$	7.3	4.3	3.0	2.7	1.3	1.2	0.4	—
$MnO_{1.4}$	3.8	2.1	1.1	0.8	0.6	0.3	—	—

Table IV. Effect of volume of solution on amount of MnOOH dissolved in 3 hr by buffered 2M $(\text{NH}_4)_2\text{SO}_4$, 25°C

Volume, ml	pH	Mn ⁺⁺ conc., M x 10 ⁴	Mn ⁺⁺ total mmoles x 10 ²
50	4.7	12	6.0
150	4.7	4.4	6.6
250	4.7	3.0	7.5
50	5.3	5.8	2.9
150	5.3	2.1	3.1
250	5.3	1.4	3.4

with electrolytes of varying pH. In a discharge the composition of the surface of the electrode changes as the discharge proceeds and the formation of appreciable Mn⁺⁺ seems to start at different stages of the discharge in different electrolytes.

The reactivity of a lower oxide resembles the reactivity of the surface of a discharging electrode in the effect of volume. Table IV shows the results of experiments on the reactivity of 50 mg portions of MnOOH with 3 different volumes of solution at pH 4.7 and 5.3, the experimental details being as described above. The total amount dissolved in 3 hr varies considerably less with volume than the concentration.

Conclusions

The above results are in agreement with the theory of the electrode reaction that has been developed in previous papers (3,4). The decrease in closed circuit potential on discharge has been ascribed to the accumulation of lower oxide on the surface of the MnO₂. This is removed by reaction with the electrolyte to give Mn⁺⁺ or by diffusion into the MnO₂ or in both ways. The rate of removal by reaction with the electrolyte is a function of pH and of the oxygen content of the surface oxide. When the pH is too high for the surface oxide to react with the solution as fast as it is produced, its oxygen content decreases as the discharge proceeds. At the higher pH values (>6.5) the lower oxide

produced in the early part of the discharge does not react appreciably with the solution. Eventually, the surface becomes reduced to such an extent that Mn⁺⁺ passes into solution. The surface then resembles in its reaction an oxide reduced considerably below MnOOH or Mn₂O₃. For the study of the electrode reaction leading only to lower oxide, electrodes of the type described above can be used at pH 8 with no Mn⁺⁺ formation during the larger part of the discharge.

It will be shown in a later paper that these observations do not apply to all types of MnO₂. They are valid for MnO₂ electrodeposited from an acid MnSO₄ bath with negligible impurities. Such MnO₂ can be expected to be γ -MnO₂ (7,8).

Acknowledgment

This work was supported in part by the Office of Naval Research. Grateful acknowledgment is also made of a grant by the Research Council of Duke University.

Manuscript received July 15, 1957. This paper was prepared for delivery before the Buffalo Meeting, October 6-10, 1957.

Any discussion of this paper will appear in a Discussion Section to be published in the December 1958 JOURNAL.

REFERENCES

1. N. C. Cahoon, *This Journal*, **99**, 343 (1952).
2. A. M. Chreitzberg, Jr., D. R. Allenson, and W. C. Vosburgh, *ibid.*, **102**, 557 (1955).
3. S. Yoshizawa and W. C. Vosburgh, *ibid.*, **104**, 399 (1957).
4. A. M. Chreitzberg, Jr., and W. C. Vosburgh, *ibid.*, **104**, 1 (1957).
5. W. C. Vosburgh, D. R. Allenson, and Stanley Hills, *ibid.*, **103**, 91 (1956).
6. A. Kozawa and K. Sasaki, *J. Electrochem. Soc. Japan*, **22**, 569 (1954).
7. H. F. McMurdie, *Trans. Electrochem. Soc.*, **86**, 313 (1944).
8. W. F. Cole, A. D. Wadsley, and A. Walkley, *ibid.*, **92**, 133 (1947).

Oxidation of Niobium between 375°C and 700°C

Earl A. Gulbransen and Kenneth F. Andrew

Westinghouse Research Laboratories, Pittsburgh, Pennsylvania

ABSTRACT

Niobium has been found to oxidize in a complex manner. At 400°C and lower a slow rate of reaction is observed with the kinetics following the parabolic rate law. At a weight gain of 55-70 $\mu\text{g}/\text{cm}^2$ a transition in the kinetics occurs to a nearly linear rate law. Between 550° and 625°C the oxidation rate is nearly constant as a function of temperature, while above 625°C the oxidation rate again increases with the temperature. The adherence of the oxide is poor above the transition point.

Owing to its high melting point of 2415°C, its relatively low neutron cross section, and its workability at room temperature, Nb has many potential uses as a metallurgical material. The metal is very inert at room temperature to gas and liquid phase corrosion. However, its reactivity with oxygen,

hydrogen, and nitrogen at elevated temperatures is a major difficulty associated with its use as a high temperature material.

Gulbransen and Andrew (1) studied the reaction of Nb in 0.1 atmospheres of oxygen over the temperature range of 250°-375°C. For this temperature

range the parabolic rate law was found to fit the data. No evidence was found for a transition in the rate of oxidation.

Inouye (2) studied the scaling of Nb in dry and in wet air over the temperature range of 400°-1200°C. At 400°C in dry air the oxide film was initially protective. After 21 hr a sharp transition occurred in the rate of oxidation. A linear rate law was found after transition. Water vapor was found to accelerate the reaction at 400°C but not at higher temperatures.

Bridges and Fassell (3) studied the oxidation of Nb from 400° to 800°C and from 14.7 to 605 psia. pressure. A linear rate law was found. The temperature dependence of the rate of oxidation showed a reversal in sign between 550° and 650°C. In this temperature region the rate of oxidation was very sensitive to pressure.

The thermochemical properties of the niobium oxides have been studied (4,5) and a comprehensive study of the oxides of Nb has been made (6). Three oxides, Nb_2O_5 , NbO_2 , and NbO exist with limited regions of homogeneity. The solid oxide Nb_2O_5 exists in three forms designated as (L) low, (M) middle, and (H) high. The x-ray diffraction patterns of the L form were isomorphous with Ta_2O_5 and were stable to 900°C. Between 1000° and 1100°C the M form was found which transforms to the H form at higher temperatures.

According to Inouye (2), Zachariasen found Nb_2O_5 to be isomorphous with Ta_2O_5 . The crystal structure was pseudohexagonalorthohombic. The cell dimensions were reported as $A_1 = 6.16 \pm 0.03 \text{ \AA}$, $A_2 = 3.65 \pm 0.02 \text{ \AA}$, and $A_3 = 3.94 \pm 0.02 \text{ \AA}$ with the metal atoms at (0,0,0) and $(\frac{1}{2}, \frac{1}{2}, 0)$. The calculated density was 4.95 g/cc. NbO_2 has a crystal structure similar to that of rutile with the following lattice constants: $a = 4.84 \text{ \AA}$, $c = 2.99 \text{ \AA}$, and $c/a = 0.618$. The solubility of oxygen in Nb between 800° and 1100°C has been investigated by Seybolt (7).

The purpose of this work is (a) to extend earlier work to the temperature range of 350°-700°C, (b) to study the transition in the rate of oxidation observed by Inouye (2), and (c) to check the negative temperature coefficient for the reaction found by Bridges and Fassell (3).

Experimental

The vacuum microbalance method was used in this work (8). Small strips of the metal were suspended from a sensitive microbalance operating inside a vacuum system. After removal of the gases from the vacuum system, the sample was heated to temperature and oxygen gas added. The reaction of the metal with oxygen was followed semicontinuously.

To extend the range of the study, two microbalances of different sensitivities were used and three sizes of samples. The samples weighed 0.6840 g, 0.1600 g, and 0.0780 g, and had surface areas of 6.6 cm^2 , 1.62 cm^2 , and 0.79 cm^2 , respectively. The specially constructed low sensitivity microbalance had a sensitivity of $0.34 \times 10^{-3} \text{ cm}^2/\mu\text{g}$ and was used with the small specimens to extend the thickness range.

Weight gains of 4.5 mg could be measured on specimens of 0.0780 g with surface areas of 0.79 cm^2 . This was equivalent to 13% of the metal reacting with oxygen.

A gas-tight mullite furnace tube was used to enclose the sample. This tube was sealed directly to the all-glass vacuum system. No metal, rubber, grease joints, or stopcocks were used. Pressures of less than 10^{-6} mm Hg could be achieved in the system.

To eliminate the reaction of Nb with the gases present in the vacuum system during the heat-up period, the sample and furnace tube were pumped at room temperature for several hours at 10^{-6} mm Hg or less. Purified oxygen gas was added after the furnace was raised around the furnace tube and after thermal equilibrium was established.

The specimens were prepared from Fansteel high purity vacuum sintered Nb sheet. The analysis of the sheet was as follows: C, 0.0162 wt %; Ta, 0.143; Fe, 0.008; Zr, 0.65; Ti, 0.013; N, 0.028; and O, 0.107. To remove surface contamination, the specimens were abraded under purified kerosene. Each oxidation was made using a new specimen. There was no indication that decarburization was a factor in the change of weight of the specimen. The experimental results were reproducible within 10%.

Results and Discussion

Effect of temperature 375° to 525°C.—Figures 1 to 5 show the results of the oxidation experiments for temperatures of 375°-525°C. In these figures the weight gain in micrograms per cm^2 was plotted as a function of the time in minutes. The usual oxidation experiment was for 6 hr. However, in several experiments longer times were used. All experiments were made at 0.1 atmospheres pressure of oxygen.

To convert the weight gain in micrograms per cm^2 to thickness in Angstroms, a factor of 67.2 was used. This factor was calculated from the oxide Nb_2O_5 , a density of 4.5, and a surface roughness ratio of unity.

Figure 1 shows the weight gain curves for the 375° and 400°C oxidation curves. After a rapid initial reaction, the rate of oxidation decreases as the oxide thickens. Table I shows a summary of the thickness data after a given time of reaction, together with the color of the oxide film and its stability to cracking on cooling. At 375°C no evidence was observed in 6 hr for a transition in the rate of oxidation.

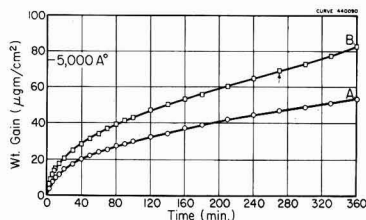


Fig. 1. Effect of temperature on oxidation of Nb abraded through 4/0, 7.6 cm Hg of O_2 . Curve A, 375°C; curve B, 400°C.

Table I. Thickness, color, and physical character of oxide films formed on Nb

Temp. °C	Time, min	Oxide thickness $\mu\text{g}/\text{cm}^2$	Å	Color	Character
375	360	53.8	3620	Blue-green	Stable
400	360	83.5	5610	Dark gray	Stable
425	330	591	39,800	Dark gray	Stable
450	360	2780	187,000	Light gray	Stable
475	190	2880	193,500	Light gray	Stable
500	120	1818	122,100	Light and dark gray	Spalled
525	100	1308	87,900	Dark gray + small amt. light gray	Spalled
550	120	3190	214,500	Light and dark gray	Spalled
575	120	3610	236,000	Light and dark gray	Spalled
600	120	3270	220,000	Dark gray + small amt. light gray	Spalled
625	120	3350	225,500	Dark gray + small amt. light gray	Spalled
650	120	4290	288,000	Dark gray + small amt. light gray	Spalled
675	95	5550	373,000	Dark gray + small amt. light gray	Spalled
700	55	5550	373,000	Dark gray	Cracked oxide film

For the 400°C experiment of Fig. 1, the oxidation reaction follows the protective pattern for 4½ hr after which a transition occurs and the rate of oxidation increases. This transition occurs at a film thickness of about 60–80 $\mu\text{g}/\text{cm}^2$. Bridges and Fassell (3) state that nearly 6 hr were required before the oxidation rate became linear at 400°C and a pressure of 1 atmosphere of oxygen. This observation could be interpreted as a transition in the oxidation rate and is in agreement with the results of Fig. 1. Transitions in the rate of oxidation have been observed in other systems (9) and may be a general phenomenon for the oxidation of a wide variety of metals and alloys. What was unusual was the low thickness value at which transition occurs.

Figure 2 shows the oxidation curve at 425°C. Again the oxidation curve shows the formation of a protective oxide during the initial stage of the reaction. However, after a film thickness of 55 $\mu\text{g}/\text{cm}^2$ was reached, the rate of oxidation underwent a transition to a linear rate. These results confirm the transformation shown at 400°C.

Figure 3 shows the course of the 450°C oxidation curve. The curve shows a very short period of protective oxide formation followed by a transition to a linear rate of reaction. The transition thickness was about 50 $\mu\text{g}/\text{cm}^2$. The weight gains corresponding to 100,000 and 200,000 Å of film thickness were noted on the figure. A film thickness of 100,000 Å corresponds to 10^{-3} cm, or 0.0004 in. This was an appreciable amount of reaction for a 3-hr period at this temperature.

Figure 4 shows the results at 475°C. Here, the initial stage of the reaction was very short. The

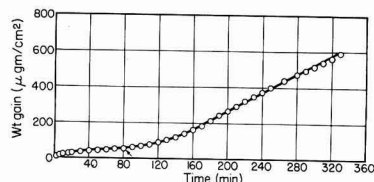


Fig. 2. Oxidation of Nb, abraded through 4/0, 425°C (797°F), 7.6 cm Hg of O₂.

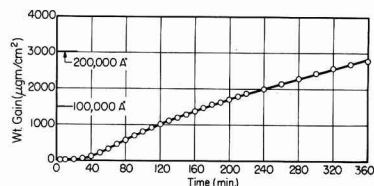


Fig. 3. Oxidation of Nb, abraded through 4/0, 450°C (842°F), 7.6 cm Hg of O₂.

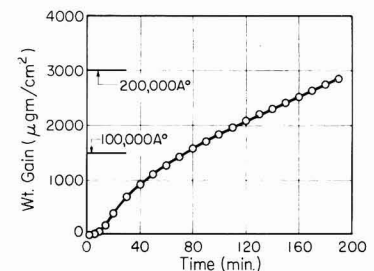


Fig. 4. Oxidation of Nb, abraded through 4/0, 475°C (887°F), 7.6 cm Hg of O₂.

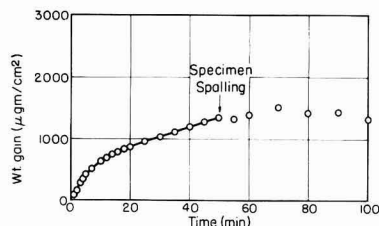


Fig. 5. Oxidation of Nb, abraded through 4/0, 525°C (977°F), 7.6 cm Hg of O₂.

extent of reaction after 3 hr of reaction was nearly 2×10^{-3} cm, or 0.0008 in. Table I shows that the oxide film was cracking on cooling, and one must conclude that the oxide was unprotective for this temperature.

Figure 5 shows several new features in the course of the oxidation curve at 525°C. First, the initial period was no longer observed. Second, spalling of the oxide from the metal was interfering with the rate measurements. Third, the previously termed linear rate law region was not linear since the rate decreases with time. This could be an indication of spalling or a change in the mechanism of reaction.

Effect of temperature 550°–700°C.—Figure 6 shows oxidation curves for experiments between 550° and 700°C. Between 500° and 625°C the rate of oxidation was nearly independent of temperature, while above 625°C the rate of oxidation in-

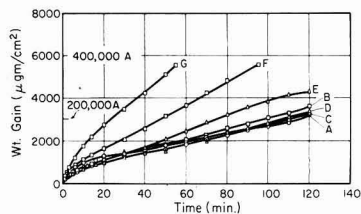


Fig. 6. Effect of temperature on oxidation of Nb, abraded through 4/0, 7.6 cm Hg of O_2 . Curve A, 550°C; curve B, 575°C; curve C, 600°C; curve D, 625°C; curve E, 650°C; curve F, 675°C; curve G, 700°C.

creased with temperature. After an initial period, the data approximately fit a linear rate law. Due to occasional spalling of the oxide, the linear rate law was not uniform. All of the oxide films formed in this temperature range spalled or cracked on cooling to room temperature. Table I summarizes the oxide thickness, the oxide color, and the stability data for these experiments. Figure 7 shows a photograph of the 675°C sample after oxidation, together with the spalled oxide collected from the furnace tube.

These experiments suggest that there exists a temperature region in which the rate of oxidation is nearly constant with temperature. No evidence was found for a reversal in the temperature coefficient of the oxidation reaction as noted by Bridges and Fassell (3).

Rate law correlation.—Both the linear and parabolic rate law have been used to explain the oxidation rate of Nb (1-3). The parabolic rate law states

$$W^2 = At + C$$

Here W is the weight gain, t is the time, and A and C are constants. Wagner and Grünwald (10) and later Mott (11) derived this equation from fundamental principles of diffusion and lattice defects. The linear rate law states

$$W = At + C$$

and suggests that diffusion processes are not rate controlling. The symbols have the same meaning as before.

To test the fitness of the parabolic rate law and to show the transition to the linear rate law, plots were made of the weight gain squared vs. time. Three plots were made for 375°, 425°, and 475°C runs. Figure 8 shows the parabolic rate law plots

Table II. Comparison of parabolic rate constants for oxidation of Nb

Temp, t°C	Older work (1) parabolic constants (g/cm ²) ² /sec	Temp, t°C	This study parabolic constants (g/cm ²) ² /sec
200	1.06×10^{-15}	375	1.25×10^{-18}
225	4.45×10^{-15}	400	2.96×10^{-18}
250	6.25×10^{-15}	425	6.50×10^{-18}
275	5.52×10^{-14}	450	1.12×10^{-17}
300	7.39×10^{-14}	475	1.75×10^{-17}
325	9.38×10^{-14}		
350	2.8×10^{-13}		
375	9.03×10^{-13}		

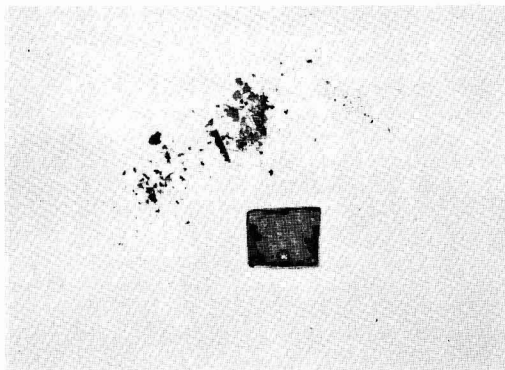


Fig. 7. Oxidation of Nb, 650°C, 7.6 cm Hg of O_2

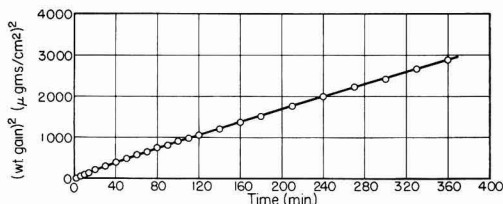


Fig. 8. Oxidation of Nb parabolic plot, abraded through 4/0, 375°C (707°F), 7.6 cm Hg of O_2 . $A_{1-2 \text{ hr}} = 1.35 \times 10^{-18}$ (g/cm²)²/sec; $A_{1-6 \text{ hr}} = 1.25 \times 10^{-18}$ (g/cm²)²/sec.

for 375°C run. After the initial period a fairly good fit was obtained. This confirms the earlier results of Gulbransen and Andrew (1). Figure 9 for the 425°C oxidation shows the parabolic rate law to fit the initial part of the reaction. The transition to the linear rate law occurs after 80 min of reaction. Figure 10 shows a parabolic rate law plot for the 475°C experiment. No fit was obtained at this temperature.

Table II shows a comparison of the parabolic rate law constants obtained in this study with those obtained in the authors' earlier work. Results for the commercial grade of Nb show lower rates of reaction than results on a somewhat purer grade of Nb used in our earlier study.

Figure 11 shows a logarithmic plot of the parabolic rate law constant vs. $1/T$. The results of the earlier study were included. The figure shows that the temperature coefficients of the parabolic rate

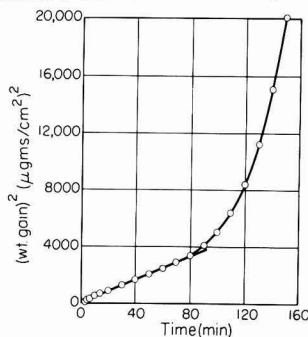


Fig. 9. Oxidation of Nb parabolic plot, abraded through 4/0, 425°C (797°F), 7.6 cm Hg of O_2 . $A = 6.95 \times 10^{-18}$ (g/cm²)²/sec.

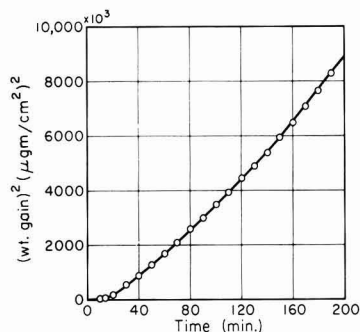


Fig. 10. Oxidation of Nb parabolic plot, abraded through 4/0, 470°C (887°F), 7.6 cm Hg of O₂.

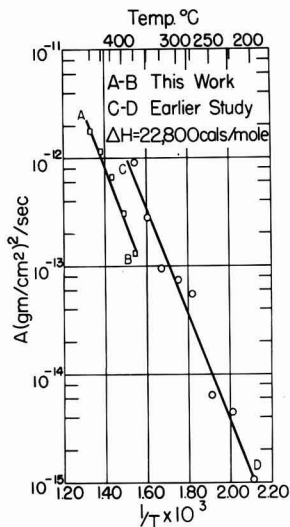


Fig. 11. Oxidation of Nb, log A vs. 1/T

law constant for the two sets of results were about the same. However, the actual constants for the commercial grade of material were smaller. A heat of activation of $22,800 \pm 3,000$ cal/mole was calculated. Since the studies of Inouye (2) and Bridges and Fassell (3) were for the linear range of oxidation, no comparisons can be made with their data.

Table III shows a summary of the linear rate law constants for the temperature range of 400°–700°C. The values identified as initial values were obtained immediately after transition and do not represent the long period rate of reaction.

Figure 12 shows a logarithm linear rate constant vs. $1/T$ plot of the linear rate law data, together with the data of Inouye (2) and Bridges and Fassell (3). Below 500°C the data from the three studies were in agreement, while above 500°C the three studies are not in agreement. The present study shows no evidence at 0.1 atmosphere pressure of oxygen for a negative temperature coefficient for the rate of oxidation as noted by Bridges and Fassell (3). Although Inouye only studied the reaction at 100°C intervals, his data also show no evidence for this phenomenon.

Table III. Linear rate law constants, oxidation of Nb

Temp, °C	Linear rate law const g/cm ² /sec	Temp, °C	Linear rate law const g/cm ² /sec
400	5.7×10^{-8} *	550	3.3×10^{-7}
425	4.3×10^{-8} *	575	3.76×10^{-7}
450	1.13×10^{-7}	600	3.81×10^{-7}
450	2.05×10^{-7} *	625	3.88×10^{-7}
475	2.07×10^{-7}	650	5.53×10^{-7}
500	1.9×10^{-7}	675	8.8×10^{-7}
525	2.66×10^{-7}	700	1.39×10^{-6}

* Initial values.

Transition in the rate of oxidation data.—Niobium undergoes a transition in the rate of oxidation from the parabolic rate law to the linear rate law at film thicknesses of 50–67 $\mu\text{g}/\text{cm}^2$ in the temperature range of 400°–450°C. This confirms the results of Inouye (2).

After transition the oxide was not adherent to the metal. The early onset of transition is a major difficulty in the use of the material at high temperature. In the protective range of the oxidation of Nb the parabolic rate constants were considerably higher than those found for Zr, Ni, and other metals.

The data of Table I suggest that there is a definite relation between the fact that the oxide spalls at temperature or cracks on cooling and the transition to a linear rate law. However, the 400°–475°C experiments indicate that the oxide did not crack on cooling. This suggests that the oxide film had lost adhesion on a local basis long before the necessary stresses were reached for cracking of the oxide from the metal. We associate, therefore, the transition in the rate of oxidation to local loss of adhesion or to cracking or spalling of the oxide from the metal. The cracking or spalling of the oxide was a later stage of the process which starts as one involving a local loss of adhesion.

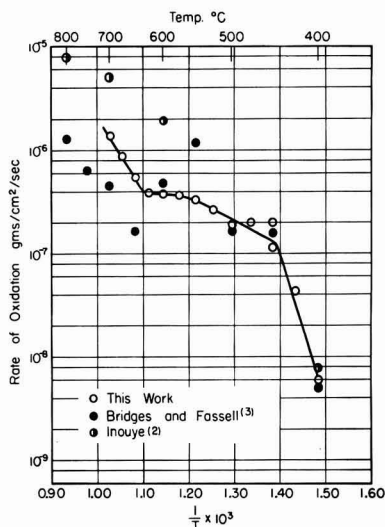


Fig. 12. Oxidation rate Nb vs. $1/T$ O₂ at 7.6 cm Hg, 400°–700°C.

Table IV. Comparison of x-ray diffraction data on spalled oxide with Nb₂O₅ (L-form) Ni K_α

550°C Oxide		700°C Oxide		Nb ₂ O ₅ (L-form) (6)	
d _{hkl}	I/I ₀	d _{hkl}	I/I ₀	d _{hkl}	I/I ₀
3.9231	10	3.8854	9	4.0550	1
3.1260	8	3.1258	10	3.9482	8
3.0758	8	3.0575	5	3.1661	8
2.9199	1	2.4394	4	3.0867	5
2.8177	1	2.4120	2	2.4661	5
2.7252	tr	2.1051	tr	2.4364	3
2.4479	7	2.0028	tr	2.1319	1
2.4197	7	1.9626	7	2.0213	2
2.1136	tr	1.8205	6	1.9729	5
2.0011	tr	1.7852	7	1.8377	3
1.9585	7	1.6560	9	1.8004	5
1.8232	1	1.6253	5	1.6664	5
1.7884	3	1.5696	3	1.6380	3
1.6564	5	1.5375	1	1.5798	3
1.6267	2	1.4574	3	1.5508	2
1.5668	tr	1.3365	3	1.5276	1
1.5390	tr	1.3207	3	1.4977	1
1.4589	tr	1.2265	1	1.4687	3
1.4318	tr	1.2088	1	1.4435	1
1.3205	tr	1.1930	1	1.4029	1
		1.1429	1	1.3429	3
		1.1227	tr	1.3280	3
				1.2333	2
				1.2161	1
				1.1995	1
				1.1493	2
				1.0084	1

X-ray diffraction studies.—An x-ray diffraction study was made of the oxides formed in the oxidation of Nb for the temperature range of 500°–700°C. The x-ray diffraction d_{hkl} values can best be correlated with the L-form of Nb₂O₅, although important deviations are found. Table IV shows a correlation between the d_{hkl} values for the 550° and 700°C spalled oxide films with the L-form of Nb₂O₅.

(6). X-ray studies on the spalled oxide agree with those of Inouye (2).

Attempts were made to strip the oxide film electrochemically from the 375° and 400°C experiments where adherent oxide films were formed. These efforts were not successful.

It was concluded that the low temperature modification of Nb₂O₅ was formed. However, the parameters were not exactly those observed by Brauer (6). A phase diagram study of the niobium oxide system must be made to understand the observed structures and those of Brauer. Also, the important oxide films to study were those for the adherent scales. Methods must be developed for removing the base metal from the oxide film.

Manuscript received May 27, 1957. This paper was prepared for delivery before the Washington Meeting, May 12–16, 1957.

Any discussion of this paper will appear in a Discussion Section to be published in the December 1958 JOURNAL.

REFERENCES

1. E. A. Gulbransen and K. F. Andrew, *Trans. Am. Inst. Mining Met. Engrs.*, **188**, 586 (1950).
2. H. Inouye, A.I.M.E. Reactive Metal Conference, Buffalo, New York, March 19–21, (1956). To be published.
3. D. W. Bridges and W. M. Fassell, Jr., *This Journal*, **103**, 326–350 (1956).
4. G. Grube, O. Kubaschewski, and K. Zwiaur, *Z. Elektrochem.*, **45**, 885 (1939).
5. O. Kubaschewski, *ibid.*, **62**, 818 (1940).
6. G. Brauer, *Z. anorg. u. allgem. chem.*, **248**, 1 (1941).
7. A. U. Seybolt, *J. Metals*, **6**, 774 (1954).
8. E. A. Gulbransen, *Trans. Electrochem. Soc.*, **83**, 301 (1943).
9. E. A. Gulbransen and K. F. Andrew, Unpublished work.
10. C. Wagner and K. Grünwald, *Z. Phys. Chem.*, **40B**, 455 (1938).
11. N. F. Mott, *Trans. Faraday Soc.*, **36**, 472 (1940).

The Action of Lead Pigments and Lead Soaps on Aluminum

M. J. Pryor, R. J. Hogan, and F. B. Patten

Department of Metallurgical Research, Kaiser Aluminum & Chemical Corporation, Spokane, Washington

ABSTRACT

Aqueous extracts from metallic lead and litharge are corrosive to aluminum due to their initially high pH and to the galvanic corrosion resulting from lead deposition on the aluminum. Aqueous extracts from red lead and basic lead carbonate have lower pH, do not deposit metallic lead on aluminum, and are much less corrosive. Aqueous extracts from lead linoleate, lead ricinoleate, and lead laurate inhibit the corrosion of aluminum and the galvanic corrosion of aluminum coupled to lead. Inhibition is believed to be due to the adsorption of fatty acid anions on the oxide covered aluminum surface. Since the diameter of the fatty acid anions is large, the electric fields accelerating aluminum ions from the metal through the oxide film are very weak. Consequently the corrosion of aluminum in lead soaps is prevented. Inhibition by lead soaps is easily broken down by the simultaneous presence of small quantities of chloride ions.

The question of whether organic coatings pigmented with lead compounds accelerate or reduce the corrosion of aluminum has never been fully resolved. It has been argued (1) that paints containing lead pigments should accelerate corrosion due

to deposition of metallic lead which forms damaging galvanic cells. However, Wagner (2) has suggested that red lead primers may be used safely on aluminum provided all alkaline cleaning compounds are first removed. This uncertainty has been accen-

tuated by the varied service experience with aluminum which had been coated with lead based paints.

Mayne (3) demonstrated that oxygen and water pass through organic films at a relatively high rate but that the passage of other more corrosive anions such as chloride ions is largely prevented. Therefore it follows that the effectiveness of a primer depends to a considerable extent on the rate of corrosion of the base metal in an oxygen-containing aqueous extract from the pigment or from the products of interaction of the pigment with the vehicle.

Several investigations have been carried out in the past (4-6) which have shown that aqueous extracts from certain lead pigments such as litharge, metallic lead, and red lead have an inhibitive action on the corrosion of steel. Furthermore, lead linoleate (5), a product of reaction of a lead pigment with a linseed oil vehicle, is a corrosion inhibitor for steel.

These observations have been of great assistance in furthering the understanding of how lead pigmented paints control the corrosion of steel. Therefore it was considered that an investigation of the corrosion rate of aluminum in aqueous extracts from litharge, red lead, basic lead carbonate, and metallic lead pigments and in certain lead soaps might clarify the effect of lead pigmented paints on aluminum. Lead soaps of unsaturated linoleic ($C_{18}H_{32}O_2$) and ricinoleic acids ($C_{18}H_{34}O_2$) together with the lead soap of saturated lauric acid ($C_{12}H_{24}O_2$) were selected for this investigation because these acids are commonly found in the vehicles of many air-drying and baking coatings. In particular it is desirable to determine whether sufficient lead passes into aqueous solution from lead pigments or lead soaps to initiate metallic deposition on aluminum. Should this occur, the problem becomes primarily one of galvanic corrosion between aluminum and lead. Consequently, the intensity of the galvanic corrosion between aluminum and lead in the different pigment and soap extracts must be investigated in some detail.

Experimental

Materials.—The aluminum used in this investigation was high purity, cold rolled sheet 0.088 cm thick. Its chemical composition together with those of the litharge, red lead, basic lead carbonate (white lead), metallic lead, and lead soaps are shown in Table I. All other solutions were prepared from C.P. chemicals and distilled water.

Preparation of the Aqueous Extracts

Extracts from the four inorganic lead compounds were prepared by exposing 50 g of each compound

Table II. Properties of aqueous extracts

Extract	Initial pH	Lead content mg per liter		Avg Spec Res after filtration through glass wool ohm/cm ² /cm
		After filtration through glass wool	After filtration through Whatman #1 paper	
Lead	9.1	70.0	6.9	40,500
Litharge	9.0	82.5	2.0	29,500
Red lead	6.1	7.5	2.1	49,000
Basic lead carbonate	6.3	2.0	0.18	33,000
Lead linoleate	5.1	218.0	—	4,400
Lead ricinoleate	6.0	20.8	—	24,000
Lead laurate	5.5	296.0	—	4,200
Distilled water	6.0	—	—	1,500,000

to one liter of distilled water for eight days in a stoppered flask at $25 \pm 0.05^\circ\text{C}$. The flasks were shaken at frequent intervals to ensure dispersion of the fine particles of pigment. After eight days the solutions were filtered rapidly through glass wool and contained in well-stoppered bottles. Since the conductivities of the extracts changed markedly with time, even after filtration, all experiments described below were carried out on fresh extracts. The extracts from lead soaps were prepared in a manner similar to that previously described by Mayne (5). The lead soaps were dispersed in hot xylene and applied to the inside of glass beakers. After drying in air for eight days the beakers were filled with distilled water at 25°C for a further eight days. After this period the solutions were decanted and stored in well-stoppered bottles.

Properties of the aqueous extracts.—The properties of the aqueous extracts are shown in Table II. The lead content of each extract was determined colorimetrically using diphenyl thiocarbazon (11). Both the litharge and lead extracts are initially markedly alkaline. However on standing in contact with the atmosphere they become less alkaline due to the absorption of carbon dioxide and the resulting precipitation of basic lead carbonate (6). Furthermore both the litharge and lead extracts after filtration through glass wool are buffered to some extent (Fig. 1). The reserve alkalinity of 100 ml of extract will be defined arbitrarily as the volume of 0.01N hydrochloric acid required to lower its pH to a value of 6.0. The reserve alkalinities of lead and litharge extracts are dependent not only on the quantity of lead in solution but also on the form in which it is present. Table II shows that most of the lead from litharge and lead extracts may be removed by filtration through Whatman No. 1 filter

Table I. Compositions of the materials used

Aluminum	Silicon 0.001%	Iron 0.001%	Copper 0.002%	Balance Al
Lead powder	Silicon 0.004%	Iron—trace	Magnesium—trace	Balance Lead
Sheet lead	Bismuth 0.06%	Silver 0.003%	Copper 0.03%	Balance Lead
		Silicon 0.004%		
Litharge	PbO assay 99.9%	Moisture 0.04%		
Basic lead carbonate	Lead carbonate 63.5%			
Red lead	Pb ₃ O ₄ assay 97.0%			
Lead linoleate	25% Lead			
Lead ricinoleate	25% Lead			
Lead laurate	32.3% Lead			

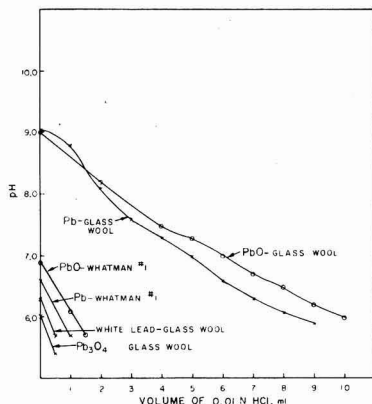


Fig. 1. Neutralization curves for pigment extracts filtered through glass wool and through Whatman No. 1 filter paper.

paper. This is probably due to the removal of massive lead hydroxide, lead dioxydihydroxide [$\text{Pb}_2\text{O}_2(\text{OH})_2$] (12) and to the adsorption of lead compounds by the filter paper (13).

The lead linoleate extract has a relatively low pH (5.1) and specific resistance together with a high lead content similar to the value previously reported by Mayne (5). The lead laurate extract contains even higher quantities of lead but otherwise its properties are similar to those of lead linoleate. Lead ricinoleate is less soluble than the other two lead soaps and shows a correspondingly increased specific resistance and pH value.

Twenty-five ml of the inorganic extracts were filtered through glass wool and enclosed in semipermeable membranes of untreated (nonwater-proofed) cellophane. These "bags" of cellophane were then placed in 25 ml of distilled water for 48 hr in order to investigate whether detectable quan-

Table III. Weight losses of aluminum specimens in fifteen days in aqueous extracts

Extract	Filtration method	Weight losses (mg/cm ²)
Fresh distilled water	None	0.195, 0.27, 0.29, 0.34, 0.18, 0.42
Distilled water after 8 days' contact with glass	None	0.43, 0.47, 0.40
Metallic lead	Glass wool	0.52, 0.68, 0.49
	Whatman #1 paper	0.22, 0.22, 0.235
Litharge	Glass wool	0.65, 0.65, 0.55
	Whatman #1 paper	0.23, 0.23, 0.26
Red lead	Glass wool	0.00, 0.00, 0.01
	Whatman #1 paper	0.00, 0.00, 0.00
Basic lead carbonate	Glass wool	0.00, 0.00, 0.00
	Whatman #1 paper	0.00, 0.00, 0.00
Lead linoleate	None	0.00, 0.00, 0.00
Lead ricinoleate	None	0.00, 0.00, 0.00
Lead laurate	None	0.00, 0.00, 0.00

ties of ionic lead were present in the aqueous extracts. Using the sensitive lead sulfide test it was found that in no case did detectable quantities of lead ions pass through semipermeable membranes into the surrounding water. In the case of the litharge extract this result differs from previous work (6) in which it was found that a substantial quantity of the lead in the litharge extract was present as $\text{Pb}(\text{OH})^+$ ions. Evidently the properties of litharge extracts are dependent on the source of the pigment.

Reactions between Aluminum and Aqueous Extracts in the Presence of Dissolved Air

Aluminum specimens measuring 5.6×2.5 cm were degreased in benzene, etched for 1 min in cold 10% NaOH, rinsed, dried, stored in dry air for 24 hr, and weighed. Triplicate specimens were totally immersed for fifteen days at $25 \pm 0.05^\circ\text{C}$ in 100 ml of fresh extracts which had been filtered through glass wool. The tops of the specimens were located 1 cm below the water line of the solution. Evaporation was largely prevented by covering the tops of the vessels with Saran plastic tissue. Control experiments in fresh distilled water and in distilled water that had been stored in glass vessels for eight days were also carried out.¹ At the end of the experiments the specimens were treated with nitric acid to remove the corrosion products together with any lead compounds, then they were dried in acetone and re-weighed. The weight losses² for these experiments are shown in Table III. This table also contains the results of similar experiments in which the extracts were filtered through Whatman No. 1 filter paper before use. Potential/time curves measured by means of a Speedomax recording potentiometer are shown in Fig. 2.³

Specimens immersed in litharge and lead extracts that had been filtered through glass wool rapidly developed a plating of metallic lead. However, after a short while the lead plate transformed into a white powder which was identified by x-ray diffraction as having $2\text{PbCO}_3 \cdot \text{Pb}(\text{OH})_2$ as the major constituent and lead as a minor one. The quantity of lead deposited, as indicated by approximate weight gain figures, was greater in litharge extracts

¹ This was to investigate the suggestion made previously for iron (7) that silicate leached from the glass might influence the results.

² All weight losses in this paper are corrected by subtracting the small weight loss resulting from the chemical cleaning process itself.

³ All potentials in this paper are expressed on the Standard Hydrogen Scale.

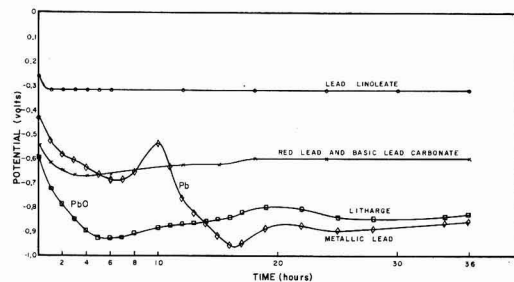


Fig. 2. Potential-time curves of aluminum specimens immersed in inorganic pigment extracts filtered through glass wool and in lead linoleate at $25 \pm 0.05^\circ\text{C}$. All specimens carried an air-formed oxide film.

than in lead extracts. Conductivity measurements indicated that lead was not completely stripped from the solution by deposition on aluminum. When the lead-plated aluminum samples were removed from the solution, transformation of the deposited lead to basic lead carbonate was greatly hastened.

Specimens immersed in fresh distilled water remained apparently uncorroded for around six days after which time a continuous gray film and later white β $\text{Al}_2\text{O}_3 \cdot 3\text{H}_2\text{O}$ formed. Specimens immersed in distilled water that had been contained in a glass beaker for eight days before the experiment not only formed gray films and white corrosion product somewhat faster than those immersed in fresh distilled water but were more severely corroded. The silicate leached out of the glass raised the initial pH of the water by around one pH unit and evidently increased the corrosion rate of the aluminum.

Specimens immersed in the extracts of red lead, basic lead carbonate, lead linoleate, lead ricinoleate, and lead laurate were not visibly attacked and suffered no loss in weight.

Galvanic Experiments

Galvanic experiments were carried out using the apparatus shown in Fig. 3. The lead (see Table I for composition) and aluminum electrodes had equal areas of 25 cm^2 immersed in 320 ml of the aqueous extract under investigation and were held firmly in place 5 cm apart by means of a Lucite holder. The back surfaces of the electrodes were masked with water-proofed Scotch pressure-sensitive tape. Surface pretreatment of lead involved degreasing in benzene, etching for 1 min in 50% nitric acid, followed by rinsing, drying, weighing, and storage in dry air for 24 hr. Surface pretreatment of aluminum was carried out in a similar manner except that etching was done in cold 10% NaOH for 1 min. The cell was contained in a water-bath thermostatted at $25^\circ \pm 0.05^\circ \text{C}$.

The electrodes were short-circuited for the test period for 96 hr. Current values at zero external resistance were measured periodically by introducing a zero resistance microammeter into the circuit. Potential measurements of the aluminum electrodes were made against a saturated calomel electrode using a high resistance bridge. Diffusion of the dilute chloride solution contained in the reference elec-

trode vessel was prevented by a bentonite plug (8). The tip of the tubulus was situated 1 mm from the aluminum electrode surface since, in high resistance solutions, there is a significant potential drop across the solution in addition to localized undetermined potential changes at the double layers next to the electrodes (9). The potentials of aluminum electrodes coupled to lead were somewhat more noble than those measured during corrosion of uncoupled aluminum specimens in the same solution.

After 96 hr the experiments were discontinued and corrosion products removed chemically so that weight loss of the electrodes could be determined. The aluminum specimens were cleaned by immersion in nitric acid whereas the lead specimens were cleaned by 10-min immersion in boiling 1% acetic acid (10). The total number of coulombs flowing in each experiment was calculated from the appropriate current/time curve. By knowing the weight loss of uncoupled specimens in the appropriate extract, the decrease in weight loss of the cathodic member of the couple and the current efficiency of the anodic process can be calculated. The weight losses of lead specimens immersed in the four inorganic pigment extracts for 96 hr are shown in Table IV.

Current/time curves for the aluminum/lead couple in aqueous extracts from lead, litharge, red lead, basic lead carbonate, and in distilled water were erratic. The total number of coulombs flowing in triplicate experiments together with the weight losses of the aluminum and lead are shown in Table V. However, aluminum invariably behaved as the anode in the galvanic studies of the aluminum-lead couple.

Initial values of current flow in aqueous extracts from the four inorganic lead compounds were primarily dependent on the resistance of the extract. Later however the resistance of the extracts decreased as the lead cathodes corroded. In these experiments the greatest proportion of the corrosion of the aluminum was the result of the deposition of metallic lead on the aluminum anodes. Lead is fairly readily attacked by extracts from the inorganic lead compounds and the galvanic currents are insufficiently strong for complete cathodic protection. Therefore the extracts may be regarded as providing a reservoir of lead ions from which metallic lead may be deposited on the aluminum. Substantial quantities of basic lead carbonate were precipitated from the extracts over a period of four days and the lead cathodes also became blanketed with this compound.

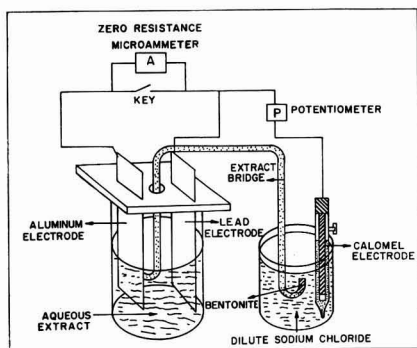


Fig. 3. Apparatus for galvanic studies in pigment and lead soap extracts.

Table IV. Weight losses of lead specimens in 96 hr in aqueous inorganic extracts filtered through glass wool

Extract	Weight loss of lead specimens (mg/cm ²)
Distilled water	2.8, 2.3, 2.6
Metallic lead extract	3.4, 2.7, 2.6
PbO extract	3.9, 2.5, 2.4
Pb ₂ O ₃ extract	3.1, 2.6, 2.7
Basic lead carbonate extract	3.2, 2.9, 2.7

Table V. Galvanic corrosion data for the aluminum-lead couple in aqueous extracts filtered through glass wool

	Wt loss of lead cathode mg/cm ²	Wt loss of Al anode mg/cm ²	No. of coulombs flowing in 96 hr	Calculated Al wt loss due to galvanic current flow mg/cm ²	Al wt loss due to local action mg/cm ²
Distilled water	5.2	0.33	17.7	0.085	0.245
	5.5	0.31	11.8	0.055	0.255
	4.2	0.31	14.2	0.065	0.24
	4.3	0.36	20.2	0.095	0.265
Metallic lead	5.15	0.205	11.3	0.055	0.15
	3.0	0.23	12.5	0.065	0.165
	5.4	0.155	11.5	0.055	0.10
PbO	4.1	0.20	29.9	0.14	0.06
	3.1	0.165	18.2	0.085	0.08
	3.0	0.12	12.1	0.060	0.06
Pb ₃ O ₄	5.6	0.09	8.4	0.04	0.05
	4.2	0.09	11.1	0.05	0.04
	4.8	0.06	8.0	0.035	0.025
Basic lead carbonate	5.9	0.095	14.1	0.065	0.030
	3.5	0.05	8.6	0.04	0.01
	4.1	0.05	8.4	0.04	0.01
Lead linoleate	2.4	0.00	0.06	0.00	0.00
	2.3	0.00	0.19	0.00	0.00
	2.4	0.00	0.05	0.00	0.00
Lead ricinoleate	3.4	0.00	0.4	0.00	0.00
	4.6	0.00	0.9	0.00	0.00
Lead laurate	1.2	0.00	0.04	0.00	0.00
	1.5	0.00	0.03	0.00	0.00

Table V also contains the results of experiments on the aluminum/lead couple in lead soap extracts. In this case, little galvanic current flow was observed (Table V) and such minute currents that could be detected were very constant (Fig. 4). The minimum galvanic current flow was observed in lead laurate and the maximum current flow in lead ricinoleate. Weight loss determinations showed that galvanic corrosion of the aluminum and metallic lead deposition were completely prevented in all lead soap solutions despite the high soluble lead content of the extracts and their lower specific resistance. The corrosion rates of the lead cathodes were lower than in distilled water and were lowest in lead laurate extract.

Electrochemical Studies in Lead Soaps

Potential/time curves for initially "film-free" aluminum specimens were determined by first removing the air-formed oxide film by abrading the specimen with fine, high purity aluminum oxide in a high pressure stream of helium and then introducing the specimens immediately into the soap extract which had been presaturated with dissolved air. Alternatively the oxide film may also be removed by similar alumina/helium abrasion under the lead soap extract. In either case the results are identical and are shown in Fig. 5. Bubbling purified helium through the lead linoleate extract did not alter the potential of an aluminum specimen that originally carried an air formed oxide film and shifts the potentials of originally "film-free" specimens in the

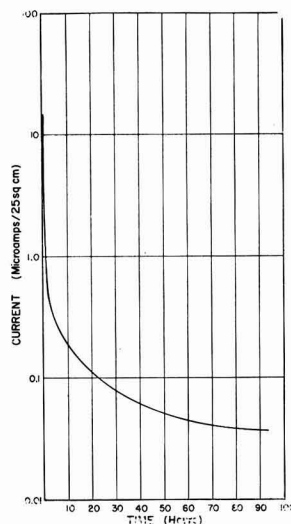


Fig. 4. Current vs. time curve at zero external resistance for the aluminum-lead couple in lead linoleate extract at 25°C.

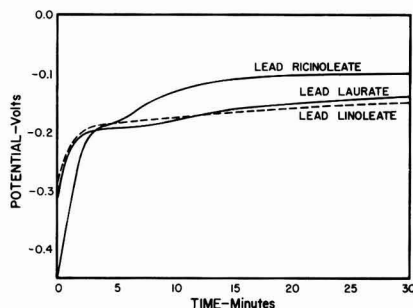


Fig. 5. Potential-time curves for initially "film-free" aluminum in lead soap extracts at 25°C ± 0.05°C. The air-formed oxide film on the aluminum specimens was removed by abrasion with aluminum oxide in a high pressure stream of helium.

soap solutions only slightly in the less noble direction.

Anodic polarization curves for aluminum after 24-hr immersion in lead soap extracts are shown in Fig. 6. The aluminum specimens carried an initial air-formed oxide film before immersion in the solutions. Polarization curves were obtained by applying small constant currents for a fixed 5-min period and recording the potential at that time. The actual values of potential, although not the shape of the curves, are purely arbitrary since the potentials, except at the inflections in the curves, show a steady and reproducible shift with time to more noble potentials. An anodic polarization curve in normal sodium chloride solution is included for comparison.

Discussion

Composition of Inorganic Pigment Extracts

Examination of the pigment extracts by dialysis shows that there is no evidence of appreciable quantities of lead being present in the ionic form. Therefore it is probable that the inorganic pigment extracts contain lead mainly in the form of colloidal

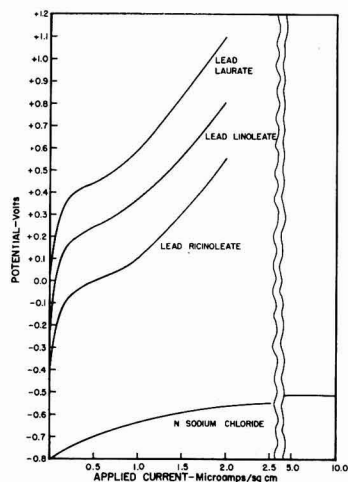


Fig. 6. Anodic polarization curves for aluminum in lead soap extracts and in normal sodium chloride at $25^{\circ} \pm 0.05^{\circ} \text{C}$. The specimens initially carried an oxide film formed in dry air for one day and were immersed in the solutions for 24 hr before the curves were determined.

lead hydroxide as had been found previously for metallic lead extracts (6). On standing, the colloidal lead hydroxide may subsequently age to the more insoluble lead dioxydihydroxide $\text{Pb}_2\text{O}_2(\text{OH})_2$ (12). In the presence of atmospheric carbon dioxide insoluble basic lead carbonate will also be precipitated. The presence of colloidal lead hydroxide together with the other two reaction products evidently gives rise to some considerable buffering action as shown in Fig. 1. The values of reserve alkalinity for the four pigment extracts are approximately proportional to the total quantities of lead in solution. Since the rate of interaction of hydrogen ions with massive and colloidal lead hydroxide must be quite rapid, lead need not be present in the ionic form for buffering of an extract. Because lead is present largely as hydroxide in the massive and/or colloidal forms it is relatively easily removed by filtration (Fig. 1). Filtration through Whatman No. 1 paper removes the lead dioxydihydroxide and basic lead carbonate together with any residual pigment particles. Filtration also removes much colloidal lead hydroxide by adsorption on the paper (13). Consequently the buffering action in metallic lead and litharge extracts is almost destroyed by filtration (Fig. 1).

Corrosion of Aluminum in Inorganic Pigment Extracts

The results contained in Table III demonstrate that the weight losses of all aluminum specimens immersed in inorganic pigment extracts are fairly low. Metallic lead and litharge extracts alone corrode aluminum more rapidly than distilled water. In part, the stimulation of corrosion may be attributed to deposition of metallic lead. However, the higher initial pH values of the lead and litharge extracts must also contribute to the increased corrosion rate, since distilled water which had been con-

tained for eight days in a Pyrex glass beaker corroded aluminum somewhat more rapidly than fresh distilled water (Table III). This effect is probably associated with the slow leaching of sodium silicate from the glass which raises the initial pH value of the solution. That higher initial pH values of lead pigment extracts stimulates corrosion of aluminum is consistent with previous suggestions of Wagner (2).

Evidently in the immersion tests, metallic lead is deposited on the aluminum from lead and litharge extracts. Initially gas bubbles, presumably of hydrogen, form on the lead plate. However the carbon dioxide contained in the extracts reacts rapidly with the finely divided lead deposit, forming relatively insoluble basic lead carbonate. Since basic lead carbonate is not an efficient electronic conductor it should not be capable of acting as a preferential cathode and should not stimulate corrosion of the aluminum. Undoubtedly, in the absence of carbon dioxide, deposited lead would act as a more efficient cathode than in the present experiments. Consequently, under CO_2 -free conditions a greater rate of corrosion of the aluminum might be anticipated in litharge and metallic lead extracts.

The very low rates of corrosion of aluminum in red lead and basic lead carbonate extracts are probably due to a combination of low dissolution rate of the two pigments combined with control of pH within the range 5-6 (Table II). Although the degree of buffering resulting from the very slight dissolution of both compounds is small (Fig. 1) it is sufficient to result in a marked decrease in corrosion rate. Whereas the results in Table III suggest that extracts from red lead, basic lead carbonate, and lead soaps are inhibitive towards aluminum, the subsequent galvanic experiments (Table V) indicate that only lead soaps are truly inhibitive. Therefore the negligible weight losses of aluminum in red lead and basic lead carbonate extracts are probably due to a lengthening of the induction period before corrosion of the aluminum begins. In distilled water the induction period is around 100 hr, and in red lead and basic lead carbonate extracts it must be in excess of 360 hr. Thus the aluminum specimens exhibit the phenomenon of metastable passivity in red lead and basic lead carbonate extracts.

Galvanic Corrosion of the Aluminum-Lead Couple in Inorganic Pigment Extracts

Results of galvanic experiments in which aluminum invariably behaves as the anode are contained in Table V and Fig. 4. For distilled water and the four inorganic pigment extracts, comparison of Tables IV and V shows that the corrosion rate of lead is somewhat stimulated by coupling to aluminum, possibly on account of the increased local pH values at the cathodes. The current flow values in the galvanic cells are generally low and erratic; therefore only the total number of coulombs flowing are recorded. The generally low value of current flow is attributed to the high resistance of the solution and the moderately high value of hydrogen overpotential on lead (14). Initially the current flow appears to be controlled by the specific re-

sistance of the electrolyte (Table II), but after appreciable corrosion of the lead cathodes the current in the cells involving red lead and basic lead carbonate extracts increases to approximately that in the litharge and metallic lead extracts. However, Table V shows that the corrosion rates of aluminum anodes in distilled water, litharge, and metallic lead extracts are generally higher than those in red lead and basic lead carbonate extracts. In the first three solutions calculation from Faraday's Law shows that the weight loss due to the galvanic current flow constitutes only a small portion of the total weight loss of the anode. In red lead and basic lead carbonate extracts a greater proportion of the total aluminum weight loss is due to the galvanic current flow.

When aluminum is coupled to steel in sodium chloride appreciable quantities of aluminum are corroded by local action (9). This was attributed to incomplete suppression of the local cathodes on active aluminum anodes. The weight loss of an aluminum anode due to local action was independent of the area of steel cathode and decreased with decreasing area of the aluminum anode. At equal areas of steel and aluminum about 10% of the total aluminum weight loss was due to local action. In the aluminum-steel couple there was, of course, no question of metallic deposition on the aluminum anode.

It is evident that, in distilled water and in extracts from metallic lead and litharge, as much as 80% of the total weight loss is due to local action, whereas in basic lead carbonate and red lead extracts up to 50% of the total weight loss is due to local action. The much higher local action weight losses of aluminum coupled to lead are clearly due to deposition of metallic lead on the local cathodes on an active aluminum anode. Previous work (15) has demonstrated that the cathodes on aluminum in neutral solutions are small and that high cathodic polarization exists primarily because of the high electronic resistance of the air-formed aluminum oxide film. The high cathodic polarization at local cathodes on aluminum undoubtedly explains why the local action weight losses on aluminum anodes are much less than those on zinc anodes under similar experimental conditions (9). When metallic lead is deposited at these local cathodes local action corrosion is greatly intensified despite the relatively high hydrogen overvoltage on lead (14). An even higher intensification of local action corrosion would be anticipated if a metal of lower hydrogen overpotential such as copper was deposited.

Inhibition of the Corrosion of Aluminum by Lead Soaps

The weight loss experiments (Table III) and galvanic experiments (Table V and Fig. 4) demonstrate that lead linoleate, ricinoleate, and laurate completely inhibit the corrosion of aluminum and the galvanic corrosion of aluminum coupled to lead. The potential of aluminum initially freed from oxide is strongly ennobled (Fig. 5) in these extracts and the anodic polarization curves (Fig. 6) suggest an anodic form of inhibition. The negligible values

of galvanic current in lead soap extracts cannot be attributed to high values of electrolyte resistance since Table II shows that, with the exception of lead ricinoleate, the values of specific resistance are very low. There is no evidence of lead deposition on either aluminum panels or aluminum anodes despite some dissolution of lead from the cathodes in the galvanic experiments.

More recent work by Mayne and Van Rooyen (16) has demonstrated that the water-soluble degradation products of lead linoleate are responsible for inhibition of the corrosion of steel. The effect of oxygen is to increase the apparent solubility of lead linoleate in water from around 0.002 to 0.07%. A saturated solution of lead linoleate prepared in the absence of air does not inhibit the corrosion of steel. Mayne and Van Rooyen identified lead salts of formic acid, azelaic acid, and an unsaturated hydroxyacid derived from pelargonic acid as comprising the primary degradation products of lead linoleate. Small quantities of acetic, propionic, butyric, and suberic acid were also detected. Lead azelate, lead suberate, and lead pelargonate inhibited the corrosion of steel at concentrations of around 35 ppm within the pH range 4.5-6.0. Lead salts were more inhibitive than calcium salts which in turn were more effective than sodium salts.

It would be anticipated that some degradation of lead ricinoleate might occur in the presence of oxygen since ricinoleic acid is also unsaturated. However from the solubility measurements (Table II) it is evident that degradation by oxygen occurs to a lesser extent in lead ricinoleate than in lead linoleate. Since lauric acid is saturated, lead laurate probably does not degrade in a similar manner in the presence of oxygen. Instead its high solubility must be attributed mainly to the shorter carbon chain length.

Inhibition of corrosion of aluminum by lead soaps must be associated with the adsorption of fatty acid anions since small quantities of basic lead carbonate are precipitated when large areas of aluminum are immersed in small volumes of lead soap extracts; similar precipitation is not observed in the absence of an aluminum surface. Because, under most conditions examined in this investigation, the aluminum is covered with an oxide film, adsorption of long chain fatty acid anions must occur on the surface of the oxide. Furthermore it is considered that the oxide film is continuous rather than containing holes or cracks which penetrate to film-free metal. Since adsorption is involved as part of the inhibition process it becomes easier to understand why lead soaps are more effective inhibitors for steel than calcium or sodium soaps (16). The pH value of sodium and calcium soaps will be higher than those of lead soaps (5.1-6.0). In the more alkaline solutions less acid soap will exist and above pH values of 8.0 it should be virtually absent. Since $-\text{COONa}$ has a much greater attraction for water than $-\text{COOH}$ (17) it follows that an acid soap should be more strongly adsorbed at an interface than a neutral soap. The undeniably weaker inhibitive action of lead ricinoleate must therefore be attributed to a combination of somewhat higher pH

and lower concentration (Table II) which makes the anions less readily adsorbed.

If fatty acid anions are adsorbed on oxide covered aluminum as a condensed film, each anion should occupy an area of 20.5 sq Å at zero compression (18). However it is somewhat more likely that laurate would be adsorbed as an expanded film, which, at low compressions, should show an area of around 48 sq Å per ion. Unsaturated acids exhibit larger limiting areas which increase with increasing number of double bonds (20). For instance, elaeostearic acids with three double bonds may exhibit limiting areas of 100 sq Å or more which probably means that the ions are lying almost flat on the surface. If such unsaturated acids are permitted to oxidize, as in the case in this investigation, the adsorbed films still remain coherent with a limiting area of around 125 sq Å per ion. This figure is probably close to the effective areas of adsorbed linoleate and ricinoleate ions or their degradation products.

It follows that if fatty acid anions of large effective areas are adsorbed on an oxide surface, the electric field accelerating aluminum ions through the oxide will be very weak—much weaker than those fields resulting from the adsorption of smaller ions such as the chloride ion. Therefore the corrosion rate of aluminum will be negligible as is in fact observed. Furthermore since considerable energy must be supplied to transport aluminum ions through the oxide film and the adsorbed fatty acid anion layer, the potential of the aluminum is strongly ennobled. Assuming this model of an electrode surface, which is described later in more detail, the actual value of the "corrosion" potential will depend on the thickness and defect structure of the oxide film on the aluminum and on the energy required to transport aluminum ions through the adsorbed fatty acid anion layer. Experiments not reported in this paper demonstrate that lead soaps and their degradation products have no appreciable solvent action on aluminum oxide. Therefore, local intensification of the adsorption field cannot be obtained by local film thinning as is the case with fluoride and chloride ions.

When soaps are adsorbed on initially film-free aluminum, Fig. 5 shows that there is first an ennobled potential which increases with increasing time. This progressive ennoblement is not observed to anything like the same degree in lead linoleate when the aluminum initially carries an oxide film resulting from the exposure to dry air for 24 hr (Fig. 2). The initial ennoblement of potential in the virtual absence of oxide must be due to the high energy required for transport of aluminum ions through the adsorbed layer of fatty acid anions. Evidently this energy is lower when film-free aluminum is immersed in more weakly adsorbed ricinoleate solutions. Clearly the magnitude of this energy is sufficiently high that adsorption must be considered to be the primary cause of inhibition. The subsequent ennoblement of potential with time

shown in Fig. 5 is attributed to the formation of aluminum oxide primarily by discharge of fatty acid anions at anodic areas on the aluminum; the fatty acid anions are probably reduced to complex alkyne or possibly ketonic compounds. The formation of oxide is apparently not dependent on the presence of dissolved oxygen in solution since the extracts may be saturated with helium without markedly altering the corrosion rate or potential. Neither is oxide formation believed to occur uniformly over the surface but instead occurs locally at areas of maximum ionic conductivity, i.e., at the local anodes. Oxide formation by adsorption of dissolved oxygen is probably of some importance in the presence of more weakly adsorbing anions such as ricinoleate. This would serve to explain the higher rate of ennoblement of potential of initially film-free aluminum in lead ricinoleate extract (Fig. 5). Thus the additional formation of aluminum oxide films in these systems is an important secondary cause of inhibition. Work to be reported elsewhere shows that at current densities of 0.5-1.0 $\mu\text{A}/\text{cm}^2$ the formation of oxide by anodic discharge of fatty acid anions proceeds at current efficiencies in the region of 85-92%. Since oxide is not formed in similar experiments in distilled water, its formation in lead soap solutions may be attributed with some certainty to discharge of fatty acid anions. That aluminum oxide is formed by anodic discharge of fatty acid anions at potentials of the order of 0.0 v on the Hydrogen Scale indicates that the oxygens in the RCO^0 groups are in intimate contact with the electrode surface.

Since some small local corrosion currents are presumed to flow initially during the inhibition of corrosion of aluminum in lead soaps, these corrosion currents should result in local thickening of the oxide film by the mechanism outlined above at areas of higher ionic conductivity in any initial oxide film. Since the local currents are presumably very small the current efficiency of aluminum oxide formation may be less than at higher current densities. Local thickening of the oxide film will result in a further decrease in the electric fields accelerating aluminum ions into solution. Thus inhibition must be due to a combination of adsorption and oxide film formation. If aluminum is coupled to a lead cathode in the soap extracts the somewhat higher initial galvanic currents (Fig. 4) are considered to result in the formation of oxide at higher efficiencies on the aluminum anodes. Thus as the oxide film progressively thickens it becomes steadily more difficult to pass further current and so the galvanic current rapidly decays (Fig. 4).

That oxide formation due to very small local corrosion currents may proceed at lowered current efficiencies is supported by the polarization curves in Fig. 6. These all show a marked inflection at a current density of around 0.5 $\mu\text{A}/\text{cm}^2$ which is not observed in similar polarization curves measured in distilled water. It is believed that this inflection represents the occurrence of the Kolbe reaction:



⁴The electric field across the oxide film is proportional to the adsorbed charge density and inversely proportional to the oxide thickness. The charge density is proportional to the anion valence and inversely proportional to the anion area.

⁵In electrolysis of the higher fatty acids olefines rather than paraffins are usually evolved at the anode (22).

which at very low currents may be an alternative reaction to oxide formation in these systems. Latimer (21) quotes a value of -0.16 v for the Standard Electrode Potential of the Kolbe reaction for acetic acid. Since an increase in the carbon chain length should not greatly influence the E_0 value, this reaction must be considered to be thermodynamically possible at the potentials shown in Fig. 6. Attempts were made to hold the potential of aluminum electrodes constant in the region of the inflection in the polarization curves with a view to collecting and, if possible, identifying the olefines which might form on the aluminum anodes. These attempts were invariably unsuccessful since in a short while oxide began to form at higher current efficiencies and the potentials of the aluminum anodes were displaced to much more noble values. Therefore it is concluded that the Kolbe reaction in the lead soap systems probably proceeds with a very high steric hindrance factor. At very low currents of less than $0.5 \mu\text{a}/\text{cm}^2$ it must be considered as an alternative anodic reaction to the formation of aluminum oxide by discharge of soap anions. At extremely low current density the very slow leakage of aluminum ions into solution may also occur to a very limited extent although this is not detectable by microchemical analysis using the alizarin test.

Since inhibition of aluminum by lead soaps is attributed to the adsorption of large radius fatty acid anions on the oxide surface and the resultant weak electric fields accelerating aluminum ions through the oxide film, it follows that the simultaneous adsorption of even a small number of chloride ions of much smaller diameter should produce intense local fields which would effectively transport aluminum ions into solution. Accordingly the inhibition afforded by lead soaps is broken down by the addition even of 5 ppm chloride.

From the more practical standpoint of performance of lead based paints on aluminum, this implies that lead paints, particularly those pigmented with red lead or basic lead carbonate, would be expected to perform well on aluminum provided that chloride (or sulfate) ions were absent at the metal-paint interface. According to the work of Mayne (3) this condition should be realized, at least initially, since organic films can effectively prevent the passage of anions such as chloride and sulfate ions for considerable periods. Therefore, provided that the paint completely covers the aluminum, inhibition of corrosion by virtue of the presence of lead soaps should occur. However once the paint suffers breakdown or if it is discontinuous initially so that chloride or

sulfate ions reach the metal surface, inhibition of corrosion would not be obtained. Particularly, in paints pigmented with litharge, rather severe corrosion of the aluminum should result. It is felt that these two opposing tendencies may be the reason for the very variable performance of aluminum covered with lead pigmented paints.

Acknowledgments

The authors wish to acknowledge some careful experimental work by P. G. Sprang and the many helpful suggestions of J. J. McMullen. They wish to thank A. J. Eickhoff of the National Lead Company for supplying the pigments, W. J. Stewart of Nuodex Products for supplying the lead soaps, and the Kaiser Aluminum & Chemical Corporation for their support of this work and for their permission to publish the results.

Manuscript received April 2, 1957. This paper was prepared for presentation before the Cleveland Meeting, Sept. 30-Oct. 4, 1956.

Any discussion of this paper will appear in a Discussion Section to be published in the December 1958 JOURNAL.

REFERENCES

1. H. Rohrig, *Korr. u. Metallschutz*, **5**, 85 (1929).
2. H. Wagner, *ibid.*, **16**, 329 (1940).
3. J. E. O. Mayne, *Research*, **6**, 278 (1952).
4. K. G. Lewis and U. R. Evans, *J. Soc. Chem. Ind.*, **53**, 25T (1934).
5. J. E. O. Mayne, *ibid.*, **65**, 196 (1946).
6. M. J. Pryor, *This Journal*, **101**, 141 (1953).
7. R. S. Thornhill, *J. Soc. Chem. Ind.*, **65**, 197 (1946).
8. M. J. Pryor and M. Cohen, *This Journal*, **100**, 203 (1953).
9. M. J. Pryor and D. S. Keir, *ibid.*, **104**, 269 (1957).
10. H. H. Uhlig, Editor, "Corrosion Handbook," p. 1081, John Wiley & Sons, Inc., New York (1948).
11. Snell and Snell, "Colorimetric Methods of Analysis," Vol. III, p. 1 (1949).
12. M. Pleissner, *Arb. kaiserl. Gesundh.*, **26**, 398 (1907).
13. J. C. Thresh, *Analyst*, **49**, 124 (1924).
14. J. A. V. Butler, "Electrocapillarity," p. 126, Methuen, London (1940).
15. M. J. Pryor and D. S. Keir, *This Journal*, **102**, 605 (1955).
16. J. E. O. Mayne and D. Van Rooyen, *J. Appl. Chem.*, **4**, 384 (1954).
17. N. K. Adam, "The Physics and Chemistry of Surfaces," p. 128, Oxford (1941).
18. N. K. Adam, *Proc. Roy. Soc.*, **A99**, 336 (1921).
19. N. K. Adam, "The Physics and Chemistry of Surfaces," p. 60, Oxford (1941).
20. E. K. Rideal, *Proc. Roy. Soc.*, **A140**, 253 (1933).
21. W. M. Latimer, "Oxidation Potentials," p. 123, Prentice Hall, New York (1950).
22. G. Kortum and J. O. M. Bockris, "A Textbook of Electrochemistry," Vol. II, p. 457, Elsevier Publishing Co., New York (1951).

Analysis of Films on Copper by Coulometric Reduction

R. H. Lambert and D. J. Trevo

Research Laboratories, Eastman Kodak Company, Rochester, New York

ABSTRACT

A technique is described for coulometric reduction of films on copper and other electropositive metals which utilizes a granular electrode for rapid and thorough pre-electrolysis of electrolyte to remove dissolved oxygen and traces of plateable cations. The sensitivity of the method has been thereby increased, and as little as a quarter of a monolayer of a reducible film can be detected readily. Results are reported for reversible cell potentials, overpotential as a function of pH and current density, and the effect of oxygen in the electrolyte, for the reduction of films of cuprous oxide, and for reduction of hydrogen ions at a copper surface. Data are also reported on the reduction of thick films of cuprous oxide formed at 125°C, and the usefulness of the coulometric method in providing information about the topography of reducible surface films is demonstrated. Other films studied included cuprous sulfide, cupric oxide, and cupric hydrogen phosphate, occurring alone or as mixed films. The effectiveness of various preparatory and rinsing techniques in eliminating phosphate contamination from copper surfaces electropolished in *o*-phosphoric acid has been evaluated. With the most favorable technique, the residual phosphate appears to be much less than a monolayer.

Many important operations involving the surfaces of solids, such as flotation, lithography, boundary lubrication, corrosion inhibition, and adhesion, depend ultimately on the interaction of substances with the outermost layer of atoms or molecules that constitutes the surface of the solid. In the case of certain metals, information about both the nature and the amount of inorganic films which may be present initially can often be obtained by controlled electrochemical reduction of the films *in situ*. The early experiments of Evans and Bannister (1), in which iodide films on silver foil were reduced electrochemically at constant potential, were followed by the work of Evans and Miley (2) on the reduction at constant current of oxide films on Cu and Fe. In subsequent work, the constant-current method has been preferred, and the technique has been considerably refined.

In theory, the method is capable of readily detecting and measuring very thin films, even fractions of a monolayer. When such sensitivity is desired, the problem is to decrease the concentrations of plateable cations and dissolved oxygen to sufficiently low levels, since these substances also compete for the reduction current. Campbell and Thomas (3) pre-boiled the 0.1N KCl electrolyte, bubbled N₂ through the solution before an experiment, and passed N₂ over the solution during an experiment. Prior to use, the N₂ was passed over hot reduced Cu.

Early experiments conducted here indicated that with such techniques the sensitivity was still limited by dissolved oxygen. To lower the oxygen level even farther, the aqueous solution was pre-electrolyzed by a modification of the pre-electrolysis technique which has found favor in studies of hydrogen overpotential (4). The present paper describes an apparatus for rapid and thorough pre-electrolysis of

electrolyte by circulation of the liquid through the interstices in a large granular electrode. Films on Cu of the order of one Å have been detected, and reduction potentials observed for a variety of films agreed with theory in most instances.

Experimental

Apparatus

The apparatus consists of two interconnected cells, one for pre-electrolytic treatment of the solution, and the other for reduction of the film on a specimen. The electrical circuit is essentially the same for each cell, constant current being obtained from a 90-v dry-cell supply by placing the reduction cell in series with a large resistor. With suitable switching to change the size of the large resistor, the current may readily be varied in the range 0.008-1000 μ a, and is measured with a microammeter and suitable shunts. A Ag-AgCl reference electrode with a Luggin capillary is coupled with the cathode to provide a potential signal which is amplified by an electrometer,¹ the output of which operates a recorder.² The recorder is connected to the output of the electrometer by a potential divider in parallel with an appropriate condenser-resistor combination which slightly damps the response of the recorder. A plot of potential as a function of time is thereby obtained without drawing appreciable current from the electrode pair. In parallel with the electrometer, a pH meter is also included to provide more accurate values of the potential when desired. The experimental points indicated in all of the figures were obtained in this way. Shielded conductors are used for all connections involved in

¹ Keithley, Model 210, input impedance 10¹⁴ ohms across a capacitance of 6 μ f.

² Bristol, range 0-5 mv d.c., rate of chart travel 3/4 in./min.

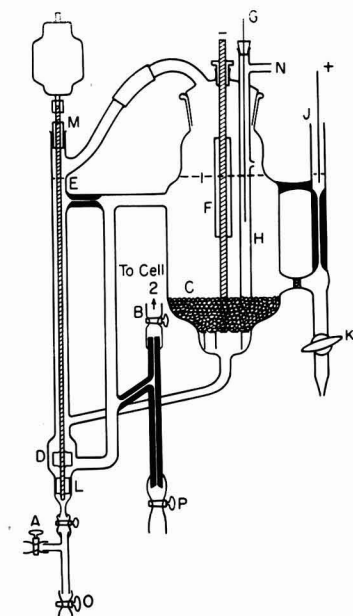


Fig. 1. Cell 1 for pre-electrolysis of electrolyte

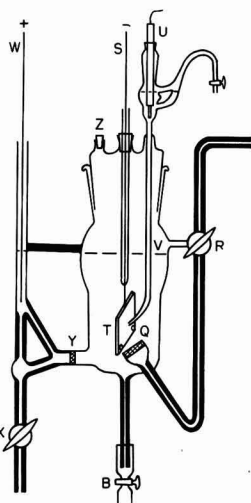


Fig. 2. Cell for reduction of films on metal surfaces

measuring or recording the potential, and the shielding is grounded.

Cell 1, shown in Fig. 1, and Cell 2, shown in Fig. 2, are similar in principle in that Cu is the cathode, and the anode and cathode sections are separated by a fritted-glass diaphragm. Cell 1 receives its solution at A from a 4-liter supply bottle through which hydrogen has been vigorously bubbled for a considerable time. After pre-electrolysis in Cell 1, a portion of the solution is passed to Cell 2 through the Tygon connection at B.

Cathode C of Cell 1 consists of a 3.2-mm Cu rod embedded in a large mass of Cu granules (Merck reagent). These granules have an average diameter

of 2 mm and all are retained on a No. 18 sieve. Their total weight is 713 g, and the apparent surface area is estimated to be 1300 cm². The granules are supported on a Cu tripod, the upper plate of which is a Cu disk having many perforations. When the glass pump, D, is energized, the solution flows into the cathode chamber near the top, down through the granular electrode and Cu disk, and back to the pump in a cyclic path, thus making intimate contact with the large surface of the electrode. A small fraction of the flow passes through the capillary, E, thereby maintaining positive circulation of liquid in all parts of the cell. Around the Cu rod which forms part of the cathode a tightly fitting Teflon sleeve, F, eliminates any spurious effect which might arise at the gas-liquid interface. The Ag-AgCl reference electrode, G, passes through a cork into a glass tube, H, which extends into the granular Cu mass and has an orifice (0.05 cm in diameter) at its extremity, thus acting as a Luggin bridge. A hole in tube H just above the catholyte surface, I, permits entry of hydrogen or nitrogen gas, thereby maintaining an inert atmosphere over the solution. Anode J is at Pt wire. Diffusion of electrically formed Cl₂ from anode to cathode compartments is hindered by use of a fritted-glass disk and capillary tubing. Drainage of the anode compartment is effected at K. The pump shaft is supported by Teflon bearings at L and M, a slot in the upper bearing allowing for escape of gas entering at N. The volume of catholyte is about 800 ml. When the electrolyte has been sufficiently freed of oxygen and plateable cations, it is forced from Cell 1 to Cell 2 by suitably adjusting the speed of the pump and opening the clamp at B. The electrolyte may be drained from Cell 1 at O, and samples for pH determinations are obtained at P.

In Cell 2, Fig. 2, agitation may be secured by passing hydrogen or nitrogen through the solution in fine bubbles formed by the fritted-glass disk, Q. If agitation is not desired, the gas is passed over the solution by adjustment of the three-way stopcock, R. The Pt wire, S, is led through a sealed glass tube to a Pt saddle, T, which holds the Cu specimen. The Ag-AgCl electrode, U, is mounted in a Teflon sleeve, and the electrolyte is drawn up by suction through the Luggin capillary, V. The anode compartment with Pt anode, W, is attached with capillary tubing to allow for ready elimination of bubbles and for draining through a stopcock, X. A fritted-glass diaphragm, Y, separates the two compartments. Gas entering the cell through stopcock R escapes through a groove in the cork, Z. The volume of the cathode compartment is about 80 ml. Screw clamps on Tygon tubing are used wherever contamination of electrolyte by stopcock grease might occur, and glass stopcocks are used to control drainage from anode compartments and to regulate gas flow.

Method of Operation

A 0.1N KCl solution is prepared in a 4-liter bottle from reagent-grade KCl and conductivity water, and is bubbled with H₂ for 1 hr. Bubbles are formed by a submerged, medium-porosity, fritted-glass disk. A portion of electrolyte is then allowed to

enter Cell 1 until the level is at I (Fig. 1), and a current of about 1 ma is applied while electrolyte is circulated at a moderate rate. The observed cathode potential measured against the reference electrode is about -0.25 v, corresponding to reduction of oxide, and is substantially constant for 15-30 min, after which it rapidly changes to -1.0 to -1.2 v, corresponding to reduction of hydrogen ions. By this time, most of the oxygen has been removed from the electrolyte, but traces are still present. Some measure of the amount remaining can be obtained by reducing successively the current in the circuit to determine the value at which the potential returns to about -0.25 v. This change occurs when the rate of arrival at the electrode of oxygen from the electrolyte is just equal to the rate of reduction of that oxygen (or oxide) by the imposed current. To further decrease the oxygen level in the electrolyte, reduction is continued with a moderate flow of electrolyte for approximately 1 hr, the current being just sufficient to reduce the oxygen as fast as it arrives. By this time, the oxygen content is usually sufficiently low so that the potential corresponding to evolution of hydrogen in Cell 1 does not move in the more positive direction by more than 25 mv in 30 min with a current of $20 \mu\text{a}$ through the cell. In the present work, pre-electrolysis is arbitrarily considered sufficient when such a condition is attained, and, if done correctly, the pH of the resulting electrolyte will not be above 8.5.

During pre-electrolysis of the solution in Cell 1, the Cu specimen, usually a 1-in. square of 16-gauge metal,³ is placed in position in Cell 2 and hydrogen is passed through the cell prior to introduction of pre-electrolyzed solution from Cell 1. The film on a specimen is usually reduced without agitation, and hydrogen is passed over the surface of the electrolyte during reduction to prevent entry of oxygen from the air. The inflection point in the potential-time curve is taken as the endpoint, and the film thickness is calculated by the relation,

$$T = \frac{100itM}{aNFd} \quad (I)$$

where T is the thickness in \AA , i is the current in microamp, t is the time in sec, M is the formula weight, a is the area in cm^2 , N is the number of faradays required to reduce one gram formula weight, F is the faraday value in coulombs, and d is the density of the film in g/cm^3 . The pH of the electrolyte is measured just before and just after many of the runs, and it is customary to discard the electrolyte before the pH reaches 11.0. Most of the work reported here was done in the pH range of 9.0-10.5, and the preferred current density for reduction of films in the thickness range of 20-40 \AA was $2.5 \mu\text{a/cm}^2$. The time required for the actual reduction was 15-25 min.

Overpotential and pH

Potential data presented below are compared with the reversible values calculated from data on

free energy of formation compiled by Latimer (5), using the sign convention of Glasstone (6), a value of 0.770 for the activity coefficient of 0.1N KCl, and equating activity and concentration for hydrogen ions and hydroxyl ions. This procedure leads to the following relations for the reversible cathode potential with respect to the Ag-AgCl electrode in 0.1N KCl:

$$\text{Cu}_2\text{O} \rightarrow \text{Cu} \quad E = 0.181 - 0.0591 \text{ pH} \quad (II)$$

$$\text{H}^+ \rightarrow \frac{1}{2} \text{H}_2 \quad E = -0.288 - 0.0591 \text{ pH} \quad (III)$$

$$\text{CuO} \rightarrow \text{Cu} \quad E = 0.281 - 0.0591 \text{ pH} \quad (IV)$$

$$\text{CuO} \rightarrow \text{Cu}_2\text{O} \quad E = 0.381 - 0.0591 \text{ pH} \quad (V)$$

The change in potential with respect to current density when cuprous ion is being reduced to Cu is shown for two values of pH in Fig. 3. The curves approach the theoretical reversible values, calcu-

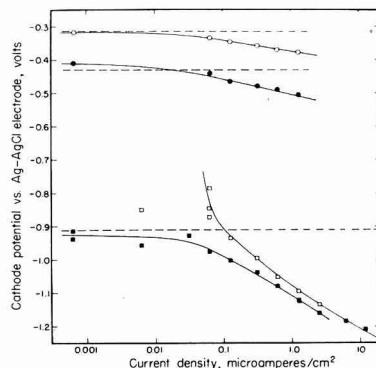


Fig. 3. Observed and calculated values of the potential for reduction of Cu_2O at low current density, and for reduction of hydrogen ions at a Cu surface: open circle, reduction of oxide at pH = 8.50; closed circle, reduction of oxide at pH = 10.45; open square, reduction of hydrogen ions at pH = 10.5, with hydrogen bubbling; closed square, reduction of hydrogen ions at pH = 10.5, with no bubbling; ——— observed; — — — reversible.

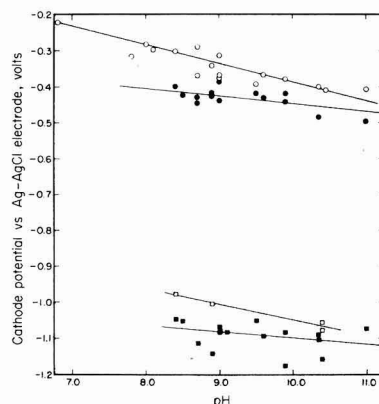


Fig. 4. Variation with pH of the potential for Cu_2O reduction and for reduction of hydrogen ions at a Cu surface for various values of current density: open circle, oxide reduction at $0.00063 \mu\text{a/cm}^2$; closed circle, oxide reduction at $2.51 \mu\text{a/cm}^2$; open square, hydrogen ion reduction at $0.63 \mu\text{a/cm}^2$; closed square, hydrogen ion reduction at $2.51 \mu\text{a/cm}^2$.

³ Photoengravers' copper, Edes Manufacturing Co., Plymouth, Mass.

lated by Eq. (II), as the current density becomes small. The deviation at higher current densities may be considered to be due to the "copper overpotential" which is analogous to the more familiar hydrogen overpotential. The variation of potential with current density for reduction of hydrogen ions at a Cu surface is also shown in Fig. 3 for a pH of 10.5. As for the cuprous ion, the approach to the reversible value is satisfactory at very low values of the current density. Bubbling hydrogen through the liquid during reduction is believed to reduce concentration polarization and thereby to shift the cathode potential to more positive values. At a current density of about $0.1 \mu\text{a}/\text{cm}^2$, bubbling had increased the rate of arrival of dissolved oxygen at the cathode to such a level that a substantial part of the current was used in reducing this oxygen. At even lower current density values, the rate of arrival of oxygen at the cathode in the agitated electrolyte exceeded that which could be taken care of by the available current, and the potential became much less negative. This effect is believed to be due not to oxygen transferred from the hydrogen bubbles but to the increased rate of arrival at the cathode of residual oxygen already present in the electrolyte. Once the oxygen content of the electrolyte is quite low, tank hydrogen may be bubbled vigorously through the solution for 2 hr without producing any measurable oxide film on the specimen, the sensitivity of measurement being about 0.5Å.

Some idea of the effect of pH on the observed potentials for reduction of cuprous oxide films and for reduction of hydrogen ions was obtained by plotting the data obtained from many months of operation; Fig. 4 is typical of the results obtained. Considerable scatter was observed, and the number of observations was insufficient, at many values of current density, to provide highly significant correlations. For very low values of current density, however, the slopes of the lines of best fit on a pH-potential plot were in fair agreement with theory (-0.0591), but, at normal values of current density, the lines were more nearly horizontal. Measurements on a single specimen were consistent within themselves, but pronounced scatter was often observed when different specimens were compared. This suggests that subtle variations may occur from

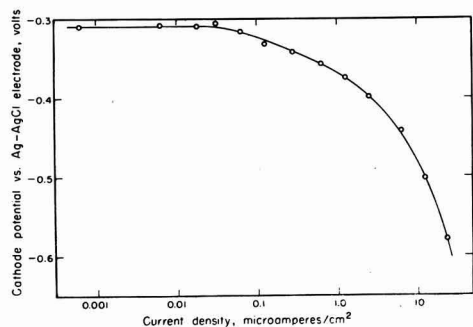


Fig. 5. Variation of reduction potential with current density for a thick Cu_2O film at a pH of 9.6.

one run to the next in the nature of the surface, residual stresses in surface crystals, the real surface area, the number and nature of any adsorbed molecules (7), and the topography of the surface film.

By subtracting the calculated reversible values from particular values taken from the lines of best fit, values of overpotential were obtained for the two electrode processes as a function of pH, and are given in Table I. It is observed that, for both electrode processes, the values of overpotential decrease with increasing pH at about the same rate. The overpotential for oxide reduction is much lower than that for reduction of hydrogen ions, an observation which suggests a smaller potential energy barrier in the case of oxide reduction. A slight extrapolation of the data for reduction of cuprous oxide indicates that the overpotential would become zero at $\text{pH} = 11.0$. In a discussion of Cu and its oxides by Pourbaix (8), a stability diagram is presented which indicates that the metal is passivated and Cu_2O is the stable phase in the pH range 8.0-11.5. For more alkaline solutions, the diagram indicates that Cu_2O films are not stable, and should dissolve spontaneously, in which case the overpotential would be zero. In a qualitative way, the authors' measurements of overpotential are in accord with this prediction.

In the present study, many measurements of oxide thickness on both abraded and electropolished surfaces have been made by the coulometric technique, but little difference in thickness of oxide has been observed as a result of differences in the method of surface preparation. It appears that a protective Cu_2O film of 20-40Å is formed very rapidly on exposure to air, tank hydrogen, or tank nitrogen, and the particular thickness seems to depend more on rinsing and drying conditions than on the method of surface preparation.

Thick Oxide Films on Copper and Topography of the Oxide Layer

It is generally agreed that only Cu_2O is formed by aerial oxidation of Cu below 150°C , although the sensitivity limits of the diffraction techniques normally used do not exclude the possible existence of a few percent of CuO . Thick oxide films on Cu in the range of 200-400Å were prepared by storing cleaned specimens in air at 125°C for several hours or days. The films were then reduced coulometrically. With a very low current density, $6.3 \times 10^{-4} \mu\text{a}/\text{cm}^2$, these specimens always showed an initial potential in the range of -0.13 to -0.20 v, substantially less negative than that observed for much

Table I. Overpotential as a function of pH at a current density of $2.51 \mu\text{a}/\text{cm}^2$

Electrode process	Overpotential, volts			
	pH = 8.5	pH = 9.0	pH = 10.0	pH = 10.5
Reduction of Cu_2O to Cu	-0.095	-0.077	-0.038	-0.018
Reduction of hydrogen ions at a Cu surface	-0.288	-0.265	-0.219	-0.198

thinner films (-0.30 to -0.35 v). With time, the potential became more negative, and finally became comparable to that of thin films of Cu_2O . The rate of change of potential with time was not accelerated by changing the current density over a wide range or by stirring the electrolyte.

As a tentative explanation for these phenomena, it is pointed out that the initial potential approximates that for reduction of CuO to Cu_2O , as shown by Eq. (V), and may therefore indicate traces of CuO . When immersed in the electrolyte, a change in the film occurs which is not dependent on the rate of charge transfer and which results in the attainment of the normal potential for a Cu_2O film after sufficient time has elapsed. If the initial potential is actually due to traces of CuO , this oxide may be converted slowly to Cu_2O , or may perhaps be dissolved on standing in the KCl solution.

The phenomena observed during reduction of thick films and the uncertainty of the speculation concerning the origin of these effects led the authors to present the data on thick films separately from those for thin films formed at room temperature, the typical variation of reduction potential with current density being shown in Fig. 5 for thick films formed at 125°C .

Because the reduction potential is strongly dependent on current density in the range of current density normally used, considerable information concerning the topography or uniformity of distribution of a film over the surface of the metal can be obtained from the reduction curve. Very thin films, having a thickness of the order of 20\AA , might be expected to be quite uniform in thickness, and, on reduction, such films yield a rather flat plateau, followed by a rapid change in potential when the film is exhausted. In this case, the transition from one plateau to the next probably requires the period of time needed for the reduction of the last monolayer of the almost exhausted component in the film. To prove that the shape of the curve in the transition region is not controlled by some other process, such as diffusion, a specimen having about the usual thickness of oxide was reduced at half the usual current density. The transition occupied twice as much time as previously, and, when the curve was replotted with the abscissa compressed by a

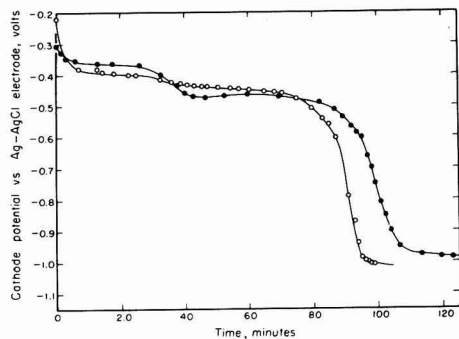


Fig. 6. Effect of variations in topography of Cu_2O films on the reduction curves: open circle, thick film on 50% of area, $2.53 \mu\text{A}/\text{cm}^2$; closed circle, thick film on 10% of area, $1.29 \mu\text{A}/\text{cm}^2$.

factor of two, the shape of the curve was identical with that obtained by reducing at the higher current density. If one relates the change in potential with current density, shown in Fig. 5, to the shape of the curve in the transition region for a specimen having a thin film of Cu_2O , it is evident that 90% or more of the last monolayer of Cu_2O has been reduced when the potential-time curve reaches the inflection point.

A thick film, on the other hand, is often less uniform in thickness over the area of the specimen. This could conceivably result in a gradual increase in potential along the plateau, as some areas are virtually freed of film while others still have a considerable coating. When the film is almost gone, its persistence in local areas which were thicker originally might tend to produce a more gradual change in potential in the transition region. The validity of these ideas was confirmed by reducing specimens with nonuniform film distributions on which interference colors varied over the area. A further check was provided by reduction of specimens which carried both a thick and a thin film on adjacent areas of the same specimen. One of these was prepared by forming a thick oxide deposit at 125°C , then dissolving the oxide on half the specimen by dipping in $0.02N$ HCl , followed by rapid rinsing in water and in alcohol. When dry, the specimen was thereby covered over half the area with a thick oxide deposit and the remainder had only a thin film. In another case, nine-tenths of the thick film was dissolved in the dilute acid. Reduction potential curves for these specimens are shown in Fig. 6, and, in each case, one observes two plateaus arising from the fact that the effective current density changes rather abruptly when the thin film becomes exhausted.

When a thick film is prepared by a 5-min aerial oxidation at 500°C , only cupric oxide is formed, according to Dixit and Agashe (9). Such a film gave potentials generally about 0.09 v more negative than were obtained for thick films of cuprous oxide, although Eqs. (II) and (IV) indicate a potential 0.10 v more positive, as the limiting case of zero current is approached. The present experiments do not agree well with those of Miley (10), who observed for reduction of CuO a potential 0.315 v more negative than that required for reduction of Cu_2O .

Other Films on Copper

Measurement of mixed sulfide and oxide films on Cu yielded results similar to those of Campbell and Thomas (3), the sulfide being formed by dipping a pumiced specimen in H_2S water. When reduced at a current density of $2.51 \mu\text{A}/\text{cm}^2$, the first plateau occurred at -0.394 v, a reasonable value for Cu_2O reduction, and the second plateau occurred at -0.956 v, a value believed to correspond to the reduction of Cu_2S to Cu . The mixed-film experiment demonstrates that many reducible films can be analyzed by this technique if they are relatively insoluble in the electrolyte, and if the reduction occurs at a potential less negative than the evolution of hydrogen or other limiting reaction.

The nature of electropolished surfaces is of considerable interest in other studies currently being

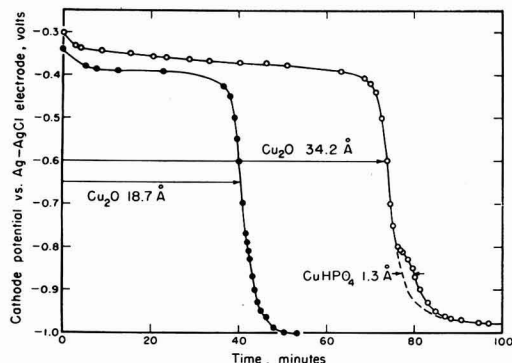


Fig. 7. Reduction at $0.62 \mu\text{a}/\text{cm}^2$ of the film on electropolished Cu rinsed in 10% *o*-phosphoric acid, and for the same specimen after reoxidation in tank nitrogen: open circle, pH = 8.5; closed circle, pH = 9.0.

conducted here. When a smooth Cu specimen was prepared by electropolishing in an aqueous solution containing 63% by weight of *o*-phosphoric acid, followed by thorough rinsing in redistilled water and ethanol before drying, two plateaus were observed in the reduction curve. The first at -0.413 v probably indicated Cu_2O , while the second at -0.792 v is believed due to a phosphate salt insolubilized during rinsing of the electropolished specimen. [Following Walton (11), it is assumed that the salt is cupric hydrogen phosphate.] Allen (12) has reported similar results but claims that the phosphate film can be removed completely by a rinse with 10% *o*-phosphoric acid, followed by a thorough rinse with water. Our reduction experiments, which are believed to be more sensitive than Allen's, have not verified the absolute removal of phosphate by this rinsing technique. It seemed likely that the phosphate salt might reside largely in pits or irregularities in the surface, and these were minimized by polishing in a vertical plane and by filing the lower edge of the specimen to a knife-edge before polishing to eliminate attachment of bubbles and subsequent pitting. This technique reduced the estimated amount of phosphate to about 1.3\AA , as shown in the upper curve of Fig. 7. [Using a radioactive tracer technique, Simpson and Hackerman (13) recently studied the elimination of phosphate contamination from electropolished Cu surfaces, but the 10% phosphoric acid rinse was not employed in their work.]

After reduction, the specimen was lifted out of the electrolyte and left for three days in nitrogen

gas above the solution. The surface film was then reduced again, and the data provide the lower curve of Fig. 7, indicating complete absence of the phosphate salt. If the reduced specimen was allowed to remain in the electrolyte in which the phosphate salt had been reduced, no re-formation of a phosphate film on the specimen was observed on subsequent reduction. After reduction of a sulfide film, however, gradual re-formation of the sulfide film was observed when the reduced specimen was left in the electrolyte. This difference in behavior may be due to a difference in the solubility product constants of the sulfide and phosphate salts.

Films on Electronegative Metals

The results just described demonstrate that coulometric reduction is a valuable tool for the study of reducible films on Cu, the sensitivity being sufficient for measurement of fractional monolayers. Application of the method to electronegative metals in aqueous solution is precluded, however, by the evolution of hydrogen at potentials less negative than are necessary for reduction of surface films. It was hoped that a nonaqueous system could be found which would avoid this difficulty without introducing other problems, but preliminary experiments have not led to the discovery of such a system.

Manuscript received Feb. 19, 1957. Communication No. 1882 from the Kodak Research Laboratories.

Any discussion of this paper will appear in a Discussion Section to be published in the December 1958 JOURNAL.

REFERENCES

1. U. R. Evans and L. C. Bannister, *Proc. Roy. Soc. (London)*, **A125**, 370 (1929).
2. U. R. Evans and H. A. Miley, *Nature*, **139**, 283 (1937).
3. W. E. Campbell and U. B. Thomas, *Trans. Electrochem. Soc.*, **76**, 303 (1939).
4. J. O'M. Bockris, *Chem. Revs.*, **43**, 544 (1948).
5. W. M. Latimer, "Oxidation Potentials," 2nd ed., Prentice-Hall Inc., New York (1952).
6. S. Glasstone, "Textbook of Physical Chemistry," 2nd ed., D. Van Nostrand Co., New York (1946).
7. R. S. Hansen and B. H. Clappitt, *J. Phys. Chem.*, **58**, 908 (1954).
8. M. J. N. Pourbaix, "Thermodynamics of Dilute Aqueous Solutions," p. 55, Edward Arnold and Co., London (1949).
9. K. R. Dixit and V. V. Agashe, *Z. Naturforsch.*, **10a**, 152 (1955).
10. H. A. Miley, *J. Am. Chem. Soc.*, **59**, 2626 (1937).
11. H. F. Walton, *This Journal*, **97**, 219 (1950).
12. J. A. Allen, *Trans. Faraday Soc.*, **48**, 273 (1952).
13. N. H. Simpson and N. Hackerman, *This Journal*, **102**, 660 (1955).

June 1958 Discussion Section

A Discussion Section, covering papers published in the July-December 1957 JOURNALS, is scheduled for publication in the June 1958 issue. Any discussion which did not reach the Editor in time for inclusion in the December 1957 Discussion Section will be included in the June 1958 issue.

Those who plan to contribute remarks for this Discussion Section should submit their comments or questions in triplicate to the Managing Editor of the JOURNAL, 1860 Broadway, New York 23, N. Y., not later than March 1, 1958. All discussion will be forwarded to the author, or authors, for reply before being printed in the JOURNAL.

Acid Copper Plating on Aluminum

J. T. N. Atkinson

Naval Research Establishment, Dartmouth, Nova Scotia

ABSTRACT

A method for plating copper on aluminum and its alloys is recorded that eliminates the need for special pretreatments, zincate dips, etc. A moderately acid copper solution containing oxalates, pyrophosphates, ammonia, and triethylamine has been found to be most effective. Rack and barrel plated work can be controlled to give adhesion better than the ultimate properties of tin-lead solder; continuously plated wire has been produced on a small scale.

Following an initial observation that, when a Cu-Al couple is immersed in glacial acetic acid, the Cu is attacked preferentially, an attempt was made to apply this phenomenon to useful systems for plating Cu on Al. This seemed to open the possibility of using strongly acid solutions for the direct electrodeposition of Cu or other metals on Al, in marked contrast to the normal practice of using neutral or nearly neutral solutions for the electroplating step (1, 2), except for the method of Burgess and Hambuechen (3).

Their method depends on mechanical keying for adhesion, but removes final traces of the Al_2O_3 film by cathodic action in the mildly acid zinc sulfate plating solution prescribed. Otherwise there has been an implicit assumption (4) that electroplating on Al from an acid solution is impossible. Only within the last few months has a reference to an acid Cu solution for direct plating on aluminum been published (5), although this process requires pretreatment steps under vacuum and its practical utility is unknown.

A review of plating various metals from acid solutions led to an interesting rediscovery of the Gauduin (6) process. Unfortunately the original patent was as vague as the brief references found, and merely established that the bath consisted of ammonium oxalate, copper oxalate, and oxalic acid and should be operated at from 40° to 60°C.

Although heating large plating tanks was difficult, the process was used for Cu plating some cast iron statuary for the Paris exhibition of 1878, the largest pieces being two cast iron bulls weighing 1600 kg each. Later, attempts to heat the plating tanks were apparently abandoned, and the process was modified to operate at room temperature but at lower current density.

This modification appears to have ruined the Gauduin process. It was not revived even when, around the turn of the century, practical methods of heating plating tanks paved the way for general acceptance of cyanide copper plating. It is indeed strange that there has been no re-examination of the Gauduin process, as there has been a good deal of interest in replacing cyanide baths by less toxic formulations of comparable usefulness, particularly in view of the technical excellence of the process in its early stages.

Once it was established here experimentally that even a moderate Cu-Al adhesion could result from direct plating methods, effort was concentrated on such methods. These would have considerable practical as well as theoretical interest. Removal of oxide film concurrently with the deposition of another metal such as Cu from a plating bath of otherwise normal characteristics should provide an elegant solution of the oxide film difficulties previously associated with plating on Al. Elimination of acid treatment and zincate immersion steps would naturally appeal to the practical plater.

Experimental Work

Experiments showed that Al did not corrode rapidly in a wide variety of more or less conventional acid Cu plating solutions and attempts were made to use these to plate on Al. However, poor adhesion resulted from attempts to plate from standard formulations. Addition of an agent designed to increase corrosion of Al by the electrolyte resulted, in certain cases, in the marked improvement of the adhesion of the plate to the basis metal. All of these tests were conducted using commercially pure Al that had been solvent or vapor cleaned, and degreased in a conventional phosphate-carbonate cleaner.

The initial criterion of adhesion was an 180° bending test without a mandrel. The practical criterion (in spite of objections to simple testing procedure) of Ehrhardt and Guthrie (8) was later adopted. That is, an adequate test for plated Al is the mechanical destruction of a soldered joint without causing the plate to part from the basis metal. Essentially, the adhesion in shear was measured via a soldered joint of 1/16 in.² area; the final refined version of this test has been published elsewhere (9). Much of the work reported in this paper preceded this development, and adhesion is therefore characterized as good, intermediate, and poor when it exceeds 5000 psi, is between 2000 and 5000 psi, and is less than 2000 psi, respectively. Confirmatory tests of samples considered to have good adhesion showed that no plating failure by repeated bending could be detected. In the case of some such samples annealed at 350°C after plating, metallographic examination showed extensive formation of intermetallic compound at the interface.

Table I. Results of initial plating trials

Metal plated	Other cations	Anions present	Other additions	Adhesion	Remarks
Cu	—	Acetate	Various	Poor	Solubility of Cu too low
Cu	—	Citrate, nitrate	—	Poor-inter.	—
Cu	—	Citrate, nitrate, fluoride	—	Inter.	—
Cu	Ammonium	Citrate, nitrate, fluoride	—	Inter.	—
Cu	—	Citrate, sulfate, fluoride	—	Inter.	—
Cu	—	Sulfate	—	Poor	—
Cu	—	Sulfate	Various*	Poor-inter.	—
Cu	Ammonium	Oxalate	—	Inter.	Gauduin's bath—pH 5
Cu	Ammonium	Oxalate	Various†	Inter.-good	Approx. pH 5

* To increase solubility of Al_2O_3 film; complexing agents such as aluminon and corrodents such as grapefruit juice were helpful.

† See Table II.

Results of initial experiments with Cu plating are consolidated into Table I. The pH of the plating solutions, except where noted, was less than 2, and often less than 1. Similar tests with Zn, Cd, Ni, Sn, Pb, and Ag were generally less promising. In the case of Pb and Ag there was serious corrosion of the Al cathode.

Development of Solutions Based on Oxalates

Although considerable effort was directed toward development of plating solutions related to the conventional acid sulfate bath and the systems including citric acid, only in the case of the oxalate solutions were the best results obtainable. Since the published information on Gauduin's bath was so meager, work had to start with solubility studies. The preferred bath composition consisted of 20 g of cupric oxide dissolved in a hot solution of 100 g of ammonium oxalate crystals and 60 g of oxalic acid crystals, the final volume being made up to 1 liter. This bath gives a fully adherent immersion deposit on steel in addition to giving good matt electrodeposits at about 2 amp/dm² at 50°–60°C. By modern standards the rate of deposition is too low and the anode corrosion inferior. For direct plating on Al the adhesion was as good as the best obtained in alternative systems referred to in Table I.

Limitations of the Gauduin bath appeared to be twofold: low solubility of ammonium oxalate and/or a Cu complex; insufficient reactivity with aluminum

oxide to develop good adhesion. Modifications were made to overcome these defects, and are summarized in Table II.

Without question, the most effective of the initial modifications was the replacement of all the ammonium oxalate in the original formulation by a like amount of ammonium pyrophosphate. This definitely overcomes the solubility limitations noted earlier and also puts the adhesion on Al consistently in the good range for the relatively thin deposits employed. Anode corrosion was still somewhat inferior, however, so attempts were made to remedy this.

Since the adhesion of Cu to Al fell off as pH was increased, this method of improving anode corrosion was not acceptable. The influence of a large number of amines on anode corrosion was then studied, and it was found that those with soluble Cu complexes were generally helpful in promoting adhesion. However, only the tertiary alkyl amines were stable to extended electrolysis, and triethylamine appeared to be the preferred addition.

The solution composition which has been tested most extensively is: ammonium pyrophosphate, 100 g; oxalic acid crystals, 60 g; copper oxide, 20 g; triethylamine, 50 g; water to make 1 liter; initial pH, 5.6–5.8.

The ammonium pyrophosphate was prepared by reaction of ammonia and pyrophosphoric acid at or near 0°C to avoid excessive hydrolysis. In view of this complication, and the difficulty of dissolving copper oxide, the use of copper pyrophosphate as starting material may be superior, particularly for large-scale use.

Details of Plating Procedure

The bulk of the work with this solution has been performed on rack plated work, in solution batches ranging up to 55 gal and using the same batch of solution for periods of up to the order of months. Barrel plated work has been, so far as can be judged with the limited adhesion test used, fully satisfactory, while wire plated in the low speed continuous wire plating device developed intermediate adhesion only.

Typical procedure is as follows: the work, following vapor degreasing, is cleaned by immersion for

Table II. Modifications to Gauduin bath

Anion replacing or added to oxalate:	Other addition	Adhesion	Comments
Sulfate, nitrate, Citrate, acetate, Tartrate, malate, Salicylate, sulfo Salicylate, or succinate	—	Not improved	
Boric acid	—	Slight improvement	10 g/l
Fluoride	—	Slight improvement	0.2 g/l
	Aluminon	Slight improvement	Up to limit of solubility
Pyrophosphate	—	Major improvement	

about 45 sec in a solution containing 3% each, by weight, of trisodium phosphate and soda ash, at a temperature of about 65°C. The time of immersion cleaning is varied slightly according to the alloy used, being greater for the more corrosion resistant alloys. The work is then rinsed and immersed in the plating solution, with the plating current being applied at up to a minute or two after the immersion of the work. Plating then proceeds at 2.7 amp/dm² at a temperature of 60°C with cathode bar agitation at 90 in./min. Under these conditions, deposits of good adhesion, according to the solder adhesion test, can be obtained at least up to 0.0005 in. in thickness.

The step requiring closest control in the above sequence appears to be the immersion cleaning step. This step is not drastic enough to remove any appreciable contamination, yet adhesion can suffer from overcleaning. Wide variations in solution composition seem to be acceptable for the plating bath, and satisfactory results have been obtained with compositions running from one half to three times that of the example given. Too high a ratio of pyrophosphate to Cu appears to be undesirable, as it appears to lead to more rapid hydrolysis of the pyrophosphate, but otherwise there seems to be considerable leeway in solution formulation. As would be expected, the more concentrated solutions give good plating at higher current densities and temperatures.

An interesting series of observations is connected with the relation between plating adhesion, plating conditions, plating thickness, and a number of possible intermediate treatments. Some inconsistencies in adhesion had been noted, but appeared to correlate with the observation that good adhesion could only be obtained for thin deposits, unless effective cathode agitation was employed. Without such agitation, good adhesion could only be obtained for deposits below 0.0001 in. in thickness, with the Cu-Al adhesion of deposits over 0.001 in. decidedly poor. Poor Cu-Al adhesion also resulted from transferring the work to other solutions for deposits of acid copper, cyanide copper, pyrophosphate copper, Watts nickel, etc. However, this defect could be ameliorated by leaving the work with the thin Cu strike at room temperature for a few days, or immersing it for 20 or 30 min in boiling water prior to continued plating. Adhesion of moderately thick deposits was also improved by plating with interrupted d.c., although this was not so effective as cathode bar agitation. It should be noted that Cu plated from this bath on solid surfaces and subsequently stripped was only slightly curled, suggesting that stress levels in the plate were quite low.

Aluminum wire plated continuously from this bath gave intermediate adhesion only. This is believed to be due to the inability to operate the plating device used at high wire speed. A trial on a larger, high speed device seems warranted.

Discussion of Results

The general field of oxalate plating of Cu on Al has shown promise, a number of additives being available to enhance the performance of the am-

monium oxalate-oxalic acid-copper oxalate type of bath.

The original formulation was improved by the addition of fluorides or boric acid, and by replacing all or part of the ammonium oxalate by ammonium pyrophosphate. The properties of the pyrophosphate-oxalate system noted above could be improved still further by the addition of triethylamine. Unfortunately, solubility limitations prevented the operation of these solutions at pH values below about 5, where more rapid dissolution of the aluminum oxide film could be expected. This is probably why a brief immersion period prior to plating was sometimes helpful.

The principal shortcoming noted in the experimental work was associated with attempts to produce deposits of several ten thousandths of an inch in thickness under improper conditions. The improvement in adhesion resulting from leaving plated work for a few days at room temperature or for a few hours at 100°C strongly suggests the possibility of gas accumulation at the Cu-Al interface. That this occurs with a variety of plating solutions suggests that codeposited hydrogen accumulates in molecular form at the Cu-Al interface. This hypothesis requires an abnormally high diffusion rate for hydrogen in electroplated Cu, analogous to that recently reported by Ewing, Tobin, and Foulke (11) for hydrogen in electroplated Ni.

The results obtained appear to suggest that the amine modified pyrophosphate-oxalate process for plating Cu on Al shows promise of providing a significant technical advance. The fully successful barrel plating operations and the highly promising continuous wire plating are especially noteworthy.

The concept of a plating bath for Al incorporating an acid pickling as well as a plating action also seems to be substantiated by the results obtained. It is evident, however, that the action of the pyrophosphate-oxalate baths is highly specific, since this type of bath produces so much better results than those found for other solutions.

Returning to the Gauduin process itself, there is some reason to believe that its rediscovery may lead to important practical applications in the plating of metals other than Al, notably Zn and Fe. For this, some modification of the original process would likely be more effective than to use the original three component formulation.

The successful use of acid Cu solutions for direct plating on Al implies that the corrosion of Al in acid Cu solutions is much less than expected. Since both Pb and Ag show normal acceleration of Al corrosion in acid solution, it may be speculated that Cu ions tend to behave as corrosion inhibitors for Al in acid solution. In connection with this, Cobb and Uhlig's (12) conclusion that Cu ions inhibit corrosion of Ti in acid solution should be mentioned parenthetically.

Acknowledgments

The work reported in this paper constitutes part of Defense Research Board Project D12-75-20-01. The author is grateful to the Chairman of the Board for permission to publish this work. The author wishes to acknowledge the assistance of Messrs.

J. Bannerman, J. L. Cromwell, R. A. Stuart, R. A. Brown, J. M. Roberge, and T. Sorensen in performing parts of the experimental work.

Manuscript received Sept. 24, 1956. This paper was prepared for delivery before the Cleveland Meeting, Sept. 30-Oct. 4, 1956.

Any discussion of this paper will appear in a Discussion Section to be published in the December 1958 JOURNAL.

REFERENCES

1. H. K. Work, *Trans. Electrochem. Soc.*, **53**, 361 (1928).
2. A. G. Gray, Editor, "Modern Electroplating," John Wiley & Sons, Inc., New York (1953).
3. C. F. Burgess and C. Hambuechen, *Electrochem. Ind.*, **2**, 85 (1904).
4. J. E. Stareck (to United Chromium Inc.), U. S. Pat. 2,437,865, Mar. 16, 1948.
5. R. Kumagaya (to Fuji Industries Co.), Japan. Pat. 860, Feb. 12, 1955.
6. Gauduin, Mignon, et Rouart, French Pat. 97030, Oct. 30, 1872.
7. H. C. Schlaupitz and W. D. Robertson, *Plating*, **39**, 750, 862 (1952).
8. R. A. Ehrhardt and J. M. Guthrie, *Monthly Rev. Am. Electroplaters Soc.*, **34**, 421 (1947).
9. J. D. McIntyre and A. F. McMillan, *Can. J. Technol.*, **34**, 212 (1956).
10. S. Heiman, J. (and Trans.) *Electrochem. Soc.*, **95**, 205 (1949).
11. D. T. Ewing, J. M. Tobin, and D. G. Foulke, *This Journal*, **103**, 545 (1956).
12. J. R. Cobb and H. H. Uhlig, *ibid.*, **99**, 13 (1952).

Energy Transfer and Sensitization in Single Crystal Phosphors

R. Leach

Department of Physics, The University of Hull, England

ABSTRACT

Previous investigations, showing that calcium fluoride activated with cerium and manganese forms a sensitized phosphor of high efficiency, are confirmed as a result of measurements on activated single crystals. Measurements of oscillator strength enable the absorptive transitions at the cerium center to be identified, and the transition giving rise to the observed manganese emission is also identified. Evidence is presented to show that the transfer involves a spin exchange interaction between the unlike impurity ions which must be situated within a few lattice sites of each other in the fluorite lattice.

In recent years the subject of sensitized luminescence has been studied extensively, both on account of the applications to the fluorescent lamp industry and also because of the great theoretical interest attached to the solution of a problem intrinsically much simpler than most others in the field of luminescence. A fundamental study of the problem involves the determination of the mechanism of interaction between the sensitizer center, which is responsible for most of the energy absorption, and the activator center, which gives rise to the main emission band.

A variety of theories has been proposed to explain the transfer mechanism, and these have been summarized in an excellent article by Botden (1). As a result of an extensive experimental study of many different sensitized systems it is possible to eliminate most of the theories, chiefly on the grounds that the dependence of the activator emission on excitation intensity is linear and not quadratic, and because sensitized systems are nonphotoconducting. The most likely explanation of the energy transfer process involves the concept of resonance between the excited states of sensitizer and activator centers, which possess a similar amount of energy with respect to the energy level scheme in the host material. Transfer of energy by a quantum mechanical resonance process will be strongly dependent on the distance over which the energy must be transferred and also on the precise nature of the optical transition at each center.

The theoretical treatment of the resonance process is directly analogous to that developed by Perrin (2) and also Förster (3) to account for certain energy transfer processes in gases. However, in the solid state the activator emission usually originates from a forbidden transition and thus the resonance process differs from that in gases where only electric dipole interactions need be considered. Dexter (4) has extended the theoretical treatment and calculates, for transitions of differing multipole order, the number of lattice sites over which transfer is possible. The transfer range is large for dipole-dipole transitions falling off to small values for exchange interactions, and becoming negligibly small for dipole-magnetic dipole interactions.

It is difficult to account for the high observed transfer efficiencies occurring with quite low activator concentrations on the basis of the above simple picture alone, and most workers have attempted to overcome the deficiency by postulating successive sensitizer-sensitizer transitions until the excitation energy reaches a sensitizer center sufficiently close to an activator center for the transfer to be possible. However, in many systems large Frank-Condon shifts occur between the maxima of the sensitizer absorption and emission bands whereas it is essential in all resonance transfers for the excited states concerned to have similar energies with respect to the level scheme of the matrix lattice. Thus transfer to a neighboring identical sensitizer center must be necessarily unlikely in view

of the considerable energy difference between the occupied and unoccupied excited states.

This paper describes the results of experiments which have been carried out on the sensitized system formed by CaF_2 activated with trivalent Ce and divalent Mn as sensitizer and activator, respectively. It is demonstrated that the results are in agreement with the predictions of the resonance theory of energy transfer, although in the absence of sensitizer-sensitizer transitions, the high transfer efficiencies can only be explained by assuming a non-random distribution of activators.

Experimental

The CaF_2 -Ce-Mn system has been studied by Ginther (5) who made extensive measurements of reflection spectra and luminescence excitation and emission spectra. His specimens were all in the form of microcrystalline powders. The present measurements were inspired by the availability of large, synthetic, single crystals of fluorite into which the activators could be introduced either in the melt or by subsequent diffusion processes at temperatures well below the melting point of CaF_2 . The use of single crystals permits a wide range of physical measurements to be made and, in the present case, information obtained from measurements of absorption coefficients enabled the nature of the transitions at each center to be established. Diffusion experiments using small cleavage crystals provided important evidence in support of the existence of large localized impurity distributions.

The fluorite crystals were grown *in vacuo* by the Stockbarger method. In the cases where the impurities were introduced in the melt the luminescence characteristics indicated a uniform distribution of Ce, but a zone purification effect occurred in the case of Mn. This defect was overcome by making all measurements on a single slab of crystal cut perpendicular to the growth direction. The Mn content was determined by colorimetric analysis.

Thermal diffusion.—The specimens activated by thermal diffusion were produced by heating small, good-quality, cleavage crystals of fluorite in a silica tube, together with the desired quantity of manganese or cerous fluoride mixed with CaF_2 powder, which prevented the small quantities of the activators from being lost during the preliminary evacuation of the system and also provided a useful comparison with the resultant luminescence of the crystal after activation. The tube was heated in an electric furnace in an atmosphere of argon which served to prevent oxidation. Cathodoluminescent fluorite could be prepared by diffusion of Mn into the lattice at temperatures as low as 800°K , although at this temperature diffusion took place mainly along the direction of dislocations in the lattice and on the surface of the specimens. As the firing temperature was raised the activation, as judged by discharge excitation following cleaving and polishing, became more uniform. It was not possible to produce cathodoluminescent crystals by heating fluorites which had an evaporated layer of metallic Mn on the surface.

Cerium could be introduced into the lattice by thermal diffusion only with great difficulty and required periods of several days at temperatures of around 1300°K . Since the apparent nonexistence of a zone purification effect with Ce, in crystals grown from the melt, suggests that the mobility of Ce ions in the fluorite lattice is extremely small, the difficulty in obtaining activation with Ce by the thermal diffusion process was not unexpected. Thus most of the experiments were confined to the introduction of Mn into crystals which already contained Ce added to the original melt. However, in this case the amount of sensitization was very small, much less than obtained from crystals activated with similar impurity concentrations in the melt.

Paramagnetic resonance.—The paramagnetic resonance spectrum of crystals activated in the melt was compared with the spectrum of crystals and powders activated by thermal diffusion. Since Ce resonance can only be observed at 20°K (6), the only resonance observed was that due to divalent Mn. Marked differences in the fine structure of the resonance line were found according to the mode of activation. In all cases of comparable Mn content, the fine structure exhibited by crystals activated in the melt was more deeply developed than those activated by thermal diffusion. The explanation of this effect appears to be that Mn is uniformly distributed throughout the crystals activated in the melt whereas it is concentrated in aggregates, possibly along the lines of dislocations and similar faults, in crystals and powders activated by thermal diffusion. The aggregation leads to a quenching of the fine structure effect by spin exchange interaction between nearby Mn ions. Even in the unexcited state some interaction between the Ce and Mn ions, which are both paramagnetic, was found and an increase in Ce content produced a slight broadening of the six peaks in the fine structure of the Mn resonance. This effect appeared to be smaller in crystals containing Ce added to the melt and into which Mn was introduced by thermal diffusion, than in specimens activated with both impurities in the melt.

X-ray analysis.—Debye-Scherrer "powder" photographs of each of the samples showed that in all cases Ce produces an expansion and Mn a contraction of the fluorite lattice. This is expected from a consideration of the ionic radii.

Optical measurements.—Specimens used in the optical measurements were cleavage crystals 0.5 mm to 1 mm thick, polished with a commercial diamond compound. In regions far removed from any absorption bands the crystal transmission was at least 90% in all cases. No absorption was found in the wave-length region between 2 and 0.4μ and, therefore, with one exception, detailed measurements were only made in the region of the cerous ion absorption bands, between 0.2 and 0.4μ . Within this region experiments were made using 800 cps "chopped" radiation from a hydrogen arc lamp in conjunction with a Leiss pattern double prism monochromator. Transmitted light intensity was measured by an EMI 5311 11-stage photomultiplier feeding into a tuned amplifier with output matched to a penrecording milliammeter. Where necessary

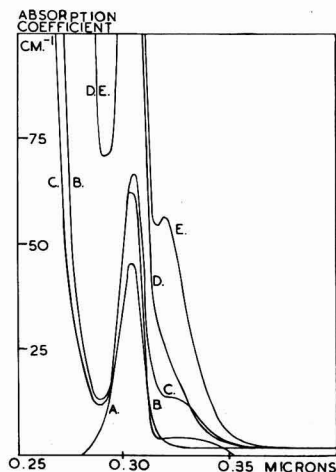


Fig. 1. Absorption spectra of activator fluorite crystals. Curve A, 0.2% Mn, 0.01% Ce; curve B, 0.45% Mn, 0.7% Ce; curve C, 0.22% Mn, 0.6% Ce; curve D, 1.1% Mn, 5.0% Ce; curve E, 5.0% Ce.

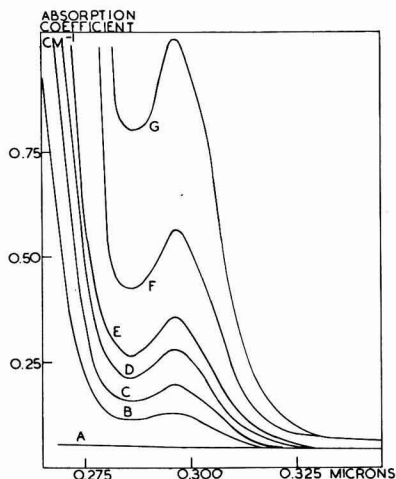


Fig. 2. Absorption spectra of cerous chloride solutions. Curve A, Zero Ce concentration; curve B, 0.00075 g/cc; curve C, 0.00126 g/cc; curve D, 0.00188 g/cc; curve E, 0.00251 g/cc; curve F, 0.00374 g/cc; curve G, 0.00753 g/cc.

correction was made for light reflected and scattered from the crystal surfaces.

Absorption spectra.—Figure 1 gives a family of curves of absorption coefficient vs. wave length for a series of specimens of varying impurity content. The curves show that absorption takes place in the three bands listed by Ginther (5). For all Ce concentrations greater than about 0.1% the absorption band in the region of 0.25μ was the most pronounced and the peak of this band could not be located. A second band peaking at about 0.305μ was very strong in specimens of any Ce concentration. The third band, with peak at about 0.33μ , was most evident in crystals of low Mn content and diminished in intensity rapidly with increasing Mn concentration. This effect was not commented on by Ginther (5), although it can be noticed in his published data.

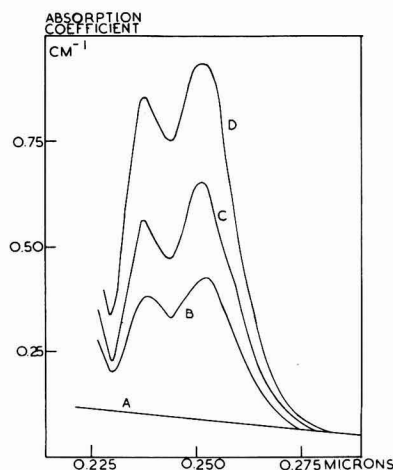


Fig. 3. Absorption spectra of cerous chloride solutions. Curve A, Zero Ce concentration; curve B, 0.000064 g/cc; curve C, 0.000096 g/cc; curve D, 0.000192 g/cc.

For the purpose of comparison, absorption coefficients of a series of solutions of cerous chloride in water were measured. These are plotted in Fig. 2 and 3. Three absorption bands were found, the first occurring with maximum absorption at about 0.305μ and the remaining two with about equal intensity at 0.2530μ and 0.2475μ . For all concentrations, absorption in the two short wave-length bands was about 100 times as intense as that in the band at longer wave lengths.

Crystals containing Mn but no Ce showed no absorption in the region of the bands described. However, in a crystal specimen 0.5 cm thick activated with about 5% Mn by diffusion, very feeble absorption was found in a broad band with maximum at about 0.375μ . This effect is shown in Fig. 4. The absorption band appears to correspond with the feeble excitation region which Ginther (5) observed at 0.4μ in specimens with high Mn concentration.

Excitation and emission spectra.—Measurements of excitation and emission spectra were not so exhaustive as those of Ginther (5) but, nevertheless, served to verify his observations. Sensitization was very pronounced in the two shorter wave-length Ce absorption bands but was extremely feeble following absorption in the 0.33μ Ce band. The broad, green, emission band attributed to the Mn ion could

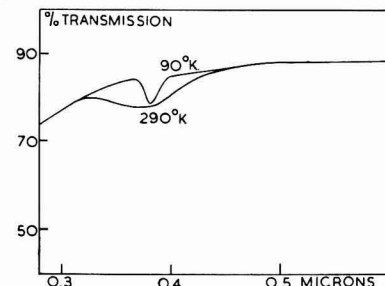


Fig. 4. Spectral transmission of CaF_2 -5% Mn. Specimen thickness 5 mm.

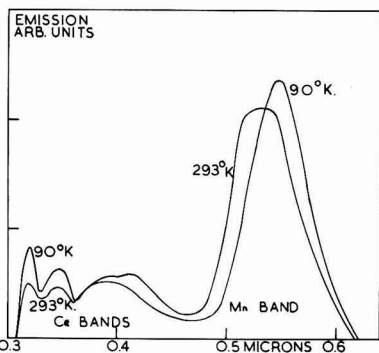


Fig. 5 Emission spectra of typical activated fluorites, at 293°K and 90°K. Impurity concentrations in this case are Ce 0.6%, Mn 0.20%.

be excited by an electrical discharge in air, in agreement with the earlier investigation. However, the sensitized emission of Mn was very feeble in crystals activated with this impurity by thermal diffusion; much less than in crystals containing a comparable amount of Mn introduced into the melt, although discharge excitation of the two types of crystal gave about equal intensities of luminescence. Measurement of emission spectra at 90°K showed little difference in form from the room temperature case, as indicated by Fig. 5. Curves of emission intensity vs. temperature are plotted on Fig. 6 as a typical crystal was allowed to warm up from 90°K.

Lifetime investigation.—The decay times for the various emission bands were investigated using a phosphoroscope wheel method. In every case the u.v. emission had a decay time less than 10^{-4} sec which was the experimental limit of measurement. The decay time for the visible Mn emission was measured at various temperatures and found to be of the order of tens of milliseconds. Figure 7 is a plot of the decay time of emission in this band as a function of Mn concentration, for a series of specimens in which the Ce concentration also varied over a wide range. The curve shows that the decay time is proportional to the Mn concentration but remains unaffected by large changes in the Ce concentration. The decrease in decay time with increasing Mn

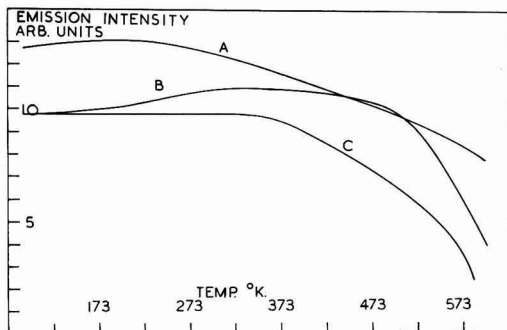


Fig. 6. Fluorescence intensity vs. temperature curves. Curve A, Ce emission, 0.254 μ excitation; curve B, Mn emission, 0.254 μ excitation; curve C, Mn emission, 0.313 μ excitation.

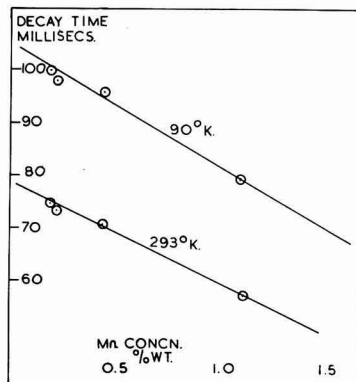


Fig. 7. Decay time for Mn emission at room temperature, and 90°K, and for varying Mn concentration.

concentration is presumably due to a spin exchange interaction between nearby Mn ions.

Discussion

By means of other experiments not described above it was possible to show that the activated crystals were nonphotoconductors, and also that the Mn emission intensity varied linearly with the excitation intensity. Thus it can be concluded that the system is an example of sensitized luminescence. As in all other luminescent systems it is of paramount importance to identify the particular levels of the impurity centers which are responsible for the emission, and energy level schemes are suggested for both activators below. Finally, the process of energy transfer by resonance, in this system, is discussed.

The Cerous Ion Center

A comparison of the absorption bands in the crystals with those for the cerous chloride solutions immediately suggests a direct correspondence between the two cases. The two dominant bands in fluorite at 0.305 μ and 0.25 μ appear to correspond exactly with the same two bands in the solutions (see Fig. 1, 2, and 3). The shape of the short wave-length absorption band, as measured in reflection spectra by Ginther (5), indicates the same form as the double peaked band in the solutions, while the band at longer wave lengths corresponds exactly.

Oscillator strengths were calculated for the 0.305 μ and 0.25 μ bands in the cerous chloride solutions, using Smakula's formula (7). The results are tabulated in Table I. Calculation of the oscillator strength for the 0.305 μ Ce band in fluorite, assuming that all of the Ce added to the melt stays in the lattice, gives values which differ from those for the solutions by a factor of only four. This relatively good agreement serves to further verify the suggested correspondence between the transitions in aqueous solution and in fluorite activated with Ce. The 0.33 μ band, which does not occur in the solutions, is assumed to be due to some interaction between a Ce ion and its surroundings in the fluorite lattice.

Because of the similarity between the absorption of cerous ions in solution and in the fluorite lattice it appears fairly certain that Ce goes into the lattice

Table I. Oscillator strengths for transitions giving rise to 0.30 μ and 0.25 μ absorption bands in aqueous solutions of cerous chloride and in cerium activated fluorite

0.30 μ Absorption band in cerous chloride					
Soln.	Conc g/cc	No. of centers/cc N_0	Max. abs. coeff. cm^{-1}	Half width ev	Oscillator strength (f)
B	0.00075	1.88×10^{18}	0.08	0.28	1.37×10^{-4}
C	0.0013	2.90×10^{18}	0.15	0.28	1.67×10^{-4}
D	0.0019	4.73×10^{18}	0.235	0.26	1.49×10^{-4}
E	0.0025	6.30×10^{18}	0.315	0.28	1.61×10^{-4}
F	0.0037	9.37×10^{18}	0.515	0.31	1.95×10^{-4}
G	0.0075	18.9×10^{18}	0.97	0.31	1.83×10^{-4}
					Mean value = 1.65×10^{-4}
0.25 μ Absorption band in cerous chloride					
Soln.	Conc g/cc	No. of centers/cc N_0	Max. abs. coeff. cm^{-1}	Half width ev	Oscillator strength (f)
B	0.000064	1.61×10^{17}	0.340	0.30	7.27×10^{-8}
C	0.000096	2.41×10^{17}	0.550	0.30	8.00×10^{-8}
D	0.000192	4.81×10^{17}	0.845	0.30	6.07×10^{-8}
					Mean value = 7.11×10^{-8}
0.30 μ Absorption band in cerium containing fluorite					
Spec.	Conc atomic %	No. of centers/cc N_0	Max. abs. coeff. cm^{-1}	Half width ev	Oscillator strength (f)
A	0.01	0.024×10^{20}	0.93	0.15	6.67×10^{-4}
B	0.7	1.75×10^{20}	62.5	0.16	6.57×10^{-4}
C	0.6	1.63×10^{20}	66.5	0.14	6.56×10^{-4}
					Mean value = 6.60×10^{-4}

as the trivalent Ce^{+++} ion, and not in the quadrivalent form. Thus one has the situation of a trivalent ion of greater size than the Ca ion being substituted into a divalent, predominantly ionic, lattice. Applying simple ideas of localized charge compensation it appears that two Ce^{+++} ions should replace two Ca ions along the 110 axis, which is the direction of least potential energy in the crystal, with a Ca ion situated midway between them. However, Bleaney (8) has stated that no axial symmetry is observed in the paramagnetic resonance spectrum of Ce in a divalent lattice and this seems to preclude the above mechanism. The alternative is to suppose that there is a direct substitution of Ce^{+++} for Ca^{++} with charge compensation resulting from the presence of a nearby interstitial fluorine ion. This situation will lead to severe local distortion of the lattice due to the large disparity in ion size.

In fluorite the short wave-length absorption band does not appear for very low Ce concentration but, as the concentration of Ce increases, absorption in this band rapidly becomes much more intense than that in any other. The 0.25 μ absorption band is the most pronounced in cerous chloride solutions of all concentrations indicating that the nature of the Ce center changes with the concentration of this activator in fluorite. Ginther (5) postulated the existence of an aggregate or "cluster" of Ce ions to account for the increased short wave length absorption with high Ce concentrations. In this case the perturbation of the local field produced by the interaction between nearby Ce ions is presumably suffi-

cient to permit absorption in the 0.25 μ band. However, severe distortion of the surrounding lattice results from the presence of localized groups of Ce ions, each ion being compensated by an interstitial fluorine ion. A detailed investigation of the paramagnetic resonance spectrum due to Ce in fluorite should yield interesting results which might demonstrate the increasing interaction between Ce ions as the concentration of this impurity is increased.

It is somewhat surprising that the same transitions appear to occur in both solutions of cerous salts and cerium ions in crystalline media. However, this is in accord with magnetic data on the rare earths and is attributed to the shielding of the solitary 4f electron by the outer filled 5s and 5p orbitals. Hund's selection rules applied to the Ce^{+++} ion give $4^2F_{5/2}$ for the ground state, since the separation of the doublet $4^2F_{5/2} - 4^2F_{7/2}$ is much greater than kT at room temperature. The screening effect of the outer electrons would be expected to result in line spectra for inner shell transitions and this suggests that the excited states of the ion, corresponding to the measured absorption bands, are outer levels. Roberts, Wallace, and Pierce (9) calculated oscillator strengths for solutions of cerous sulfate, from measurements of the Faraday effect, assuming that the outer levels were $5^2D_{3/2}$ and $5^2D_{5/2}$ for the 0.305 μ and 0.25 μ absorption bands, respectively. The values they obtained are in substantial agreement with those quoted in Table I as a result of the present optical measurements. Thus it seems likely that the excited states concerned in these transitions are at any rate perturbed Stark levels of the 3D state of this ion.

The low value of the oscillator strength is at first sight unexpected since the postulated transition is allowed by the usual selection rules. However, as pointed out by Mott and Gurney (10), the oscillator strength is essentially fixed by the product of the wave functions of the excited and ground states concerned and in this case the radial extension of the outer shell, excited state, wave function will be many times greater than that of the shielded, inner shell, ground state and thus the oscillator strength will be necessarily small. Bril, Klasens, and Zalm (11) measured the lifetime for decay of luminescence in Ce-activated phosphors and obtained values of about 1 μsec which again suggests a small oscillator strength for the lowest energy transitions of the Ce^{+++} ion, in agreement with the suggested scheme.

The Manganese Ion Center

The divalent Mn ion possesses an outer incomplete 3d electron shell containing five electrons, and in the isolated condition the ground state would be $3^4S_{5/2}$. In the crystalline state the susceptibility of transition metal ions is given by an expression of

$$\text{the form } \kappa = \frac{N\beta^2}{3kT} \cdot 4S(S+1), \text{ which can only be}$$

explained if the orbital angular momentum is completely quenched. Van Vleck (12) states that this orbital quenching is probably due to the presence of strong asymmetrical electric fields which break

down the spin-orbit coupling. This view is supported by the disappearance of all fine structure in the paramagnetic resonance spectrum of Mn at concentrations of more than a few percent. Orgel (13) has considered the spectra of transition metal complexes and the same general considerations apply to the present case where Mn^{2+} is assumed to enter the fluorite lattice substitutionally, by simple replacement of Ca ions. The degeneracy of the d orbitals completely vanishes, leaving five separate levels with transitions possible between any two of them. In general, the transitions are all forbidden, and strong associated absorption is not expected. However, some d - p hybridization occurs in the excited states and in certain cases this may lead to an increased transition probability between particular states. Thus for Mn^{2+} the ground state is a 3S level which is not significantly split by the crystalline field and the lowest excited state predicted is the 3G level (14), involving a spin reversal only. Even in the free state transitions to outer levels involve energies of many electron volts and for cubical, or octahedral, coordination in the crystalline state these separations will increase and thus may be precluded here. Orgel (13) states that the 4G state in Mn is split into three and the transition responsible for the observed luminescence in the present case is probably from one of the higher pair of these states back to the 3S ground state.

Very weak absorption has been reported for the hydrated Mn ion at about 0.39μ (15) and this seems to fit in with the above theoretical picture. The broad, weak, absorption band located in fluorite containing approximately 5% of Mn (see Fig. 4) with maximum absorption at 0.375μ , and also the excitation at 0.4μ reported by Ginther (5) further support this tentative allocation of energy states. The long luminescence decay time measured in the present experiments is in agreement with the supposition that the radiative transition is one which is normally forbidden.

Mechanism for Energy Transfer

In agreement with Ginther's conclusions (5), the present experiments support the view that CaF_2 activated with Ce and Mn forms a sensitized system of high efficiency. In view of the large spin change involved in the suggested transition at the Mn center, energy transfer by resonance must involve a spin exchange interaction between the excited states of Ce and Mn. According to the detailed theoretical calculations of Dexter (4) this type of interaction is one of extremely short range. However, exchange forces can produce the necessary strong coupling between the spins of two highly paramagnetic ions such as Ce and Mn when the ions are situated within a few lattice sites of each other.

Most previous authors have rejected the idea of a close spatial association between activator and sensitizer on the grounds that a close interaction between the two impurity centers would severely perturb the form and position of the absorption and emission spectra obtained when either activator is present alone. However, a comparison of the experimentally determined absorption and emission spectra

of the present two activators with those for the same two elements in other phosphor systems and in aqueous solution shows that the surrounding lattice has little effect on the position of the energy levels. Activator pairing would not be expected to produce any large additional perturbation and therefore the principal objection to the close association of the activators is removed. Dexter (4) calculates the upper limit for energy transfer by a spin exchange interaction to be about 40 lattice sites surrounding a given excited sensitizer center. A rapid calculation shows that in a phosphor containing 1% MnF_2 and 1% CeF_3 by weight there are only approximately two Mn ions and one Ce ion for every two normal cation points and thus pairing appears to be essential in order to explain the high transfer efficiencies found with activator concentrations of a few tenths of a percent.

Evidence for Association of Activators in Specimens

Prepared from the Melt

The ionic sizes of Ce and Mn are, respectively, larger and smaller than that of Ca and x-ray analysis showed that addition of Ce leads to an expansion, and addition of Mn to a contraction, of the fluorite lattice. When the two ions were present together in about equal proportions little change in the fluorite lattice spacing was detected, nor was there appreciable line broadening. The introduction of Ce into the fluorite lattice will lead to a severe local lattice distortion which will be particularly marked when Ce aggregation occurs. However, the lattice distortion is minimized by the presence of a nearby Mn ion. The formation of associations of impurity ions is opposed by considerations of the statistical nature of entropy and also by electrostatic repulsion, but at the temperature at which the lattice was formed from the melt these effects are less important.

The critical dependence on temperature of the factors which tend to promote pairing of Ce and Mn is well illustrated by the diffusion experiments. It was stated in a previous section that it was possible to diffuse Mn into fluorite at quite low temperatures, and so far as could be ascertained from the luminescence properties the activation was uniform throughout the bulk of the lattice. However, diffusion of Mn into a crystal which already contained Ce added to the melt did not produce appreciable sensitization, even after prolonged diffusion periods at $1300^\circ K$. It appears that the influence favoring pairing is operative only at temperatures at, or close to, the melting point of CaF_2 , where the cation mobility is high. Efficient sensitization is only found in crystals in which the association of activators has taken place. However, efficient powder phosphors were obtained by firing cerous and manganous fluorides with CaF_2 at $1100^\circ K$, but in this case it was shown by paramagnetic resonance measurements, which indicated little fine structure even for low Mn concentrations, that the impurities were mainly contained in the surface layers of the microcrystalline grains. Since this is the case for Mn which has a relatively high mobility in fluorite, the

surface distribution of Ce which has a low mobility, may be expected to be even more pronounced. Thus the local concentration in the surface of the powder grains will be high enough for interaction between Ce and Mn.

The spectral measurements provide further evidence for the formation of a nonrandom distribution of activators. Ginther's investigations (5) are in agreement with the present work in two significant respects, (a) the shift to longer wave lengths of the Mn emission with increasing Ce concentration, and (b) the diminution of the 0.33μ Ce absorption band with increasing Mn concentration. The first effect, the shift in the peak of the Mn emission band, would only be expected to result from a very close interaction between Mn and Ce ions since most reported experimental evidence shows that the spectra of transition metal elements are but little affected by their environment. The 0.33μ Ce absorption band in fluorite has been shown, by comparison with the absorption of cerous salt solutions, to be due to a transition characteristic of the Ce ion in the fluorite lattice. The disappearance of this band at high Mn concentrations suggests that the presence of a nearby Mn ion reduces, or removes, the particular field perturbation which made the transition possible in an isolated Ce center. This assumption was verified by measuring the absorption of a crystal activated with Ce in the melt, both before and after diffusion of Mn into the lattice. No diminution in the magnitude of the 0.33μ absorption band was apparent in this case, although discharge excitation showed that Mn had entered the lattice.

The data obtained from measurements of paramagnetic resonance provide strong evidence in support of the association of impurity ions in the fluorite lattice of specimens activated in the melt. For specimens activated in this way a noticeable diminution in the depth of the six fine structure peaks of the Mn resonance was found to accompany an increase in the Ce content. The effect can be attributed directly to a spin exchange interaction between Ce and Mn ions. The extremely short range of the exchange forces necessitates the assumption of a nonrandom distribution of activators since otherwise, with the activator concentrations used in the present work, an effect of observable magnitude would not be expected. It is hoped that a detailed experimental and theoretical account of the paramagnetic resonance studies will form the subject of a future communication.

Conclusion

Ginther's observation (5) that CaF_2 -Ce-Mn phosphors form a sensitized luminescence system of high efficiency has been verified. Measurements of absorption coefficients and emission spectra have enabled tentative spectroscopic states to be proposed for the ground states of both impurity ions, for the primary excited states of Ce and for the excited

state of Mn responsible for the observed emission. Evidence in favor of a close association of Mn and Ce in the fluorite lattice has been presented. This helps to explain the high energy transfer efficiency found in this phosphor system despite the extremely short range of the spin exchange forces. It has not been possible to identify the particular excited states between which the resonance occurs, nor has the precise nature of the luminescence center been established. A limit to the size of the latter is supplied by Dexter's calculation (4) which puts 40 lattice sites as the maximum distance before the exchange interaction becomes negligibly small. However, it is likely that the separation of the impurity ions comprising the center is much less than 40 lattice sites in view of the high transfer efficiency and the magnitude of the observed spectral shifts.

Acknowledgments

The author wishes to acknowledge with grateful thanks the active support and encouragement of G. F. J. Garlick, who suggested the problem and subsequently provided much valuable criticism. Thanks are also due to R. V. Jones and the staff of Mareschal College, University of Aberdeen, Scotland, who supplied the fluorite crystals, and to A. Cunliffe of this laboratory for his kind assistance with the measurements of paramagnetic resonance. During the course of this work the author was supported by an award from the Department of Scientific and Industrial Research.

Manuscript received April 26, 1957. This paper was prepared for delivery before the Washington Meeting, May 12-16, 1957.

Any discussion of this paper will appear in a Discussion Section to be published in the December 1958 JOURNAL.

REFERENCES

1. T. P. J. Botden, *Philip's Research Repts.*, **7**, 197 (1952).
2. F. Perrin, *J. phys. radium*, **7**, 1 (1936).
3. T. Förster, *Ann. phys.*, **2**, 55 (1948).
4. D. L. Dexter, *J. Chem. Phys.*, **21**, 836 (1953).
5. R. J. Ginther, *This Journal*, **101**, 248 (1954).
6. S. S. Bogle, A. H. Cooke, and S. Whitley, *Proc. Phys. Soc.*, **A64**, 931 (1951).
7. A. Smakula, *Z. Physik.*, **59**, 603 (1930).
8. B. Bleaney, Private communication.
9. R. W. Roberts, L. A. Wallace, and I. T. Pierce, *Phil. Mag.*, **17**, 934 (1934).
10. N. F. Mott and R. W. Gurney, "Electronic Processes in Ionic Crystals," Oxford University Press (1940).
11. A. Brill, H. A. Klasens, and P. Zalm, *Philip's Research Repts.*, **8**, 393 (1953).
12. J. H. Van Vleck, "The Theory of Electric and Magnetic Susceptibilities," Oxford University Press (1932).
13. L. E. Orgel, *J. Chem. Phys.*, **23**, 1004 (1955).
14. M. A. Catalán and O. García-Riquelme, "Atomic Energy Levels," Vol. 2, Circular 467, Washington, 1952.
15. G. Gielessen, *Annal. der Phys.*, **22**, 537 (1935).
16. P. A. Forrester and E. E. Schneider, *Proc. Phys. Soc.*, **96B**, 833 (1956).

The Calcium-Silicate-Tungstate Phosphor

Phase Relationships and Fluorescent Properties

D. E. Harrison

*Luminescent Materials Laboratories, Lamp Wire and Phosphors Department,
General Electric Company, Cleveland, Ohio*

and

F. A. Hummel

*Department of Ceramic Technology, Pennsylvania State University,
University Park, Pennsylvania*

ABSTRACT

An efficient phosphor can be prepared by a co-crystallization of β -CaSiO₃:Mn+Pb and CaWO₄:Pb. The fluorescence, excited by either 2537Å or cathode radiation, is that of a mechanical mixture of β -CaSiO₃:Mn+Pb and CaWO₄:Pb. In the presence of tungstic oxide, the formation of β -CaSiO₃ is greatly accelerated.

Determination of the pertinent compatibility tetrahedra in the system CaO-MnO-SiO₂-WO₃ revealed that the phosphor compositions lie in the sub-tetrahedron β -CaSiO₃-MnSiO₃-SiO₂-CaWO₄. X-ray data showed that there was no solid solubility of β (Ca_{1-x}Mn_x)SiO₃ in CaWO₄; the fluorescence of CaWO₄ is adversely affected by MnO.

Working independently Froelich (1) and Merrill and Stewart (2) made the discovery that β -CaSiO₃ could be cooperatively activated by incorporating small quantities of Pb and Mn ions into the wollastonite structure.

The properties of the β -CaSiO₃:Mn + Pb phosphor have been described by Froelich (3), Merrill and Schulman (4), Schulman, Ginther, and Evans (5), Fonda and Froelich (6).

The synthesis of wollastonite (β -CaSiO₃) involves several intermediate stages. Landiya and Mchedlov-Petrosyan (7) showed again recently that when an equimolar mixture of CaO and SiO₂ was heated between 1000° and 1100°C, the first phase to form was Ca₉SiO₆. The orthosilicate reacted with excess SiO₂ to form either Ca₃Si₂O₇ or β -CaSiO₃. Ca₃Si₂O₇ subsequently reacted with excess SiO₂ to yield β -CaSiO₃. The final reaction product consisted entirely of wollastonite.

In the absence of mineralizers, the synthesis of wollastonite is a sluggish reaction. Steadman (8) used 100% excess silica in the preparation of CaSiO₃:Mn and CaSiO₃:Pb phosphors to help promote the rate of reaction. Schulman (9) found that 0.0025-0.0088 moles of PbF₂/mole Ca served as an effective mineralizer. Froelich (10) used 0.05-5.0% of an equimolar mixture of CaF₂ and CaCl₂ to produce an efficient phosphor which required only 4-5 hr firing time between 1100° and 1200°C. Froelich (1,3,11) also found that steam was an efficient catalyst during the firing of silicate phosphors.

This paper describes the phase relationships and fluorescent characteristics of a phosphor prepared by a co-crystallization of β -CaSiO₃:Mn + Pb and CaWO₄:Pb. In the presence of tungstic oxide, wollastonite can be synthesized readily without the use of PbF₂, CaF₂, steam, or excessive temperature.

Experimental Procedure

The raw materials used for phosphor synthesis were as follows: Mallinckrodt Special Bulky silica, and Reagent Grade PbSO₄ and MnCO₃. The H₂WO₄ and CaCO₃ were prepared by Chemical Products Plant of the General Electric Company for phosphor production.

Preparation of compositions and heat treatments.—The components were mixed in a mortar with reagent grade acetone until it had evaporated and a dry powder resulted. Calcines were prepared in fused silica crucibles at temperatures ranging from 1000°-1200°C for periods of 2 hr to several days. For survey work in a temperature gradient, a Pt-wound furnace was used. For heat treatments at constant temperature, silicon carbide element furnaces were used.

Apparatus and techniques.—(A) X-ray patterns: x-ray data were obtained from Norelco and General Electric recording spectrometers using CuK α radiation ($\lambda = 1.5418\text{Å}$) filtered with Ni (Table I); (B) Infrared absorption measurements: data were obtained by means of a Perkin-Elmer Model 21, infrared spectrophotometer. Samples were prepared using pellets of KBr formed under pressure (Table II); (C) Fluorescence measurements: emission curves were obtained with an automatically recording General Electric spectroradiometer.

Results and Discussion

Calcium fluoride serves as an effective mineralizer toward wollastonite. However, when using a batch consisting of CaCO₃, SiO₂, PbSO₄, MnCO₃, and CaF₂, the material produced has coarse and variable grain size. Quench experiments disclosed the presence of considerable liquid formation in the temperature region between 800° and 900°C. This liquid results

Table I. Calcium silicate, calcium tungstate, and calcium-silicate-tungstate compositions used in x-ray analysis

CaO	Molecular ratio			Weight per cent composition			
	MnO	SiO ₂	WO ₃	CaO	MnO	SiO ₂	WO ₃
1.000	0.010	—	1.010	19.27	0.246	—	80.59
1.000	0.031	—	1.031	18.86	0.738	—	80.40
1.000	0.064	—	1.064	18.25	1.47	—	80.28
1.000	0.031	0.757	0.343	30.59	1.20	24.79	43.43
1.000	0.064	0.781	0.354	29.57	2.39	24.73	43.32
1.000	0.750	1.777	0.150	14.39	13.61	27.37	44.64
1.000	1.331	2.029	1.331	9.63	16.23	20.98	53.15
1.000	0.500	1.500	0.500	18.84	11.92	30.28	38.96
1.000	2.000	2.000	2.000	7.17	18.14	15.36	59.33
1.000	1.000	1.000	3.009	6.35	8.03	6.80	78.80

Table II. Compositions used in infrared study

CaO	Molecular ratio		SiO ₂	Weight per cent composition		
	WO ₃	SiO ₂		CaO	WO ₃	SiO ₂
1.00	1.00	—	—	19.47	80.53	—
1.00	—	1.10	—	45.91	—	54.09
1.00	0.08	1.02	—	39.86	13.18	46.96

primarily from eutectics in the system PbO-CaF₂ or PbSO₄-CaF₂ and also to a lesser extent from eutectics in the system PbO-SiO₂. The liquid formed, which serves to accelerate the reaction, has only temporary existence. However, it promotes the formation of large aggregates of β -CaSiO₃.

The addition of 10–15 wt % WO₃ to an equimolar mixture of CaCO₃ and SiO₂ facilitates the formation of wollastonite without the development of a liquid phase. In the presence of MnO and PbO, a fine-grained powder can be obtained by firing this material at 1050°C for 3 hr. A typical composition is given in Table III.

The calcium-silicate-tungstate phosphor is not a silicotungstate but an intimate mechanical mixture of β -CaSiO₃ and CaWO₄ crystals. This can be shown in several ways: (a) x-ray diffraction data showed two phases, β -CaSiO₃ and CaWO₄. (b) Microscopic examination of the composite while it was being irradiated by 2537Å excitation revealed blue fluorescing CaWO₄:Pb crystals situated in aggregates of orange fluorescing β -CaSiO₃:Mn + Pb crystals. It was not possible to separate the two phases by manipulating the aggregates with a probe. The bonding of the CaWO₄ and β -CaSiO₃ crystals was further demonstrated by noting that practically none of the co-crystallized β -CaSiO₃-CaWO₄ phosphor, which had been previously ground in a mortar, floated in tetrabromethane (sp gr 2.964) whereas much of a material prepared by mixing CaWO₄ and β -CaSiO₃ phosphors, each of which had been prepared separately, was carried in suspension because of the buoyancy of β -CaSiO₃.

Optical Properties

The fluorescent emission of the β -CaSiO₃:Mn + Pb and CaWO₄:Pb phases in the calcium-silicate-tung-

state phosphor is the same as those of the two phases when each is prepared separately. The composite is efficiently excited by 2537Å and cathode radiation and inefficiently excited by 3650Å. A relative spectral distribution curve is shown in Fig. 1.

A comparison of the x-ray data of β -CaSiO₃ and CaWO₄, each of which had been prepared separately, with the x-ray data of the phases in the composite β -CaSiO₃-CaWO₄ material revealed no modification in either the wollastonite or scheelite patterns. However, a comparison of the infrared absorption spectrograms of 0.92 β -CaSiO₃, 0.08CaWO₄:0.10SiO₂ with those of CaWO₄ and β -CaSiO₃:0.10SiO₂ showed that some modifications had occurred in the β -CaSiO₃ spectrum. The most marked change occurred at 14.0 μ ; smaller changes were observed between 9 and 11 μ . The CaWO₄ and β -CaSiO₃ + quartz absorption spectrograms were in good agreement with those reported by Miller and Wilkens (12) and by Hunt, Wisherd, and Bonham (13), respectively. Infrared absorption spectrograms are shown in Fig. 2.

Although the structural modifications in β -CaSiO₃ producing changes in the absorption spectrum are not known, it is suggested that they may be the result of surface forces bonding the β -CaSiO₃ and CaWO₄ crystals.

Phase Relationships

The behavior of Mn in the β -CaSiO₃-CaWO₄ composite was unexpected. When the phases were examined individually, manganese oxide was found to be a severe poison toward CaWO₄. Kroger (14)

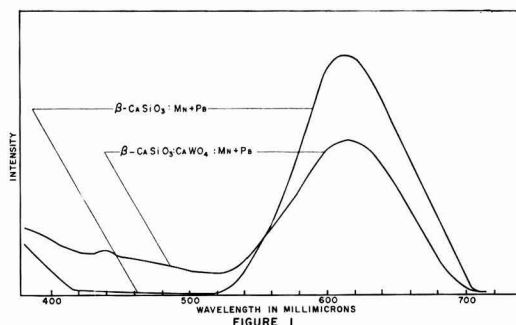


Fig. 1. Relative spectral distribution curves excited by 2537Å ultraviolet.

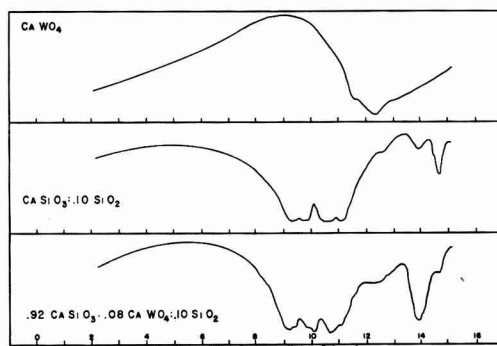


Fig. 2. Infrared absorption spectrograms

Table III. Typical calcium-silicate-tungstate composition

CaO	Molecular ratio				WO ₃	Weight per cent composition				
	MnO	PbO	SiO ₂	WO ₃		CaO	MnO	PbO	SiO ₂	WO ₃
1.000	0.062	0.018	1.112	0.085	37.15	2.90	2.72	44.22	13.01	

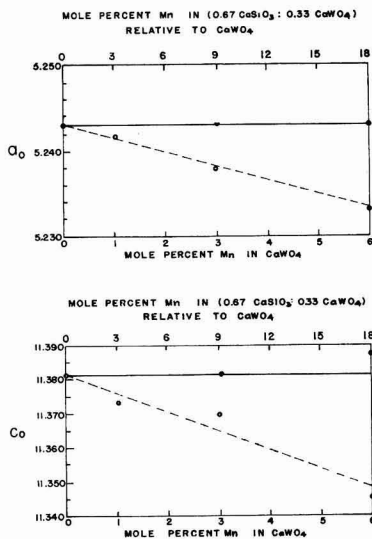


Fig. 3. Variation of unit cell dimensions of CaWO_4 with Mn substitutions in (0.67 CaSiO_3 :0.33 CaWO_4).

reported that as little as 0.1 mole % Mn in CaWO_4 decreased the fluorescent intensity by 37%.

The distribution of Mn in the β - CaSiO_3 - CaWO_4 composite was determined by measuring the changes in the lattice parameters of CaWO_4 . The results for a sample consisting of 67 mole % β - CaSiO_3 , 33 mole % CaWO_4 , with up to 6 mole % substitutions of Mn for Ca are shown in Fig. 3. The dashed line indicates the changes in the (a) and (c) lattice parameters attending substitutions of Mn for Ca in CaWO_4 . The solid line shows the results of measurements of CaWO_4 lattice parameters in the composite containing silica and Mn. The "d" spacings were determined to an accuracy of 0.0025%. The data show no detectable solid solubility of MnWO_4 in CaWO_4 .

This rather unexpected result can be explained readily by considering the compatibility tetrahedra in the quaternary system CaO - MnO - SiO_2 - WO_3 . The subsolidus phase relationships in the temperature region between 1000° and 1200°C were determined using x-ray and microscopic techniques. Only the pertinent subtetrahedra in the high SiO_2 - WO_3 region were investigated. A diagram of the system CaO - MnO - SiO_2 - WO_3 is shown in Fig. 4.

The β - CaSiO_3 : CaWO_4 phosphor compositions lie in the subtetrahedron β - CaSiO_3 - MnSiO_3 - CaWO_4 - SiO_2 . Neglecting a small excess of silica, the phosphor compositions lie in the plane β - CaSiO_3 - MnSiO_3 - CaWO_4 . Since there is complete solid solubility between β - CaSiO_3 and MnSiO_3 in this temperature region (15), two phases are involved, i.e., β - $(\text{Ca}_{1-x}\text{Mn}_x)\text{SiO}_3$ and CaWO_4 . The β - CaSiO_3 - MnSiO_3 - CaWO_4 plane is shown in Fig. 5. X-ray data showed that there was no solid solubility of β - $(\text{Ca}_{1-x}\text{Mn}_x)\text{SiO}_3$ in CaWO_4 .

On the MnWO_4 side of the plane SiO_2 - CaWO_4 - MnSiO_3 , i.e., in the subtetrahedron CaWO_4 - MnSiO_3 - MnWO_4 - SiO_2 , the situation is different, for there is considerable solid solubility between CaWO_4 and MnWO_4 . This effect can be demonstrated optically.

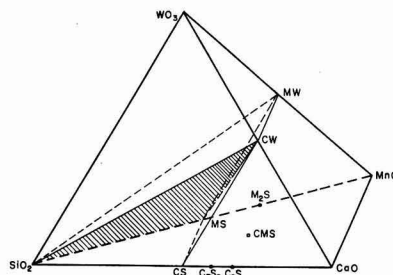


Fig. 4. The system CaO - MnO - SiO_2 - WO_3 (1100°C)

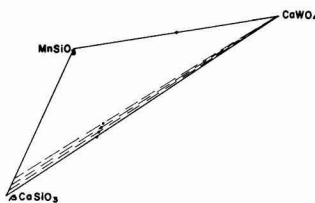


Fig. 5. The plane β - CaSiO_3 - MnSiO_3 - CaWO_4 .

Two compositions were selected, one at 10 mole % CaSiO_3 on one side of the common plane MnSiO_3 - CaWO_4 - SiO_2 and the second on the other side of the plane at 10 mole % MnWO_4 . After firing at 1100°C for 4 hr, the fluorescent characteristics were compared. The compositions containing β - CaSiO_3 fluoresced a bright blue whereas that containing MnWO_4 fluoresced only weakly.

The small addition of Pb required to sensitize the phosphor under 2537Å radiation does not appear to alter the phase relationships. Lead oxide distributes itself between the two phases. Determination of the lattice parameters of CaWO_4 :Pb in the composite β - $(\text{Ca},\text{Mn},\text{Pb})\text{SiO}_3$ - CaWO_4 :Pb showed that from 0 to 2 mole % PbO enters the tungstate phase. The retention of lead by the CaWO_4 phase is very dependent upon the firing conditions. Kroger (16) has presented data on the changes in luminescent emission with composition for CaWO_4 - PbWO_4 solid solutions.

Manuscript received June 6, 1957. This paper is a part of a thesis submitted by D. E. Harrison in partial fulfillment of the requirements for the Ph.D. degree to the Pennsylvania State University; contribution No. 56-64 from the Mineral Industries Experiment Station, The Pennsylvania State University. This paper was prepared for delivery before the Washington Meeting, May 12-16, 1957.

Any discussion of this paper will appear in a Discussion Section to be published in the December 1958 JOURNAL.

REFERENCES

- H. C. Froelich, British Pat. 577,694.
- J. B. Merrill and W. E. Stewart, British Pat. 581,951, Oct. 30, 1946; *J. Opt. Soc. Amer.*, **38**, 471 (1948).
- H. C. Froelich, *J. (and Trans.) Electrochem. Soc.*, **93**, 101 (1948).
- J. B. Merrill and J. H. Schulman, *J. Opt. Soc. Amer.*, **38**, 471 (1948).
- J. H. Schulman, R. J. Ginther, and L. W. Evans, *ibid.*, **38**, 817 (1948).
- G. R. Fonda and H. C. Froelich, *J. (and Trans.) Electrochem. Soc.*, **93**, 114 (1948).

7. N. A. Landiya and O. P. Mchedlov-Petrosyan, *Zhur. Fiz. Khim.*, **26**, 1785 (1952); *Chem. Abs.*, **47**, 6231e.
8. A. Steadman, U. S. Pat. 2,299,510, Oct. 20, 1943; *Chem. Abs.*, **37**, 1658^a.
9. J. H. Schulman, U. S. Pat. No. 2,474,193, June 21, 1949; *Chem. Abs.*, **43**, 6517g.
10. H. C. Froelich, U. S. Pat. 2,542,322, Feb. 20, 1951; *Chem. Abs.*, **45**, 5027a.
11. H. C. Froelich, U. S. Pat. 2,525,028, Oct. 10, 1950; *Chem. Abs.*, **45**, 456^b.
12. F. A. Miller and C. H. Wilkins, *Anal. Chem.*, **24**, 1253 (1952).
13. J. M. Hunt, M. P. Wisherd, and L. C. Bonham, *ibid.*, **22**, 1478 (1950).
14. F. A. Kröger, "Some Aspects of the Luminescence of Solids," p. 137, Elsevier Publishing Company, Inc., Amsterdam (1943).
15. E. Voos, *Z. anorg. u. allgem. chem.*, **222**, 213 (1935); F. P. Hall and H. Insley, *J. Am. Ceram. Soc.*, **30**, 63 (1947).
16. F. A. Kröger, *loc. cit.*, p. 123.

The Calcium-Silicate-Tungstate Phosphor

Preparation and Physical Properties

Shannon Jones

Lamp Wire and Phosphors Department, General Electric Company, Cleveland, Ohio

ABSTRACT

A typical formulation and method of preparation is given for the calcium-silicate-tungstate (CST) phosphor. The wave length of the peak fluorescent emission of the tungstate phase is a function of its lead content. From spectral distribution of the emission of a CST phosphor, one can determine the lead content and the luminous efficiency to be expected from the tungstate phase. The effect of calcium fluoride as a batch addition in increasing average particle diameter of CST phosphor is shown.

Finer-grained phosphors (CST, calcium silicate, calcium tungstate) are produced if the batch is preheated at about 500°C before firing the phosphor.

Beta calcium metasilicate and calcium tungstate can be cocrystallized in the presence of Pb and Mn to form β -CaSiO₃:Mn:Pb and CaWO₄:Pb. Harrison and Hummel (1) described the phase relationships and fluorescence of this composite phosphor. Their work showed that no Mn entered the CaWO₄:Pb phase, where it was known to be a poison (2). The fluorescent properties of this calcium-silicate-tungstate phosphor under 2537Å excitation are simply those of a mixture of β -CaSiO₃:Mn:Pb and CaWO₄:Pb. The emission spectrum of a typical composite is shown in Fig. 1.

The use of H₂WO₄ in place of CaF₂ (3) as a mineralizer in the preparation of calcium silicate phosphor permits synthesis of a finer-grained material. However, the formation of the additional fluorescent phase, CaWO₄:Pb, not only affects the color but also reduces the luminous efficiency, since a substantial portion of the CaWO₄:Pb emission occurs in the near ultraviolet and in the less luminous part of the visible spectrum.

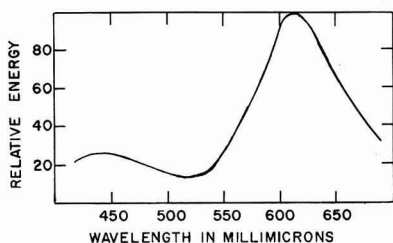


Fig. 1. Emission spectrum of CST phosphor

Fortunately an increase in the amount of PbWO₄ in solution in CaWO₄ has the effect of shifting the emission spectrum farther into the visible region. The distribution of Pb between the β -CaSiO₃:Mn:Pb and CaWO₄:Pb phases does not, in practice, reach equilibrium, but rather it is dependent on firing conditions. Under proper firing conditions it is possible to retain sufficient Pb in the calcium tungstate phase to obtain nearly maximum luminous efficiency in this phase.

Object

The primary objectives of this paper are: (a) to present data on the effect of Pb concentration on the fluorescent properties under 2537Å excitation of the calcium tungstate phase in the calcium-silicate-tungstate (CST) phosphor; (b) to compare average particle sizes of calcium-silicate-tungstate phosphor and calcium silicate phosphor prepared using CaF₂.

The particle size of the CST phosphor or of calcium silicate or calcium tungstate phosphor is dependent on the method of preparation. It was found that a preheating technique was effective in producing finer particle size, particularly in the case of CST phosphor.

Preparation

A typical CST phosphor was prepared by pebble-milling the batch given in Table I, firing it at 1140°C for 3 hr, mixing with 3 wt % of NH₄Cl, then refiring at 1140°C for 3 hr. Both firings were done in open "Vycor" crucibles in air in an electric resistance furnace.

Table I. Batch

Ingredient	Moles
CaCO ₃	1.10
MnCO ₃	0.070
PbSO ₄	0.025
H ₂ SiO ₄	0.40
H ₂ WO ₄	0.10
NH ₄ Cl*	0.94

* NH₄Cl was added after the first (or structure-forming) firing.

Table II. Phosphor

Phase	Oxide	Composition	Moles
Calcium Silicate	CaO	—	1.0007
	MnO	—	0.068
	PbO	—	0.003
Calcium Tungstate	SiO ₂	—	1.20
	CaO	—	0.0993
	PbO	—	0.0007†
	WO ₃	—	0.10

† This value was estimated from the peak wave length of the fluorescent emission band of the calcium tungstate phase.

The resulting approximate phosphor composition is given in Table II. It will be seen that the Pb content of the phosphor is much lower than that of the batch, the Mn content only slightly lower. Such variations result from selective volatilization of the compounds, particularly of the chlorides of Pb and Mn during the second (or scavenging) firing.

Role of Lead in the Calcium Tungstate Phase

Since the brightness of CST phosphor is partially dependent on the spectral distribution of the two phases, it is of value to know the changes in spectral distribution of each phase in the composite CST phosphor produced under various firing conditions.

First, examine in detail the calcium tungstate phase of CST phosphor. Kröger has published data on the fluorescent color of various CaWO₄-PbWO₄ solid solutions at room temperature under 2537Å excitation (2). He showed that, with increasing Pb content, the spectrum shifts toward longer wave lengths. However, his published data were not sufficiently detailed to be of value in determining the Pb content from the peak emission wave length. If one knows the relation between brightness and peak emission wave length of the tungstate phase, then one can, from its spectral distribution, determine whether the tungstate phase is potentially efficient.

Harrison and Hummel have shown that from 0 to at least 2 mole % Pb can be retained in the tungstate phase of CST. The Pb content of the tungstate phase is not determinable from the batch composition alone because one cannot predict either the distribution of Pb between the two phases or the total Pb retained in CST unless one knows the firing conditions and their effects on the retention of Pb.

However, from the peak wave length of the emission of the tungstate phase its Pb content and brightness can be determined. The emission bands of the calcium silicate phase do not overlap the

peak of the tungstate emission. If one knows the Pb content of the tungstate phase from its peak wave length and the Pb content of the CST composite phosphor from chemical analysis, one can determine the Pb retained in the silicate phase of the CST phosphor.

In order to determine the effect of Pb content on the spectral distribution and other fluorescent properties of calcium tungstate phosphor, five batches were made up with various amounts of PbSO₄ (none, 0.0075 mole, 0.0150, 0.0225, 0.0300) added to 1.05 moles CaSO₄ plus 1.00 mole H₂WO₄. Part of each batch was fired at about 1000°C for 3 hr, another part for 15 hr. No subsequent addition of NH₄Cl was made and no second firing was given the phosphor. There is no reason to believe that subsequent additions of NH₄Cl and refirings have any substantial effect on the fluorescent properties of the calcium tungstate phase in CST other than those effects which are due to the reduction in Pb content.

Spectral distribution curves were run on the emission of the samples at room temperature under 2537Å radiation. Relative brightness was obtained on the samples with a barrier layer photocell corrected to the visibility function. Relative photocell outputs were obtained from the phosphors when an arbitrary blue filter was placed over the uncorrected barrier-layer cell. Each blue output, divided by the brightness of the phosphor, gave a ratio which is called "blueness". The "blueness" number should not be considered as having an easily definable quantitative significance, but rather it is a subjectively descriptive number indicating the appearance of the phosphor.

Figures 2, 3, and 4, respectively, are graphs of Pb introduced vs. peak wave length, brightness, and "blueness" for various firing times. In each figure a curve extrapolated to an estimated effective zero firing time is drawn. Points defining the extrapolated curves were determined by assuming that the loss of Pb followed first-order kinetics, i.e., $A = A_0 \exp(-bt)$, where A is the amount of Pb at time t , A_0 is the amount of lead at time $t = 0$, and b is the rate constant, which is determinable from the data at 3 and 15 hr. Along these extrapolated curves one may assume that the Pb retained in the tungstate phase is determined solely by the Pb introduced in the batch. Thus the extrapolated curve in Fig. 2 pro-

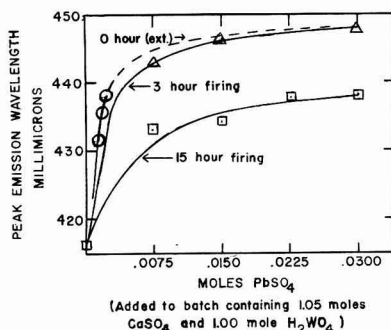


Fig. 2. Effect of Pb content and firing time on peak wave length of calcium tungstate phosphor.

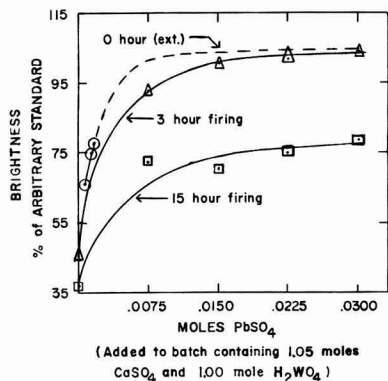


Fig. 3. Effect of Pb content and firing time on brightness of calcium tungstate phosphor.

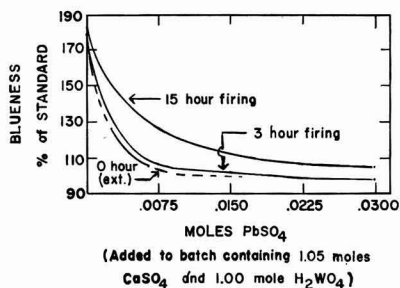


Fig. 4. Effect of Pb content and firing time on "blueness" of calcium tungstate phosphor.

vides a basis for a reasonably accurate estimate, from peak wave length of the tungstate phase, of the Pb retained in this phase. In turn, from the Pb content, one can determine the relative brightness of the tungstate phase from Fig. 3. In Fig. 3 the apparent dependence of brightness on firing time even where no Pb was introduced is probably false and the result of Pb contamination of the furnace.

The Calcium Silicate Phase in CST

The optimum amount of Pb in the calcium silicate phase is not critical. In the phosphor formulation given in Table I, variations in Pb content of the calcium silicate phase from 0.0025 to 0.0035 moles do not give significant differences in brightness.

In practice an excess of Pb must be introduced initially into the CST or into straight calcium silicate phosphor, presumably to promote a sufficiently rapid formation of the proper structure. This excess of Pb in calcium silicate phosphor produces a dark phase, which probably contains some Mn. The dark phase reduces the brightness of the calcium silicate, consequently the scavenging firing with a chloride (3) is required to whiten the calcium silicate phosphor and increase its efficiency.

Firing with chloride reduces the Mn content slightly, as indicated in Table I. In the composition region of Table I, the spectral peak of the calcium silicate phase is shifted slightly away from the red by the reduction in Mn content, but the brightness is virtually constant.

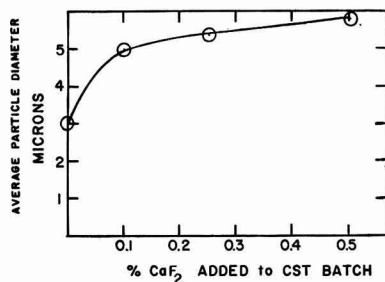


Fig. 5. Effect of CaF_2 on particle size of CST phosphor

Influence of Mineralizers on Particle Size

The strong tendency of CaF_2 to cause an increase in particle size of CST phosphor is shown in Fig. 5. The average particle diameters were determined by an air permeation method ("Fisher Sub-Sieve Sizer"). Klasens, Hoekstra, and Cox recently mentioned the effect of fluorides in promoting crystal growth in silicates (4).

Similar effects of CaF_2 on particle size of calcium silicate phosphor have been observed. Tungstic acid in the amount given in Table I catalyzes the formation of the silicate phase about as effectively as the fluoride without causing the formation of as large grains. Harrison and Hummel have attributed the formation of large grains, particularly when using CaF_2 , to the presence of liquid regions during firing (1).

Effect of Preheating on Particle Size

In the CST formula of Table I there is no fluoride to form liquid regions. However, there is a probability of lead silicate glass being formed at certain points in the batch where the ratio of lead sulfate to silica is near a eutectic composition. It is possible to minimize the formation of these liquid regions by preheating the batch for a sufficient time below the temperature of liquid formation. Such a treatment distributes the lead compound by solid and vapor state diffusion until the small local regions of batch having compositions near the eutectic have lost their excess of lead compound.

Two experiments on typical CST batches showed average particle diameter (APD) reductions due to preheating as follows: not preheated, 4.6 μ and 6.2 μ ; preheated, 450°C, 3 hr, 2.9 μ and 4.8 μ .

The above diameters apply to the phosphor after the structure-forming but before the addition of

Table III. Average particle diameter (Fisher Sub-Sieve Sizer)

Preheating treatment		Calcium silicate μ	Phosphor type	
Temp. °C	Time, hr		CST μ	Calcium tungstate μ
NONE		7.7	7.2	6.2
400	3	5.6	6.7	4.9
400	16	5.8	4.5	4.6
400	64	5.4	4.4	4.6
500	3	6.6	4.5	5.1
500	16	6.3	4.5	5.4
500	64	6.0	4.3	5.2
600	3	6.3	4.3	5.9
600	16	6.4	4.3	5.9

NH₄Cl and the scavenging firing. Qualitatively, differences in particle size which result from different procedures and which are apparent after the first firing tend to remain after a subsequent addition of NH₄Cl and a refiring. However, the method of mixing in the NH₄Cl, the second firing conditions, and other factors also affect the particle size. For these reasons, it is not possible to give a single, clear-cut relationship between particle size after the second firing and either the fluoride content of the batch or the preheating treatment.

In another group of experiments it was found that preheating of the batches produced smaller particle sizes of calcium silicate phosphor and of calcium tungstate phosphor as well as of CST. For these tests, each of three batches was divided into ten parts. One part was fired directly at 1150°C for 3 hr; the other nine parts were preheated at various low temperatures for various times before taking them up to firing temperature (1150°C for 3 hr). The samples were not refired with NH₄Cl. Results are given in Table III.

Summary and Conclusions

1. By using tungstic acid instead of calcium fluoride as the mineralizer, a finer grained calcium silicate phosphor phase can be obtained.

2. The introduction of tungstate produces a second fluorescent phase, CaWO₄:Pb whose efficiency can be determined from the spectral distribution of fluorescent emission of the composite.

3. Average particle size of CST phosphor, or of calcium silicate phosphor or calcium tungstate phosphor, can be reduced by a batch preheating technique.

Manuscript received June 6, 1957.

Any discussion of this paper will appear in a Discussion Section to be published in the December 1958 JOURNAL.

REFERENCES

1. D. E. Harrison and F. A. Hummel, *This Journal*, 105, 34 (1958).
2. F. A. Kröger, "Some Aspects of the Luminescence of Solids," Chap. III.
3. H. C. Froelich, U. S. Patent 2,542,322.
4. H. A. Klasens, A. H. Hoekstra, and A. P. M. Cox, *This Journal* 104, 93 (1957).

Heat of Formation of Titanium Tribromide by the Mercury Reduction of Titanium Tetrabromide

Elton H. Hall and John M. Blocher, Jr.

Battelle Memorial Institute, Columbus, Ohio

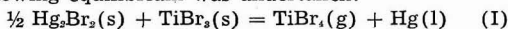
ABSTRACT

The experimentally determined heat of reaction, $\frac{1}{2}\text{Hg}_2\text{Br}_2(\text{s}) + \text{TiBr}_3(\text{s}) = \text{TiBr}_4(\text{g}) + \text{Hg}(\text{l})$, $\Delta H_{475} = 23.0 \pm 1.2$ kcal is combined with existing data for TiBr₄, Hg, and Hg₂Br₂ to obtain for the heat of formation and standard entropy of TiBr₃,

$$\Delta H^\circ_{f,298.2} = -130.6 \pm 1.2 \text{ kcal/mole}$$

$$S^\circ_{298.2} = 43.4 \pm 1.6 \text{ e.u.}$$

As part of a program directed toward the determination of the physical and thermodynamic properties of the titanium bromides, a study of the following equilibrium was undertaken:



The heat of this reaction may be combined with the heats of formation of Hg₂Br₂ and TiBr₄ to calculate the heat of formation of TiBr₃. A study by a dew-point method of the corresponding reduction of TiCl₄ has been reported by Schäfer, *et al.* (1).

Experimental

The reagents were triple-distilled Hg and TiBr₄ prepared from distilled Br and iodide-process Ti, and distilled in a 30-plate column, as described by Blocher, *et al.* (2).

Measurements of the equilibrium pressure of TiBr₄ over Hg₂Br₂, TiBr₃, and Hg were made in the apparatus shown in Fig. 1. The cell was carefully cleaned with HF, rinsed, outgassed, and charged with Hg by vacuum distillation from a reservoir attached at Point A. A small amount of pure TiBr₄, transferred in an ampoule provided with a break

seal, was distilled into the cell and allowed to react with the Hg to form a surface coating of Hg₂Br₂ and TiBr₃, after which the cell was sealed off at A and separated from the filling apparatus. The purpose of the flexible rubber tubing connecting the cell to the vacuum and controlled-pressure system was to

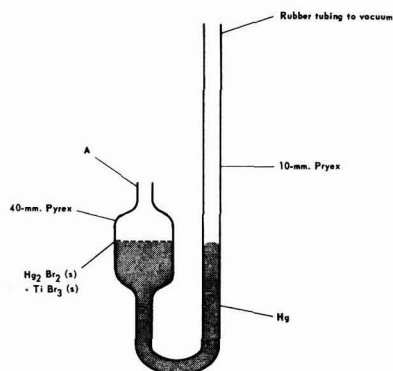


Fig. 1. Mercury reduction cell

permit outgassing by inverting the cell while evacuating the system.

The cell was used as a null indicator, the pressure above the bromides being balanced by a measured pressure of inert gas which was varied until the Hg level in the 10-mm tube was returned to the position occupied at zero pressure differential. As a check on the reliability of the technique, and of the prediction that the partial pressures of $\text{Hg}_2\text{Br}_2(\text{g})$ and $\text{HgBr}_2(\text{g})$ are negligible,¹ the cell was charged with Hg and Br to form a scum of Hg_2Br_2 over the Hg surface. The pressure-temperature data given in Table I indicate that only the partial pressure of Hg is significant, although there appears to be a small systematic error in the experimental values. In the Hg reduction of TiBr_4 , the Hg saturation vapor pressure is exerted over the Hg at unit activity in the cell along with the equilibrium TiBr_3 pressure, and must be subtracted from the observed total pressure to obtain the partial pressure of TiBr_3 .

The cell was thermostated to $\pm 0.2^\circ\text{C}$ in a salt bath whose temperature was measured by a calibrated Chromel-Alumel thermocouple. The Hg levels in the cell and the manometer were measured with a cathetometer.

The data obtained with six separate preparations are given in Tables II-IV. Figure 2 shows the results for samples E and F, which are typical. In the preparation of each of samples A through D, an undetermined amount of Br was distilled into the cell in addition to the Hg and TiBr_4 , thus providing an excess of Hg_2Br_2 . Samples E and F were prepared using only Hg and TiBr_4 , so that the Hg_2Br_2 and TiBr_3 were produced in stoichiometric ratio.

Results

The data obtained on samples C and E, when plotted in the usual manner, fell on three straight lines. The pressures exerted by a fresh sample fell on line I. However, when the sample was held at high temperature, e.g., 250°C , the pressure decreased slowly over a period of 36 hr. A new equilibrium was apparently established on line II. Finally, when the sample was cooled below 200°C , line III was obtained, the slope of which was less than the slope of I. The system was then reversible between II and III with considerable lag in the change in slope after passing the break in either

¹ Calculations based on the data given by Brewer (3) indicate a HgBr_2 pressure, e.g., of 0.13 mm at 225°C .

Table I. Total pressure over Hg(l) and $\text{Hg}_2\text{Br}_2(\text{s})$

Temp, $^\circ\text{C}$	P_{total} , ^a mm of Hg	$P_{\text{Hg}(\text{g})}$, ^b mm of Hg	$P_{\text{total}} - P_{\text{Hg}}$, mm of Hg	$\frac{\Delta P}{P}$, %
236.5	52.3	51.6	0.7	1.35
238.1	54.4	54.0	0.5	0.93
246.2	67.3	67.3	0.0	0.0
254.5	83.9	83.7	0.2	0.24
257.9	91.7	91.2	0.5	0.55
274.1	137.1	136.4	0.7	0.52

^a Observed pressure corrected for latitude, and for thermal expansion of Hg in the cell and in the manometer.

^b "Handbook of Chemistry and Physics," 35th Ed., Chemical Rubber Publishing Co., p. 2147 (1953-54).

Table II. Equilibrium TiBr_3 pressure in Mercury Reduction Reaction, Runs A and B

Run ^a	Temp, $^\circ\text{K}$	P_{TiBr_3} , mm of Hg
A	449.3	6.4
A	443.4	4.3
A	430.5	1.7
A	472.3	21.7
A	466.0	16.9
A	463.3	14.0
A	446.8	5.6
B	462.7	12.0
B	475.7	25.0
B	492.2	60.8
B	459.4	10.0
B	449.7	5.6
B	491.0	56.5
B	510.7	139.8
B	444.1	3.7

^a Data listed in order taken.

direction. The intersection of II and III occurred at 238° and 218°C for samples C and E, respectively.

A similar break in the $\log p$ vs. $1/T$ curve was observed in the data for sample A. At the time, this was considered to be anomalous behavior and precise data were not obtained during the early stages of the run. The points reported for sample A correspond to the system in state III.

The measurements on sample B were made over a very short period of time compared to sample A, and the run was completed before a drift in pressure was observed.

Runs D and F were purposely terminated while the system was still in the state leading to pressures on line I.

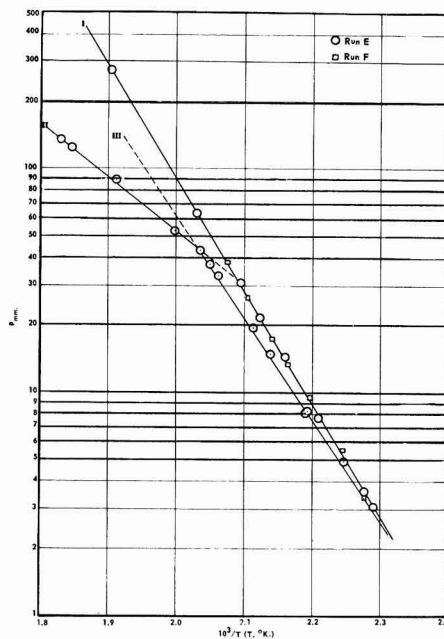


Fig. 2. TiBr_3 pressure in mercury reduction reaction (runs E and F)

Table III. Equilibrium TiBr_3 Pressure in Mercury Reduction Reaction
Runs C and D

Run C ^a		Run D ^a	
Temp, °K	P_{TiBr_3} , mm of Hg	Temp, °K	P_{TiBr_3} , mm of Hg
498.8	89.3	444.2	4.1
465.1	16.3	444.0	4.0
448.4	6.7	467.5	16.1
510.4	218.3	495.2	65.8
462.2	14.5	485.1	36.2
502.2	88.3	481.2	30.7
518.1	176.3	460.8	12.4
509.6	94.5	496.2	65.2
530.2	145.3	523.2	211.3
528.4	138.2		
522.4	121.4		
516.7	108.6		
508.2	92.8		
507.6	91.7		
501.3	78.9		
495.2	70.0		
445.7	5.3		
476.2	24.5		
471.4	19.7		
488.7	39.7		
496.8	55.2		
499.6	61.9		

^a Data listed in the order taken.Table IV. Equilibrium TiBr_3 Pressure in Mercury Reduction Reaction,
Runs E and F

Run E ^a		Run F ^a	
Temp, °K	P_{TiBr_3} , mm of Hg	Temp, °K	P_{TiBr_3} , mm of Hg
477.2	31.0	467.2	17.3
471.2	21.8	455.2	9.5
463.1	14.4	439.4	3.4
439.2	3.6	481.9	38.3
452.8	7.7	462.0	13.3
444.8	4.9	445.2	5.5
492.7	63.8	475.0	26.8
525.6	279.7		
541.2	125.1		
546.6	135.1		
523.3	89.4		
500.4	53.3		
467.7	15.0		
436.7	3.1		
473.5	19.6		
485.1	33.4		
456.2	8.2		
456.6	8.1		
491.4	43.6		
488.0	33.5		

^a Data listed in the order taken.

The slope of line I varies slightly among samples B through E. This variation, which is outside the limits set by the relatively small scatter in the data for a given sample, could not be correlated with changes in conditions or technique. For samples E and F, the initial points fall on the same line, suggesting that the data are at least reproducible for stoichiometric samples. Table V gives the ΔH values calculated from the data.

X-ray Diffraction Analysis

The breaks in the $\log p$ vs. $1/T$ curves clearly indicate a fairly energetic phase change. As an aid

in the interpretation of the data, several samples were submitted to x-ray diffraction analysis. The first such sample was prepared by placing Hg and TiBr_3 in a quartz capillary and heating for 18 hr at 120°C . The x-ray pattern taken with the sample at 250°C showed TiBr_3 and Hg_2Br_2 . At the conclusion of run C (sample in state III), a sample of the reaction product was examined. Hg_2Br_2 was found in addition to a few unidentified lines. However, no lines for TiBr_3 were seen.

Samples from runs E and F showed Hg_2Br_2 with no extra lines and no TiBr_3 lines. Two additional preparations were made by reacting TiBr_3 with distilled Hg. No pressure measurements were made on these samples. Only Hg_2Br_2 were detected in one sample, while in the other, strong Hg_2Br_2 and faint TiBr_3 lines were seen in the x-ray pattern.

No expansion of the lattice parameter of Hg_2Br_2 could be detected in any of the samples.

Hot-Stage Microscopy

The heat effect (about 12 kcal), indicated by the break in the slope of the $\log p$ vs. $1/T$ curve, is of the order of a heat of fusion rather than being characteristic of a heat of solid solution which might be about 2 to 3 kcal.

To detect possible fusion, a sample of the reaction solids was observed with a hot-stage microscope. The temperature was increased from room temperature to over 300°C . No fusion process was observed. However, at one point, a crystallization from the excess Hg was observed in the cooling process.

Solubility Experiment

In a separate experiment designed to detect possible solution of reactants in the Hg, a sample was taken at temperature from below the surface of liquid Hg which had been equilibrated with the reaction mixture at 220°C for 72 hr. A small amount (about 0.2%) of bromide-containing scum was observed to separate from the Hg sample on cooling. No Ti (<0.5%) was detected in the scum such as might be expected if solution in Hg were the explanation of the disappearance of the TiBr_3 phase in the aged samples.

Discussion

It may be assumed that the pressure-temperature data taken on a fresh sample are representative of the Hg reduction equilibrium as written in Eq. (I), since both TiBr_3 and Hg_2Br_2 were observed as sepa-

Table V. Heats of Reaction Calculated from the Slopes
of Lines I, II, and III in the Temperature Range 435°K to 525°K

Sample	ΔH_I , kcal/mole	ΔH_{II} , kcal/mole	ΔH_{III} , kcal/mole
A	—	—	20.6, 22.9 ^a
B	24.2	—	—
C	21.8	10.9	20.2
D	22.7	—	—
E	23.2	11.2	20.8
F	23.2	—	—
Mean $\Delta H_I = 23.0 \pm 1.2$ kcal/mole			

^a Mercury expansion data were not taken on the cell used for run A. The corrections determined for the cells used in runs B and C, when applied to the pressure data of run A, lead to two different lines. ΔH_{III} values calculated from each slope are reported.

rate solid phases in the x-ray diffraction patterns of fresh samples. The reason for the variation of the slope of the initial line among different samples is unknown. Therefore, the average of the initial slopes for samples B through F has been used to calculate the heat of reaction with the variation in the slopes included in the ascribed uncertainty.

To extrapolate the experimental data to 298.2°K, it was necessary to obtain a value for the ΔC_p of reaction. Unfortunately, reliable values for the heat capacities of TiBr₃ and Hg₂Br₂ are not available. However, values obtained by estimation should be entirely adequate for this purpose. The heat capacity of Hg₂Br₂ was taken as the average (24.8 cal/mole/deg at 298.2°K) of those of Hg₂Cl₂ and Hg₂I₂ given in National Bureau of Standards Circular 500. The heat capacity of TiBr₃ (also 24.8 cal/mole/deg at 298.2°K) was estimated by adding 0.8 cal/deg/gram-atom to the heat capacity of TiCl₃ obtained by averaging the heat capacities given for VCl₃ and AlCl₃. The heat capacity of Hg is also given in Circular 500. That of TiBr₃(g) was obtained by calculation from the spectroscopic data of Delwaille, *et al.* (4). The resulting value of $\Delta C_p = -6.5$ was taken as the average over the temperature range of the measurements.

This treatment of the data gives for Eq. (1):

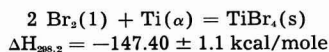
$$\log_{10} P_{\text{atm}} = -5706/T - 3.271 \log T + 19.291$$

$$\Delta H_{298.2} = 24.16 \pm 1.2 \text{ kcal}$$

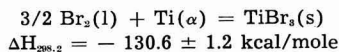
$$\Delta S_{298.2} = 44.7 \pm 1.6 \text{ e.u.}$$

Since entropy values can be estimated with greater certainty than can heats of reaction, comparison of the entropy change obtained in the above work with that calculated from the best available information gives an indication of the reliability of the experimental data. In calculating the standard entropy of TiBr₃(s), the values at 298.2°K for Hg(l) = 18.5 e.u. and $\frac{1}{2}$ Hg₂Br₂(s) = 25.45 e.u. were taken from Circular 500. The value for TiBr₃(g) = 95.02 e.u. was calculated from spectroscopic data (4). The resulting value, $S_{298.2}^\circ = 43.4 \pm 1.6$ e.u., is very close to the estimated value of 43 e.u. given by Brewer (3).

Prosen and his associates (5) at the National Bureau of Standards have obtained for



This may be combined with the above results, the heat of formation of Hg₂Br₂ (-49.42 kcal/mole from Circular 500), and the heats of vaporization and fusion of TiBr₃ [13.22 kcal of Hall, *et al.* (6), and 3.08 kcal of Kelley (7), respectively] at 298.2°C, to give the heat of formation of TiBr₃(s):



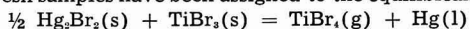
The occurrence of the break in the log p vs. $1/T$ curve and the failure of the system to return to its initial state upon cooling below the break cannot be explained on the basis of the available experimental evidence. The possibility that Hg₂Br₂(s) is the stable phase above the break is dismissed, since thermodynamic calculations indicate that the invariant

point [where Hg(l), HgBr₂(s), and Hg₂Br₂(s) coexist] lies somewhere between 1000° and 1200°C, rather than at the 225°C level of the observed break. This conclusion is confirmed by the absence of HgBr₂(s) in the x-ray patterns observed at 250°C. It appears that one or both phenomena are related to the disappearance of the TiBr₃ lines from the x-ray diffraction patterns of aged samples taken from the pressure cell. This could result from (a) formation of an amorphous form of TiBr₃, (b) formation of a solid solution or complex between TiBr₃ and Hg₂Br₂ which has the Hg₂Br₂ crystal structure or is amorphous, and (c) solution of TiBr₃ in the liquid Hg. However, neither the formation of amorphous TiBr₃ nor the formation of a solid solution would be expected to contribute as large a heat effect as that observed. Furthermore, the failure to detect any expansion of the lattice parameter of Hg₂Br₂ indicates that no solid solution is formed. The solution of TiBr₃ in liquid Hg could produce the observed heat change; however, no Ti could be detected in Hg sampled at 220°C after equilibration with the reaction solids.

Since this work was concluded, it has been suggested that the disappearance of the TiBr₃(s) phase may have resulted from a reaction with Pyrex which may not occur with quartz. Equilibrium determinations in quartz equipment would settle this point. However, it should be noted that in the present work no visible etching of the cell occurred such as might be expected if the Pyrex reacted appreciably with the relatively large amount of titanium bromide contained in the cell.

Summary

In order to permit calculation of the heat of formation of TiBr₃, a study of the Hg reduction of TiBr₃ has been made. Pressure data obtained on fresh samples have been assigned to the equilibrium:



since both Hg₂Br₂ and TiBr₃ were observed as separate solid phases in the x-ray diffraction patterns of fresh samples. The heat of reaction calculated from these data has been combined with the heats of formation of TiBr₃(s) and Hg₂Br₂(s) and the heats of fusion and vaporization of TiBr₃ to give the heat of formation of TiBr₃(s).

A break in the log p vs. $1/T$ curve was observed at high temperatures after prolonged heating. Furthermore, the TiBr₃ pattern was not seen in the x-ray diffraction studies of heated samples. A full investigation of these phenomena must be deferred. However, it is concluded that, despite these irregularities, a fairly reliable value has been obtained for heat of formation of TiBr₃.

Acknowledgment

The authors are grateful for the help and interest of the Office of Naval Research who supported this work under Contract No. Nonr-1120(00). They are also indebted to the following members of the Battelle staff: Neil D. Veigel for some of the pressure measurements, George Cocks for the hot-stage microscopy and J. Robert Bridge, for the crystallographic work.

Manuscript received July 5, 1957. This paper was prepared for delivery before the Cleveland Meeting, Sept. 30-Oct. 4, 1956.

Any discussion of this paper will appear in a Discussion Section to be published in the December 1958 JOURNAL.

REFERENCES

1. H. Schäfer, G. Breil, and G. Pfeffer, *Z. anorg. u. allgem. Chem.*, **276**, 325 (1954).
2. J. M. Blocher, Jr., R. F. Rolsten, and I. E. Campbell, *This Journal*, **104**, 553, (1956).

3. L. Brewer, "National Nuclear Energy Series," Vol. IV-19B, L. L. Quill, Editor, McGraw-Hill Book Co., New York (1950).
4. M. Delwaille and F. Francois, *Compt. rend.*, **220**, 173 (1945).
5. R. A. Nelson, W. H. Johnson, and E. J. Prosen, National Bureau of Standards Report No. 4607, November (1955).
6. E. H. Hall, J. M. Blocher, Jr., and I. E. Campbell. To be published.
7. K. K. Kelly. To be published.

Pressure Distribution within a Vacuum Arc Furnace

J. W. Suiter

Mines Branch, Department of Mines and Technical Surveys, Ottawa, Ontario, Canada

ABSTRACT

The pressure distribution within a continuously evacuated, consumable electrode arc furnace was determined when a variable leak was placed in the melting region of the furnace. This pressure distribution agreed both with that obtained from a simplified calculation based on the kinetic theory of gases and with that obtained during the melting of mild steel electrodes.

Johnson, *et al.* (1) have shown that the arc characteristics and the melting rate in a consumable electrode, vacuum arc furnace depend on a number of variables, including the gas pressure within the furnace. In current practice the pressure is usually measured at some point in the body of the furnace and not in the region of the arc. Since gas is evolved from most metals during melting the pressure in the region of the arc will be higher than that in the body of the furnace.

In the present work the pressure in the region of the arc has been calculated and measured in a simple simulated melting system and results have been compared with similar pressure measurements obtained during the melting of steel electrodes.

Apparatus and Experimental

The experiments were conducted in the furnace described by Rylski and Kinsey (2) and shown schematically in Fig. 1. Gas pressure was measured at the top of the mould and at a point 30 cm below the top by means of thermocouple vacuum gauges and probe tubes which passed through vacuum seals in a side port of the furnace. The probes were constructed from 1 cm diameter tubing and were the same length so that their response to pressure fluctuations would be the same. The pressure in the body of the furnace was measured with an Alphatron ionization gauge. The Alphatron ionization gauge was initially calibrated against a McLeod gauge. Prior to each experiment the thermocouple gauges were calibrated *in situ* against the Alphatron ionization gauge by isolating the furnace from the pumps and admitting air to a series of static pressures. These recalibrations of the thermocouple gauges were reproducible within $\pm 1\mu$ Hg pressure.

To simulate the evolution of gas during melting, a needle valve was connected to the base of the mould. The lower probe was about 9 cm from the

base plate of the mould. The leak rate for each setting of the needle valve was determined from the known volume of the furnace and the observed rate of increase in pressure when the furnace was isolated from the pumps. After each adjustment to a specified leak rate, it was necessary to allow 30 sec to elapse for the attainment of equilibrium, before measuring the pressure at the three points.

The pressure distribution within the mould was determined while melting a mild steel electrode which contained 0.13% C, 0.01% N, 0.005% O and less than 0.0001% H. During these experiments the pressure was measured only at the top and at the lower part of the mould and the temperature of the tip of the lower probe was measured by means of a thermocouple attached to it. When the arc was struck, the pressure rose quickly but, after about 90

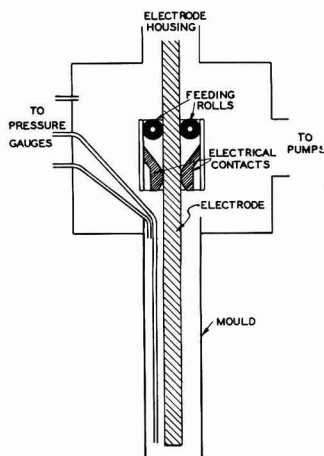


Fig. 1. Arrangement for measurement of pressure distribution with the arc furnace.

sec, dropped to a steady value when the feed rate was uniform. Before melting, the lower probe was about 4 cm from the melting zone and no melting of this probe occurred when a steady feed rate of the electrode was quickly attained and the arc length kept short.

Results

Simulated melting.—The distributions of pressure, for two electrode and two mould sizes, are shown as functions of the leak rate in Fig. 2-5. When the 11.5 cm diameter mould was used the

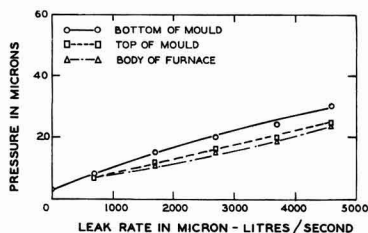


Fig. 2. Distribution in pressure for an electrode 3.2 cm x 3.2 cm in a mould of 11.5 cm diameter.

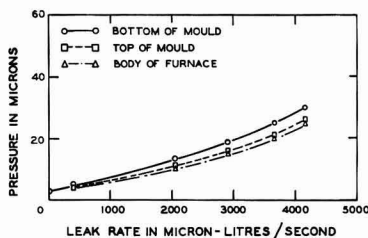


Fig. 3. Distribution in pressure for an electrode 3.2 cm x 4.9 cm in a mould of 11.5 cm diameter.

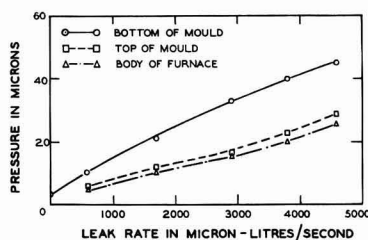


Fig. 4. Distribution in pressure for an electrode 3.2 cm x 3.2 cm in a mould of 7.5 cm diameter.

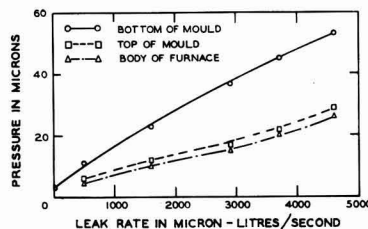


Fig. 5. Distribution in pressure for an electrode 3.2 cm x 4.9 cm in a mould of 7.5 cm diameter.

pressure difference between the top and the lower part of the mould was not very large and was only slightly affected by the electrode size. Relatively large pressure differences were obtained when the 7.5 cm diameter mould was used and these differences varied considerably with the size of the electrode.

Actual melting.—To avoid melting the lower probe, the pressure distribution in the mould was measured only when melting a 3.2 cm square steel electrode in the 11.5 cm diameter mould. Different rates of gas evolution were obtained by melting the same steel electrode at different rates. The rate of melting was controlled by the amount of current used in the arc. Because of the temperature gradient along the lower probe, there was a pressure gradient along this probe.

If the mean free path of the molecules in the hot region of the probe is greater than the diameter of the probe, then the pressure P_A in the hot region is related to the pressure P_B measured at the gauge by:

$$P_A/P_B = \sqrt{T_A/T_B} \quad (I)$$

where T_A is the temperature of the tip of the probe and T_B is the temperature of the gauge.

In the present case the mean free path of the molecules was approximately the same as the diameter of the probe and Eq. (I) gave too high a value for the pressure in the hot region. A correction factor, which depends on the ratio of mean free path to probe diameter, for Eq. (I) has been obtained from the results of other workers (3). Table I lists the measured pressures at the top and the lower part of the mould and also the corrected values of the pressure at the lower part of the mould. Once melting started, the temperature of the probe tip rose quickly for approximately 90 sec but in the following 30 sec, when steady pressure readings were obtained, the temperature of the probe tip increased by only 40°K. Variations in temperature of this order of magnitude have little effect on the calculated pressure in the hot region and the relatively steady temperature of the probe tip suggests that the measured temperature should be close to the gas temperature.

Discussion

On the basis of the kinetic theory of gases, Gruber (4) has calculated the pressure at the top of a mould and then the pressure at the lower part of that mould. In calculating the pressure at the top of the mould a formula was used which is applica-

Table I. Distribution of pressure within a mould of 11.5 cm diameter while melting a steel electrode 3.2 cm square

Arc current (amp)	Temperature of probe (°K)	Pressure at lower part of mold (μ of Hg)	Pressure at lower part of mold, corrected for temperature effect (μ of Hg)	Pressure at top of mold (μ of Hg)	Approx. melting rate (kg/min)
1200	1200	9	15	13	0.5
1500	1200	10	16	14	0.6
1800	1200	13	21	19	0.9
2100	1100	22	32	28	1.3

ble only to a thin aperture, the dimensions of which are small compared with those of the vessel from which the flow is occurring. This leads to considerably lower pressures than are encountered in practice and thus the pressure drop along the mould as calculated by Gruber will be in error.

The following calculation of the pressure drop along the mould during the simulated melting experiments is based on an equation describing the flow of gas through a simple pipe and this is modified to allow for the presence of the electrode. The flow of gas through a circular pipe over a wide range of pressures is described by a semi-empirical equation developed by Knudsen (5) and for air flowing at 25°C may be written in the following form:

$$\frac{Q}{P_1 - P_2} = C_m \left\{ 0.0145 a(P_1 + P_2) + \frac{1 + 0.246 a(P_1 + P_2)}{1 + 0.304 a(P_1 + P_2)} \right\} \quad (\text{II})$$

where Q is the quantity of gas flowing through the pipe, in micron-liters per second; P_1 and P_2 are the pressures at the ends of the pipe, in microns; C_m is the conductance of the pipe when molecular flow is occurring, in liters per second; and a is the radius of the pipe, in centimeters.

For the present case of an electrode within the circular mould, the average separation between the mould and the electrode was used rather than the radius of the mould. The molecular conductance of any duct, for air flowing at room temperature, may be calculated from the following formula (6):

$$C_m = 61.8 K \frac{A^2}{BL} \quad (\text{III})$$

where A is the cross-sectional area of the duct, in square centimeters; BL is the surface area of the walls of the duct, in square centimeters; and K is a constant equal to 1.1 for an annular duct (6) similar to the present arrangement of an electrode in a mould.

From the observed leak rate and the pressure at the top of the mould the pressure drop along the mould was calculated. These values are given in Table II together with those measured during the simulated melting experiments. Reasonable agreement is evident between the calculated and the experimental values. Particular attention is drawn to the close agreement between the values of the pressure difference measured in the actual melting experiments with those measured during the simulated melting experiments. It is possible to compare

Table II. Pressure drop along mould of 11.5 cm diameter containing an electrode 3.2 cm²

Pressure at top of mould (μ of Hg)	Measured pressure drop during simulated melting (μ of Hg)	Calculated pressure drop for simulated melting (μ of Hg)	Measured pressure drop while melting (μ of Hg)
13	3	2.2	2
14	3	2.5	2
19	4	2.7	2
28	4	3.0	4

these two sets of results because the H content of the steel used in the melting experiments is so low. The gases evolved during the melting experiments are mainly N and O or CO. Since these gases have physical properties similar to those of air, the response of the thermocouple vacuum gauges and the conditions of flow in the mould are similar in the two sets of experiments.

The flow of gas depends not only on the conditions already mentioned but also on the temperature of the gas. Therefore it might be expected that, in actual melting experiments where the flow is occurring in both a pressure gradient and a temperature gradient, the pressure drop along the mould would be considerably different from that during a simulated melting experiment where the flow is occurring in a pressure gradient alone. One reason for the close agreement may be that the water cooling of the mould cooled the gas quickly and the flow of gas through the mould occurred essentially at an uniform temperature.

The present work shows that the pressure drop along the mould of a consumable-electrode vacuum arc furnace can be measured in simulated melting experiments or can be calculated if the rate of gas evolution in the region of the arc and the pressure at the top of the mould are known. It also shows that if high pressures in the melting region of vacuum arc furnaces, with the accompanying troublesome glow discharges, are to be avoided it is essential that sufficient free space be provided between the electrode and the mould to ensure rapid removal of the gases evolved during melting.

Particularly when melting Ti, and other similar metals, it is possible that some gas (mainly H) will be evolved from the electrode some distance above the melting zone in the furnace as well as in the melting zone. Such evolution above the melting zone will tend to reduce the pressure gradient along the mould.

Acknowledgments

The work was done under the general direction of H. V. Kinsey of the Department of Mines and Technical Surveys, Ottawa, and was made possible by the award of a Fellowship by the National Research Council of Canada.

Manuscript received April 12, 1957.

Any discussion of this paper will appear in a Discussion Section to be published in the December 1958 JOURNAL.

REFERENCES

1. E. W. Johnson, G. T. Hahn and R. Itoh, "Arcs in Inert Atmospheres and Vacuum," W. E. Kuhn, Editor, p. 19, John Wiley & Sons, Inc., New York (1956).
2. O. Z. Rylski and H. V. Kinsey, *ibid.*, p. 69.
3. S. Dushman, "Scientific Foundations of Vacuum Techniques," p. 67; John Wiley & Sons, Inc., New York (1949).
4. H. Gruber, "Arcs in Inert Atmospheres and Vacuum," W. E. Kuhn, Editor, p. 118, John Wiley & Sons, Inc., New York (1956).
5. S. Dushman, *op. cit.*, p. 115.
6. A. Guthrie and R. K. Wakerling, "Vacuum Equipment and Techniques," p. 35, McGraw-Hill Book Co., New York (1949).

The Anodic Oxidation of Zinc and Zinc-Tin Alloys at Very Low Current Density

S. E. S. El Wakkad,¹ A. M. Shams El Din, and H. Kotb

Department of Chemistry, Faculty of Science, Cairo University, Cairo, Egypt

ABSTRACT

The anodic oxidation of zinc and zinc-tin alloys at very low current density was carried out in solutions of different pH values using the direct potentiometric method. In the case of zinc, the primary oxidation product was a film of zinc oxide or hydroxide less than one molecule thick. When tin was alloyed in different concentrations with zinc, the anodic process resulted in the successive formation of zinc hydroxide, stannous and stannic hydroxides before oxygen evolution. The alloys required less quantities of electricity to passivate than their pure components, thus revealing their noble character. The passivation of the alloys in 0.1N nitric acid is due to a chemical and not to electrochemical process. Critical current densities for passivation also revealed the noble character of the alloys.

The current theories of passivity are based largely on experiments performed with pure metals. Metallic alloys have attracted little attention despite their technical importance. In this laboratory, a systematic study of the anodic oxidation of metals at very low current density was undertaken (1-6). The work has now been extended to simple, two-component alloys. A start was made with speculum (Cu-Sn) alloys (7), and the present paper is a report on the results obtained with Zn-Sn alloys. By using a very small constant polarizing current, and an electrode of relatively large surface area, considerable time was taken by the electrode to pass from hydrogen to oxygen evolution potentials. This enabled the determination of the type and thickness of the oxides formed on the electrode during polarization. On the other hand, current-potential curves were helpful in determining the critical current densities for the passivation process. No work on Zn-Sn alloys from the present stand point has been published. In a publication from the Tin Research Institute (8) the mechanism of anode filming of the alloy in a bath containing sodium stannate and zinc cyanide was described.

Experimental

The electrical circuit used in obtaining the variation of the potential of the anode with the current employed a pentode valve as a constant current device; so the current passing was largely independent of changes in the back emf of the electrode system. The current was supplied from a 250-v dry battery.

The electrolytic cell used was of Pyrex glass without rubber connections. It consisted of a vessel of ca. 500 ml capacity with 5 openings. Three of these, fitted with mercury sealed covers, were for the anode compartment, cathode compartment, and the compartment for the syphon of the calomel electrode, respectively. The last two compartments

were fitted with sintered glass in order to prevent contaminations with the anolyte. The other openings were for the inlet and outlet of pure nitrogen.

The zinc electrode.—This was prepared by electrodeposition from an acidified zinc sulfate bath prepared by dissolving 145 g $ZnSO_4 \cdot 7H_2O$ in 1 liter N H_2SO_4 . Electrodeposition was carried out using a current density of 12.5 ma/cm² for 40 min on a Pt foil 2 cm² apparent area. This gave a spongy deposit with relatively large area.

Zinc-tin alloys.—These were also electrodeposited from a bath recommended by the Tin Research Institute (8), prepared by dissolving 30 g sodium stannate, 2.5 g zinc cyanide, 27.5 g sodium cyanide, and 5 g of sodium hydroxide in 1 liter of water. Electrodeposition was carried out at $65 \pm 2^\circ C$ on a Pt foil of 2 cm² apparent area for 20 min with a current density of 25 ma/cm². This bath gave a deposit containing 25% Zn. A cast anode of the same composition was used and was filmed to insure the dissolution of its tin content in the quadrivalent state (8). The area of the anode was adjusted to give an anode current density of 16 ma/cm². Alloys of 12½% and 50% Zn were prepared by varying the zinc and free hydroxide content of the bath. All deposits were analyzed for their tin content by the tannin method, and the analysis was confirmed by the Tin Research Institute. Alloys prepared either by electrodeposition on a copper substrate or by casting gave exactly the same behavior.

Each experiment was carried out with a freshly prepared electrode. Whenever the bath showed signs of deterioration, a new bath was prepared.

Measurements were carried out mainly in alkaline solutions, viz., 0.1N sodium hydroxide (pH = 13), 0.1N sodium carbonate (pH = 11.2) and 0.1M sodium borate (pH = 9.2). Measurements were also extended to neutral and acid solutions; 0.1M sodium sulfate (pH = 7), acetate buffer of pH = 6, and 0.1N nitric acid (pH = 1). All solutions were pre-

¹ Deceased.

pared from AnalaR materials and conductivity water. The solution in the cell was boiled before use and cooled in an atmosphere of pure nitrogen. The detailed experimental procedure for obtaining the anodic, cathodic, and decay curves was essentially as described before (1). All measurements were performed at 25°C.

Current-Potential Curves for Zn, Sn, and Zn-Sn Alloys

When a metal electrode is polarized anodically in a solution where passivity sets in readily, the primary oxidation process will be the oxidation of the metal itself. If the current is raised, a value is reached at which the process changes to that of oxygen evolution. This critical current for passivation is a good measure of the nobility of the metal; the nobler the metal, the smaller the current at which the potential changes to that of oxygen evolution. Critical current densities for passivation for Zn, Sn, and Zn-Sn alloys of different compositions were determined. The procedure of Uhlig and Woodside (9) was followed. Measurements were carried out in 0.1M borax solution, since in such medium the oxides of Zn and Sn possess minimum solubility. The electrode was first cathodically polarized with a current of 100 μA /electrode until a steady potential was reached. This took from 15 to 30 min. The cathodic current was then disconnected and the potential was left to decay to the open circuit value till a potential was reached which did not vary more than 20 mv in a period of 5 min. A small anodic current was then imposed on the electrode and the corresponding potential was recorded. The current was again disconnected and the open circuit value awaited. Anodic polarization was started again with a higher current. The process of connecting and disconnecting the current was repeated until the potential of the electrode changed toward oxygen evolution potential.

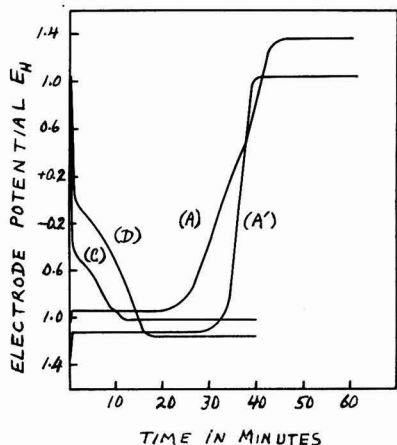
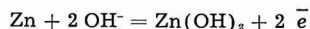


Fig. 1. Anodic polarization of Zn in: (A) 0.1M borax solution with a polarizing current of 20 μA /electrode; (A') 0.1M NaOH solution with a polarizing current of 300 μA /electrode; (C) cathodic curve in 0.1M borax with a polarizing current of 5 μA /electrode; (D) anodic decay in 0.1M NaOH solution.

Results and Discussion

Behavior of pure zinc.—Curve A, Fig. 1, is the characteristic anodic polarization curve of the Zn electrode in 0.1M sodium borate solution when using a polarizing current of 20 μA /electrode. Curve A' in Fig. 1 represents the behavior of the Zn anode in 0.1N NaOH solution when using a polarizing current of 300 μA /electrode. From these curves, which show the variation of the Zn electrode potential with the quantity of electricity passed, it can be seen that, at first, there is a rapid build up of potential, ascribed by similarity to cases studied (1-7) to the charging of the double layer. This is followed by one step before oxygen evolution. Measurements from a large number of polarization curves gave an average value for the double layer capacity of 6,000 μF /electrode in the borate solution. In the hydroxide solution, the average capacity of the double layer was comparable with that in the borate solution. The arrest in the borate solution appears to start at a potential of -0.95 v, and in the hydroxide solution at -1.15 v. In Table I are shown the potentials of this arrest in the two solutions, respectively, compared with the equilibrium potentials of the system Zn/Zn(OH)₂ at the corresponding pH values. These latter were calculated as follows: Taking the free energy of OH⁻ and Zn(OH)₂ as $-37,595$ and $-132,600$ calories, respectively (10), the free energy of the reaction:



was calculated to be $-57,410$ cal and hence E_{B}° (the potential at the extreme alkaline range of pH) is -1.245 v. By applying the ordinary equation for the variation of the potential of the system with pH, the values shown in column III of Table I were obtained.

The very close agreement between the starting potential of the arrest as obtained from polarization curves and the potential of the system Zn/Zn(OH)₂ at the corresponding pH value leaves little doubt that this step corresponds to the formation of zinc hydroxide or oxide on the electrode before oxygen evolution. The standard condition of the Zn electrode was taken to be that of the borate solution. The quantity of electricity passed from the beginning to the end of this step in the borate solution was found to be reproducible and amounting to 30,000 μC /electrode. This is sufficient for the liberation of 9.37×10^{16} atoms of oxygen. Taking the specific gravity of the Zn metal as 7.1 g/cm³, the diameter of the Zn atom was calculated to be 2.48 Å, and hence there would be 1.63×10^{15} atoms of Zn/true cm² of the Zn surface. An estimation of the ratio real/apparent area of the electrode could be determined from the capacity of the double layer

Table I

Solution	Starting potential of the arrest (v)	Equilibrium potential of the system Zn/Zn(OH) ₂
0.1M Sodium borate	-0.95	-0.96
0.1N Sodium hydroxide	-1.15	-1.18

before oxide formation. The capacity of the anodic double layer was recently determined by El Wakad and Salem (11) to be $100 \mu\text{F}/\text{real cm}^2$. As the capacity of the double of the Zn electrode amounts to $6,000 \mu\text{F}/\text{electrode}$, the ratio real/apparent area will be 30/1; hence, there would be 9.78×10^{16} atoms of Zn on the whole surface of the electrode. This shows that the quantity of electricity passed during oxide formation corresponds to the formation of less than a unimolecular layer of the oxide. In NaOH solution the quantity of electricity passed during oxide formation amounted to $594,000 \mu\text{ coulomb}$. This is sufficient for the formation of a zinc hydroxide layer ~ 19 molecules thick. This high value suggests that the oxide in such a medium is more soluble than in the borate solution. In 1N NaOH solution, using currents up to 2 ma/electrode, the potential did not rise to oxygen evolution value, but remained constant at the $\text{Zn}/\text{Zn}(\text{OH})_2$ at the corresponding pH value, viz., -1.24 v , denoting anodic dissolution of the formed hydroxide to form zincate.

In 0.1N sodium carbonate solution of $\text{pH} = 11.2$, an arrest was recorded due to the formation of zinc oxide. However, the potential of the electrode did not reach oxygen evolution value and showed irregularities due to the probable formation of non-conducting nonadherent basic carbonate film which readily peeled away from the surface of the electrode. Similar behavior was observed in the case of the nickel electrode in borate solutions (2), and in the case of the manganese electrode in phosphate solutions (12).

Cathodic curves reveal that, on reversing the polarizing current to make the working electrode the cathode, reduction of the zinc hydroxide film takes place at more or less its reversible potential. As a representative example, the cathodic behavior of zinc in sodium borate solution with a polarizing current of $5 \mu\text{a}/\text{electrode}$ is shown by curve C, Fig. 1. In NaOH solution, the reduction step corresponds to the deposition of Zn from zincate solution.

Anodic decay curves reveal that, on interruption of the polarizing current when the electrode was at oxygen evolution value, the potential dropped to a somewhat more positive value than the $\text{Zn}/\text{Zn}(\text{OH})_2$ system at the corresponding pH value, but continuously drifted with time toward the above system. The time of this drift varied from one solution to the other. Curve D of Fig. 1 is an example of the anodic decay in NaOH solution.

Anodic polarization of Zn in solutions of pH values less than 9 resulted in the dissolution of the Zn at the $\text{Zn}/\text{Zn}(\text{OH})_2$ potential.

Time-potential curves for zinc-tin alloys.—Curves A and A' of Fig. 2 are the characteristic anodic polarization curves for Zn-Sn alloys containing 25% and 12½% Zn, respectively, in sodium borate

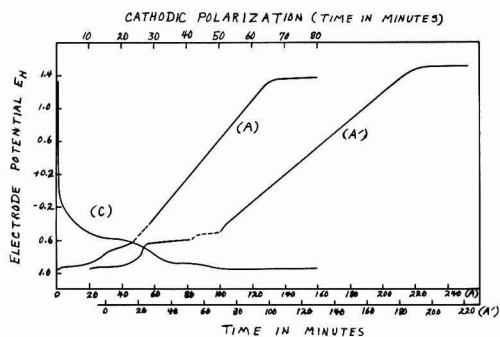


Fig. 2. Anodic polarization of 25% Zn alloy (A) and 12½% Zn alloy (A') in 0.1M borax solution; Polarizing current = $10 \mu\text{a}/\text{electrode}$; dotted parts at $1 \mu\text{a}/\text{electrode}$; (C) cathodic polarization of 50% Zn alloy with a polarizing current of $5 \mu\text{a}/\text{electrode}$.

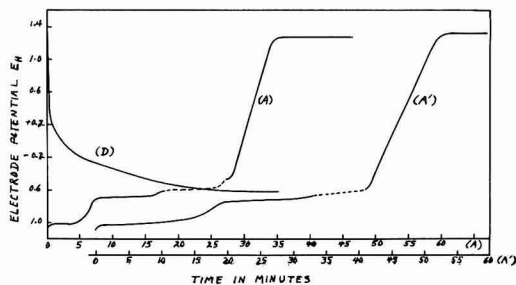


Fig. 3. Anodic polarization of 25% Zn alloy (A) and 50% Zn alloy (A') in 0.1M sodium carbonate solution; polarizing current = $60 \mu\text{a}/\text{electrode}$, dotted parts at $10 \mu\text{a}/\text{electrode}$; (D) anodic decay for 12½% Zn alloy.

solution. The polarizing current was $10 \mu\text{a}/\text{electrode}$. In the dotted parts of the curves, the polarizing current was decreased to $1 \mu\text{a}/\text{electrode}$ to decrease the rate of the anodic process to be followed by the direct potentiometric method. Curves A and A' of Fig. 3 are the same anodic polarization curves for alloys containing 25% and 50% Zn, respectively, in 0.1M sodium carbonate solution. The polarizing current was $60 \mu\text{a}/\text{electrode}$ and the dotted parts were obtained with a current of $10 \mu\text{a}/\text{electrode}$. From these curves, which show the variation of the alloy potential with the quantity of electricity passed, it can be seen that there is a rapid short build up of potential, due to the charging of the double layer, followed by 3 well-defined steps before oxygen evolution. It was difficult in this case to determine the exact capacity of the double layer because the potential of the electrode, when made the cathode, was very near to the first arrest. The starting potential of three steps, in the borate solution, were, respectively, -0.95 v , -0.66 v , and -0.52 v . In the carbonate solution, these were -1.04 v , -0.75 v , and -0.59 v . In Table II, the starting po-

Table II

Solution	1st	Starting potential of arrest			Equilibrium potential of the system		
		2nd	3rd	Zn/Zn(OH) ₂	Sn/Sn(OH) ₂	Sn(OH) ₂ / Sn(OH) ₄	
0.1M Borax	-0.95	-0.66	-0.52	-0.96	-0.64	-0.47	
0.1M Carbonate	-1.04	-0.75	-0.59	-1.08	-0.76	-0.59	

tential of the three steps in the two electrolytes are compared with the equilibrium potentials of the systems Zn/Zn(OH)₂, Sn/Sn(OH)₂, and Sn(OH)₂/Sn(OH)₄.² The last two values were obtained by taking the free energy of Sn(OH)₂, Sn(OH)₄, and OH⁻ as -117,600, -227,500, and -37,595 calories, respectively (13). The free energy of the reactions: Sn + 2 OH⁻ = Sn(OH)₂ + 2 e⁻ ΔF° = -42,410 cal. and

Sn(OH)₂ + 2 OH⁻ = Sn(OH)₄ + 2 e⁻ ΔF° = -34,710 cal. This gives E_p⁰ values of -0.92 and -0.75 v, respectively.³

By applying the ordinary equation for the variation of the potential of the above systems with pH, the values in columns 5, 6, and 7 in Table II were obtained.

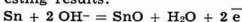
The very close agreement between these two sets of potentials leaves little doubt that these steps correspond to the consecutive formation of zinc oxide or hydroxide, stannous and stannic hydroxides, respectively, before oxygen evolution. Thus, on anodic polarization, the behavior of the alloy appears to be a combination of the behavior of its pure constituents. The same conclusion was reached in the case of Cu-Sn alloys (7).

The quantity of electricity consumed in the passivation of the alloy varied from one composition to the other, and also depended on the pH value of the solution. Thus, for example, whereas the first step (formation of zinc hydroxide) in the borate solution for the 25% Zn alloy consumed 15,000 μcoulomb, the corresponding step for the 50% Zn alloy in the carbonate solution consumed 86,000 μcoulomb.⁴ Also in the step corresponding to the formation of Sn(OH)₂ in the borate solution for the 12½% Zn alloy, the quantity of electricity amounted to 18,000 μcoulomb, while in the corresponding step for the 25% Zn alloy in the carbonate solution, the same quantity was 36,000 μcoulomb.

Alloys prepared by electrodeposition are considered to have an area more or less comparable with those of the Zn and Sn alone. The standard condition for the alloy was taken to be that of the borate solution since the oxides of both Zn and Sn show minimum solubility at that pH. Taking the alloy containing 25% Zn, which has technical importance, as an example, the quantity of electricity that passed in the formation of zinc hydroxide amounted to 15,000 μcoulomb/electrode. Comparison of this amount with that obtained in the case of pure Zn electrode revealed that the alloy required a lesser amount of electricity to passivate. The quantity of

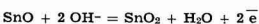
² In this comparison, no correction of the measured potentials was made to account for the fact that the activities in the alloys are less than unity. This is because such variations are uncertain and small.

³ Calculation based on the assumption that stannous and stannic oxides and not the hydroxides are formed gave the following interesting results:



$$\Delta F^\circ = -43,000 \text{ cal.}$$

$$E^\circ_{\text{p}} = -0.932 \text{ v}$$



$$\Delta F^\circ = -44,200 \text{ cal.}$$

$$E^\circ_{\text{p}} = -0.958 \text{ v}$$

which directly suggest that the oxidation of stannous oxide to the corresponding stannic oxide is improbable, since the potential of the couple SnO/SnO₂ is more negative than that of Sn/SnO. This supports the conclusion that stannous and stannic hydroxides are formed on the oxidation of the Sn electrode.

For the Zn electrode, no noticeable difference was found in the free energy if calculations were made for Zn(OH)₂ or ZnO.

⁴ The end of the step is taken as the point of intersection of the extrapolated lines from the bottom of the step with that obtained from the rising part of the following one.

electricity that passed in the second arrest (stannous hydroxide formation) was found to be 11,000 μcoulomb, which was less than the corresponding value for pure Sn under similar conditions. This supports the conclusion that alloys are nobler than their constituents (7,9).

In 0.1N NaOH solution the behavior of the alloy was rather simple. On starting the anodic polarization, a step at -1.15 v was obtained. The potential of this step is in good agreement with that of the system Zn/Zn(OH)₂ at the corresponding pH value. After a time, dependent on the Sn content of the alloy, the potential rose to -0.90 v where it remained constant. This latter value suggested that the formed stannous hydroxide is freely soluble in the hydroxide solution to give the stannite (6).

The behavior of the alloy in 0.1N HNO₃ is of extreme interest. Although the electrode was immersed in the HNO₃ solution with the current switched on cathodically, the potential was found to rise to more positive values, even when using a current as high as 1 ma/electrode. This behavior is shown for the alloys 25% Zn and 50% Zn in Fig. 4. An arrest was obtained at -0.44 v in close agreement with the Zn/Zn(OH)₂ potential at this pH, viz., -0.46 v. The potential then rose to give two steps whose potentials agreed well with those of the systems Sn/Sn(OH)₂ and Sn(OH)₂/Sn(OH)₄ at the same pH value. When the current was reduced to 400 μa/electrode and reversed to start the anodic polarization, the potential of the electrode changed directly to oxygen evolution value. The heads of the arrows in Fig. 4 show the time at which the current was reduced and reversed. Such behavior indicated that the electrode was already in the passive state. This state of affairs could be explained by taking into consideration the oxidizing effect of the HNO₃. The Zn in the alloy was oxidized by the acid to ZnO, and the rate of oxidation seems to be too high to be stopped by a cathodic current as high as 1 ma/electrode. Zinc oxide, being freely soluble in the acid, goes into solution leaving the Sn on the surface. This latter also is oxidized in a similar fashion to stannous hydroxide (6). However, after a short time, the potential changed to that of the Sn(OH)₂/Sn(OH)₄ system, where it remained constant. On reversing the polarizing current to start the anodic oxidation, the potential changed directly toward

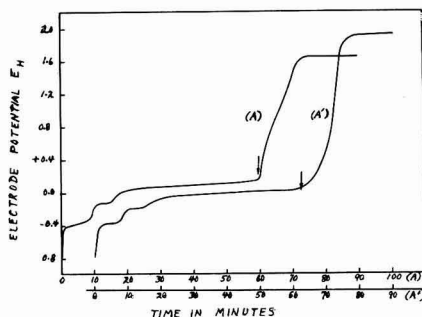


Fig. 4. Cathodic and anodic characteristics for 25% Zn alloy (A) and 50% Zn alloy (A') in 0.1N nitric acid solution; polarizing current = 1 ma/electrode; arrows point to time of start of anodic polarization with 400 μa/electrode.

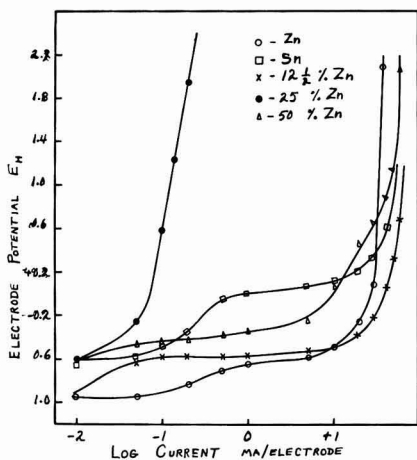


Fig. 5. Potential-log i curves for Zn, Sn, and Zn-Sn alloys in 0.1M borax.

oxygen evolution value, denoting the passivity of the electrode.

The cathodic curves reveal the reduction of both stannic and stannous hydroxides followed by the reduction of zinc hydroxide before hydrogen evolution. As a representative curve, the cathodic behavior of the 50% Zn alloy in 0.1M borax solution with a polarizing current of $5 \mu\text{A}/\text{electrode}$ is shown by curve C, Fig. 2.

The anodic decay curves reveal that, on interruption of the polarizing current, the potential dropped to a value somewhat more positive than the corresponding $\text{Sn}(\text{OH})_2/\text{Sn}(\text{OH})_2$, and changed slowly toward the value of this system. The decay curve for the 12½% Zn alloy in 0.1M sodium carbonate solution is shown by curve D, Fig. 3.

It is of interest to remark here on the effect of alloying on the potential of oxygen evolution. Thus, whereas oxygen evolution potential on pure Sn and pure Zn in 0.1M borax solution are, respectively, +1.21 and +1.36 v with a polarizing current of $20 \mu\text{A}/\text{cm}^2$, the corresponding values for the 12½%, 25%, and 50% Zn alloys in the same solution are respectively +1.51, 1.36, and 1.40 v. Although no general conclusion could be drawn at the moment, it could be said that the addition of Zn to Sn raised the oxygen evolution potential on the alloy to at least that of the Zn alone. The effect of alloying over a wider range of Zn content on the oxygen evolution potential is still under investigation.

In Fig. 5 the plot of $\log i$ vs. potential for pure Zn, pure Sn, and Zn-Sn alloys of compositions varying between 12½% Zn and 50% Zn is shown. This enables the determination of the critical current densities for passivation (see experimental section). The behavior of the electrodes on polarization varied from one case to the other. Thus, with the 25% Zn alloy, a critical current density could not

be determined easily. Any applied current raised the potential to more positive values and no sudden break in the $\log i$ -potential curve was observed. With the other electrodes on the other hand, sharper critical currents were obtained. The noble character among the electrodes studied decreased in the order 25% Zn alloy, 50% Zn alloy, Zn, Sn, and 12½% Zn alloy. These findings are in harmony with the general conclusion that the alloys are nobler in character than their components.

Summary and Conclusion

The anodic behavior of Zn and Zn-Sn alloys at very low current density was studied in solutions where passivity readily sets up. Two anodic processes occur at a Zn electrode when the current is reversed from cathode to anode: (a) the charging of an anodic double layer, and (b) the formation of zinc hydroxide film less than one molecule thick.

The anodic polarization of Zn-Sn alloys resulted in the consecutive formation of zinc hydroxide, stannous and stannic hydroxides before oxygen evolution. These oxides formed at their reversible potentials; thus the behavior of the alloys on polarization is the combined behavior of its constituents. The quantities of electricities consumed in bringing the electrode from hydrogen evolution to oxygen evolution potentials in the case of the alloys were less than those used by either Zn or Sn. This demonstrated the noble character of the alloys. The same conclusion was also reached from current potential curves.

Manuscript received Feb. 1, 1957. This paper was prepared for delivery before the Cincinnati Meeting, May 1-5, 1955.

Any discussion of this paper will appear in a Discussion Section to be published in the December 1958 JOURNAL.

REFERENCES

1. S. E. S. El Wakkad and S. H. Emara, *J. Chem. Soc.*, **1952**, 461.
2. S. E. S. El Wakkad and S. H. Emara, *ibid.*, **1953**, 3504.
3. S. E. S. El Wakkad and S. H. Emara, *ibid.*, **1953**, 3508.
4. S. E. S. El Wakkad and A. M. Shams El Din, *ibid.*, **1954**, 3094.
5. S. E. S. El Wakkad and A. M. Shams El Din, *ibid.*, **1954**, 3098.
6. S. E. S. El Wakkad, A. M. Shams El Din, and J. A. El Sayed, *ibid.*, **1954**, 3103.
7. S. E. S. El Wakkad, T. M. Salem, A. M. Shams El Din, and Z. Hanafi, *ibid.*, **1956**, 2857.
8. Tin Research Institute, Technical Publication, March, 1952.
9. H. H. Uhlig and G. E. Woodside, *J. Phys. Chem.*, **57**, 280 (1953).
10. W. M. Latimer, "The Oxidation States of the Elements and their Potentials in Aqueous Solutions," Prentice-Hall, New York, p. 168 (1953).
11. S. E. S. El Wakkad and T. M. Salem, *J. Chem. Soc.*, **1955**, 1489.
12. S. E. S. El Wakkad and A. M. Shams El Din, Unpublished work.
13. Reference (10), p. 148.

The Anodic Oxidation of Cadmium

I. Mechanism of Film Formation

Phyllis E. Lake and E. J. Casey

Defence Research Chemical Laboratories, Ottawa, Canada

ABSTRACT

Cadmium oxidizes anodically in hydroxide solutions to form films of reaction products which control the subsequent anodic processes. The electro-metrics of film formation and reduction were determined, and various other definitive experiments were done which permit an interpretation of the general mechanism of oxidation to be made. The film forms as CdO which is converted into Cd(OH)₂ at a rate dependent upon various experimental factors.

Interest in the Ni-Cd battery has focused our attention on the behavior of Cd during electrolytic oxidation and reduction in KOH electrolyte, both with and without K₂CO₃ impurity.

The purpose of this work was to establish the nature of the anodic reactions on Cd metal in caustic electrolytes, and to try to determine the general mechanism of the process.

Experimental Materials and Methods

The Cd electrodes were prepared by casting reagent grade Cd into rectangular blocks, and painting all but a known apparent area with stop-off lacquer; thus the sample had a polycrystalline surface. The electrode was rinsed with dilute HNO₃ and running distilled water. It was then placed in the test cell and reduced at 0.5 ma cm⁻² until hydrogen was evolved. Even with these precautions to insure a clean surface by removal of all oxide, reproducibility was poor. The real area of the electrodes probably varied from sample to sample. In addition, a finite thickness of metal was removed from the electrode face during each oxidation and cleaning, so that the crystal faces presented to the electrolyte at the beginning of each experiment were different. These factors lead to variations in current density and therefore in measured passivation times. Values plotted in Fig. 2, 3, and 4 are average values for several determinations.

To keep the current distribution as uniform as possible a cylindrical cell of which the anode and cathode formed the ends was used in most experiments. For measurement of gas evolution a bell shaped cell was used with the electrodes placed one above the other. Experiments were done in both air-free and air-saturated solutions, but no significant differences were noted in the amount of Cd oxidized before passivation occurred.

Using solutions freshly prepared from reagent grade chemicals, oxidation studies were done at 25°, 0°, and -40°C; gas evolution and rate of depassivation were measured at 25° only. Oxidation current densities ranged from 10 μa to 5 ma cm⁻². The KOH and K₂CO₃ solutions ranged from 0.72 to 7.2N; mixed solutions were always 7.2N with respect to

potassium ion and contained varying proportions of OH⁻ and CO₃²⁻.

The operating voltage of the Cd was measured against an Hg/HgO/KOH reference electrode and the recorded potential values are given with reference to this electrode. The additional liquid junction potential introduced was constant throughout each experiment and was therefore disregarded.

To prepare samples of film material for x-ray diffraction studies, the electrode was removed from the solution immediately after the oxidizing current was switched off, washed quickly with distilled water to remove the electrolyte clinging to the film, then rinsed with absolute methanol. The electrode was then air dried and the film scraped off. All samples were prepared from passivated electrodes. During the early part of the oxidation the film was too thin to be removed mechanically from the metal. For all photographs the Unicam rotation camera S25 was used (radius 30 mm, copper radiation, 40 kv, 15 ma, and a nickel filter).

Results

Electrometrics.—Figure 1 is a typical voltage vs. time curve for anodic oxidation of Cd at constant current in a caustic electrolyte. The potential remained flat near the reversible value for Cd/Cd(OH)₂ while the electrode became covered with film. The voltage then rose and oxygen started to evolve. The voltage continued to rise quickly to ~1

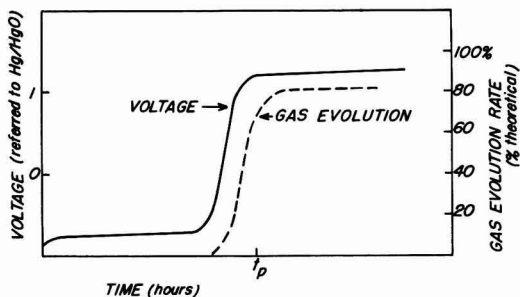


Fig. 1. Variation of voltage with time for oxidation of Cd at constant current.

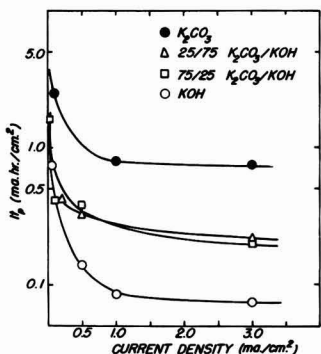


Fig. 2. Variation of It_p with current density at 25°C

v , then flattened off (E_p) and rose very slowly (a few mv/hr) for periods of up to 24 hr. The voltage vs. time curve for the mixed and carbonate electrolytes was similar in shape, except that E_p was higher and more constant. Gas evolution started slowly and rose to a steady value which depended on the current density and electrolyte composition. In K_2CO_3 solutions at high current densities, it was very close to 100% of theoretical (based on total current); it was somewhat less in hydroxide solutions and at lower current densities.

The amount of Cd oxidized before passivation occurred (It_p , where I is current density in $ma\ cm^{-2}$ and t_p is the time in hours taken to reach a relatively constant potential at which oxygen is evolved) is dependent on current density, temperature, and composition of the electrolyte (Fig. 2, 3, 4). At low current densities at room temperature the curves It_p vs. composition follow the "U" shape of the curve solubility of CdO vs. composition. Increasing the current density decreases It_p , the effect being most marked in pure hydroxide solutions. Decreasing the temperature also decreases It_p , but the effect is most pronounced in high carbonate solutions. These results are considered in detail later.

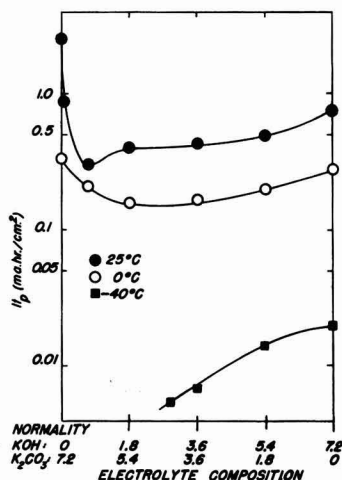


Fig. 3. Variation of It_p with temperature and composition at 0.07 ma/cm^2 .

To determine the efficiency of the oxidation process, reductions were carried out at the same current density as the preceding oxidation and the time taken to reach a constant potential at which hydrogen was evolved (t_r) was measured. If the oxidation time (t_{ox}) was shorter than t_p , then $t_r = t_{ox}$, if t_{ox} was equal to or somewhat longer than t_p , $t_r = t_p$. If the electrolyte in which the electrode was oxidized was replaced with fresh electrolyte of the same composition before the reduction was carried out, the same values for t_r were found. Thus, all the current passed (experimental error $\pm 3\%$) up to time t_p was utilized in the oxidation of Cd and all the Cd was present in the film. However, if oxidation was continued for a long time, i.e., $t_{ox} \gg t_p$, some of the outer film sometimes fell off the electrode, and $t_r < t_p$. A small amount of Cd was also dissolved in the electrolyte, since Cd was found on the cathode after long oxidations ($t_{ox} \gg t_p$).

Film composition.—The color of the film depends on the electrolyte and current density. At low current densities in KOH solutions interference colors

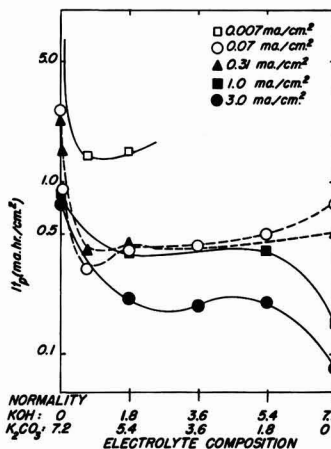


Fig. 4a. Variation of It_p with electrolyte composition and current density at 25°C.

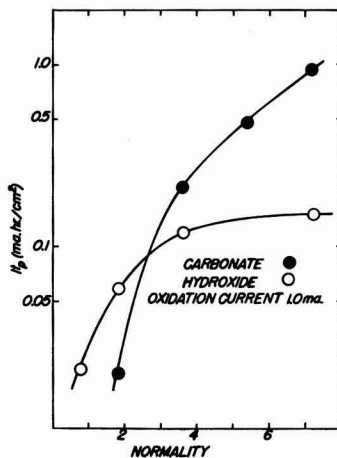


Fig. 4b. Variation of It_p with OH^- and CO_3^{2-} concentration at 25°C.

were noted as the film thickened, and in some cases different rates of film growth on different crystal faces could be thus observed. In mixed and carbonate electrolytes and at higher current densities these colors could not be observed, and the initial film was brown or black.

After the electrode was passivated the film consisted of a dark, tightly adherent layer next to the metal and an outer layer of a loose, scaly or powdery, yellow material which was easily scraped off. X-ray diffraction patterns showed that the outer material was essentially $\text{Cd}(\text{OH})_2$ in all but the pure carbonate solutions. The samples taken from films formed in carbonate solutions consisted of CdCO_3 contaminated with $2\text{K}_2\text{CO}_3 \cdot 3\text{H}_2\text{O}$ which had not been removed during the washing. There was no evidence of other Cd compounds in the outer film, and only weak traces of unidentifiable materials in a few samples. It was not possible to remove the inner layer mechanically for x-ray studies.

Huber has shown (1) by electron diffraction photographs that the initial film formed on Cd in NaOH and Na_2CO_3 solutions is the oxide, and that on continued oxidation this primary product is converted to $\text{Cd}(\text{OH})_2$ in NaOH solutions, and through basic carbonate to CdCO_3 in Na_2CO_3 solutions. Since Huber's observations of composition of the outer layer are parallel to the authors' and the inner layer was always the dark color of CdO, it is assumed that the inner layer of film was essentially cadmium monoxide.

Autocorrosion.—The reduction time t_r was measured for samples which had been cleaned and then exposed to the solutions for varying lengths of time with no external current flowing. When the electrode was first immersed in the solution, the autocorrosion rate was equivalent to a few microamperes, but decreased with time. Therefore, it is of little importance except at very low current densities.

The depassivating reaction.—Passivated electrodes allowed to stand in contact with the electrolyte with no current flowing became "depassivated". That is, when the oxidizing current was turned on again, Cd oxidized at a voltage near the reversible value for a time t_p' before the voltage again rose to the passivation voltage. Thus, some of the passivating film was removed or changed to nonpassivating film during the stand time (t_s), and the passivating film was rebuilt during t_p' .

The amount of Cd oxidized to repassivate the electrode (It_p') should be equal to the amount of passivating film converted into nonpassivating film during the time $t_s + t_p'$. This enables one to calculate the current which would be equivalent to the average rate R_2 of the depassivating reaction during the time $t_s + t_p'$. These equivalent currents are plotted against time in Fig. 5a and 5b. It can be seen that the rate of the depassivating reaction decreases with time and depends on the composition of the electrolyte, being higher in carbonate solutions.

It is well known (2,3) that cadmium monoxide and hydroxide are soluble in alkaline solutions, and indeed Rozentsveig, *et al.*, (2) have evidence that the Cd is present in a negative ion complex.

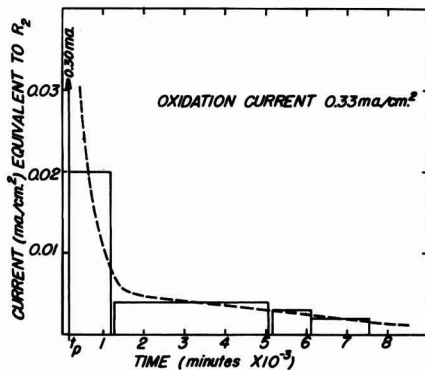


Fig. 5a. Determination of R_2 for K_2CO_3 solution

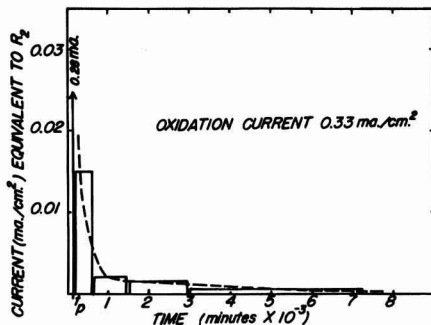


Fig. 5b. Determination of R_2 for KOH solution

The amount of Cd present in samples of the test electrolytes which had stood in contact with CdO for 8 days at 25°C was measured polarographically and results are plotted in Fig. 6a and b. Agreement with Rozentsveig's data is quite good. However, Dirkse (4) has shown that KOH solutions, previously saturated with respect to ZnO, continue to dissolve the reaction products formed by the anodic oxidation of Zn, and that on standing the excess eventually precipitates out as ZnO. The amount of Cd oxidized before passivation (i.e., It_p) in solutions which had been previously saturated with cadmium [KOH with $\text{Cd}(\text{OH})_2$ and K_2CO_3 with CdCO_3] was smaller than in the corresponding unsaturated solution, but was much larger than would be expected if no supersaturation occurred. Rosentsveig, *et al.*, (2) have estimated that 3-8 monolayers of oxide are necessary for passivation. This is equivalent to approximately $0.01 \text{ ma hr cm}^{-2}$. The measured values are shown in Table I.

Thus, it appears that the behavior of Cd with respect to alkaline and carbonate solutions is parallel to that which Dirkse found for Zn in alkaline solutions and that the depassivation reaction depends not only on the actual solubility of CdO, but also on

Table I. Values for It_p

	Measured		Calculated
	Unsaturated	Saturated	
KOH	0.52	0.25	~ 0.01
K_2CO_3	0.89	0.75	~ 0.01

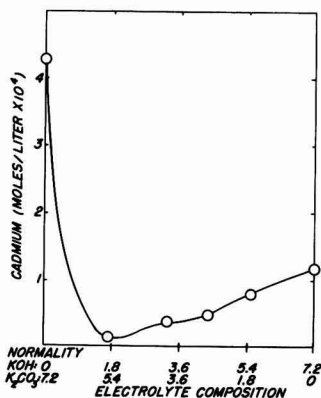


Fig. 6a. Variation of solubility of cadmium oxide with electrolyte composition.

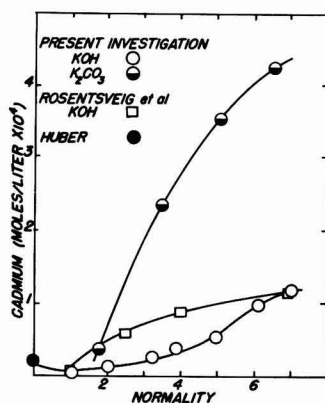


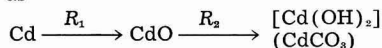
Fig. 6b. Variation of solubility of cadmium oxide with KOH and K_2CO_3 concentration.

the degree of supersaturation which can exist before precipitation occurs.

Discussion

From considerations of the detailed results a mechanism has evolved. For simplicity, the mechanism is presented first, and then the experimental results interpreted in these terms.

The formation of the film must be at least a two-step process, formation of CdO and chemical conversion to $Cd(OH)_2$ or $CdCO_3$, and can be represented as



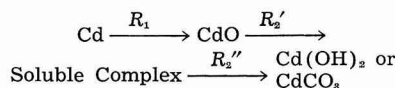
where R_1 depends on the anodic current and R_2 on the rate of supply of the converting species to the outer surface of the CdO.

There are two ways in which current may pass through the oxide film (a) electron transfer with O_2 evolution at the surface, and (b) ion transfer (Cd^{++} out or O^- in) through the film. The electronic resistance of CdO is low at room temperature and the ionic resistance would be expected to be much higher (5). But Hickling has shown that O_2 overvoltage on Cd is high (6). Since large amounts of Cd are oxidized before the electrode becomes passive, it appears that the high oxygen overvoltage permits ionic migration to take place during oxida-

tion, until the CdO builds to such a thickness that $IR_{ionic} = IR_{electronic} + E_{overvoltage}$, at which time oxygen starts to be discharged.

Huber (1) observed that no carbonate precipitate was formed until after the electrode had been oxidized for some time, and the same observation was made under the present conditions. This behavior can be explained if an amount of CdO far in excess of that to be expected from solubility product considerations must be dissolved to produce the degree of supersaturation necessary to initiate precipitation. Precipitation of the carbonate or hydroxide then begins, and continues at a rate which depends on the degree of supersaturation. The degree of supersaturation, in turn, depends on the rate of precipitation and the rate of dissolution. The rate of dissolution depends on the thickness of the precipitated film through which the "dissolving agent" must pass to dissolve the CdO. Thus, the dissolution reaction goes at its maximum rate until supersaturation is reached; it then decreases as the thickness of the precipitated film increases. The precipitation reaction does not start until the critical concentration is reached. It then starts and rises until the rate of precipitation exceeds the rate of dissolution, after which it decreases in a manner which is interdependent with the decrease in rate of the solution reaction.

In summary, the over-all reaction can now be represented as three steps,



where R_2' is the rate of solution and R_2'' the rate of precipitation. The time dependence of R_2' and R_2'' can be roughly sketched as seen in Fig. 7,

Nature of the Passivating Film.—Hickling, in his studies of oxygen overvoltage on metals (6), found that below 10^{-5} amp cm^{-2} no oxygen discharge occurred on Cd. The authors' work has shown that at 10^{-5} amp cm^{-2} at $25^\circ C$, a Cd electrode continues to oxidize at -0.8 v for periods of at least 28 days ($It = 8.7$ ma hr cm^{-2}). Figure 5 shows that, in this case, the removal rate R_2 is much greater than R_1 , thus the CdO would be removed as fast as it is formed. The porous conversion product accumulates, the oxide film does not, and the electrode does not passivate. On electrodes oxidized at higher current densities, such that $R_2' < R_1$ initially or that R_2' becomes smaller than R_1 after some accumulation of conversion product, the monoxide film builds

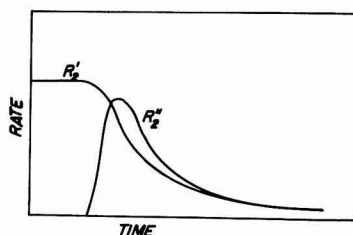


Fig. 7. Schematic representation of the variation of R_2' and R_2'' with time.

up, and the electrodes do passivate (Fig. 2). Thus, the oxide layer appears to be the primary passivating layer, while the outer layer of conversion product affects passivation only insofar as it controls R_2' . The growth pattern of the cadmium monoxide film affects the amount of Cd which must be oxidized to produce a passivating layer. Further work is in progress on this problem.

Effect of current density and temperature on I_t .—(Fig. 2 and 3). These effects are similar since increasing I increases R_2 , and hence increases $(R_1 - R_2')$, while holding I constant and decreasing the temperature decreases R_2 , and increases $(R_1 - R_2')$. It must be noted that, although the equations allow for the case of $R_2' \gg R_1$, R_2' can in fact never be greater than R_1 , since the oxide film cannot dissolve more quickly than it is formed. That is if $R_2' \gg R_1$ (at low current densities, high temperatures) the electrodes will not passivate, and $I_t = \infty$.

If $R_2' \approx R_1$ (medium I at high temperature or very low I at low temperature) an oxide film eventually builds up, and large amounts of conversion product form, so that I_t is large. The rate of accumulation of CdO depends on $(R_1 - R_2')$: it is zero or small at first, and after critical supersaturation is reached increases as R_2' decreases. If $R_1 \gg R_2'$ (high current densities or low temperatures) the oxide film reaches the thickness required to produce passivation before very much conversion product is formed, and I_t is small. It is interesting to note that the values of I_t obtained at -40° (0.1–0.16 ma hr cm $^{-2}$) are very close to the value calculated from Rozentsveig's (2) estimate of the thickness of the CdO which causes passivation (3–8 monolayers).

Results plotted in Fig. 3 show that the variation of I_t with temperature is much larger in carbonate solutions than in hydroxide solutions. Since the rate of the depassivating reaction depends on the mobility of the ions in solution, R_2' approaches zero at the freezing point of the solution. The freezing point of 7.2N KOH is below -60°C , while the freezing point of 7.2N K_2CO_3 is about -25°C ; thus the temperature coefficient of R_2 (and hence I_t) is larger in the carbonate solutions.

Effect of electrolyte composition.—The value of I_t in pure carbonate solutions is much higher than in mixed solutions (Fig. 4a). In pure K_2CO_3 the solubility of CdO is high; hence R_2' can operate at its maximum rate for longer periods before supersaturation is reached. At low current densities there is a minimum in the I_t vs. composition curve at a composition close to that at which the minimum in the solubility occurs. This minimum may have been masked at higher current densities, but the data are not complete enough to be sure. At low current densities I_t increases as hydroxide concentration is increased, as does solubility, but at high current densities the value of I_t drops sharply in pure KOH solutions. This drop can be explained by a low value of R_2' : if $R_2' \gg R_1$ initially, the CdO film may build up even before supersaturation is reached.

Figure 4b shows the variation of I_t with variations of CO_3^{2-} and OH^- . I_t decreases with decreasing concentration as would be expected, since the solu-

bility of CdO and R_2' decrease with decreasing OH^- and CO_3^{2-} concentrations. There is, in fact, a linear relation between activity and I_t in solutions of varying K_2CO_3 concentration. However, this relation does not hold in KOH solutions, and its significance is still obscure.

General Observations

The passivation voltage (E_p) and gas evolution rate in the various solutions are of interest. In pure K_2CO_3 solutions E_p was high (~ 1.4 v) and the gas rate after t_p was very nearly 100% of theoretical; in mixed electrolytes the E_p was lower (~ 1.1 v) and the gas rate was somewhat lower ($\sim 70\%$); in pure KOH, E_p was only ~ 1.0 v, while the gas rate was much lower (as low as 30% at low current densities). Since the dissolution and precipitation reactions continue beyond t_p , a part of the current must always be utilized to maintain the passivating film.

Later work on voltage decay curves has shown that oxygen overvoltage is smaller in hydroxide solutions than in carbonate solutions. In hydroxide solutions oxygen evolution may occur before the CdO film has reached its maximum thickness. That the CdO film continues to build up after t_p is indicated by the gradual increase in E_p noted above.

The two essential transport processes in the oxidation mechanism have not been considered in this paper. Firstly, there is the "outer" transport process: once the conversion product has begun to form, the conversion species (H_2O , OH^- , CO_3^{2-} ?) must move across the final product from electrolyte to the CdO surface to permit conversion. Second, the "inner" transport process essential to the oxidation involves the movement of either Cd^{2+} or an oxygen-containing species across the CdO layer to permit formation of CdO.

Summary

1. Studies have been made of the anodic oxidation of Cd in KOH, K_2CO_3 , and mixed electrolytes. The effect of experimental conditions on electrical behavior and film composition have been examined.

2. The general mechanism has been determined: The primary reaction is the formation of cadmium monoxide. The monoxide is converted to either the hydroxide or carbonate (depending on the electrolyte) through a soluble intermediate. The rate of conversion is governed by the solubility of the monoxide and the rate of transport of the dissolving species through the conversion product from the electrolyte.

3. Cadmium monoxide is the passivating species. When resistance polarization through the film is high enough to drive the CdO surface beyond the oxygen overpotential, oxygen is evolved.

4. The following factors, which vary with experimental conditions, determine the time required to produce this passivating film: (a) rate of formation of CdO: f (current density); (b) solubility and rate of dissolution of CdO: f (temperature, composition); (c) rate of precipitation and degree of supersaturation necessary to initiate precipitation: f (temperature, composition); and (d) conductivity of the oxide: f (temperature, current density).

Acknowledgments

The authors wish to express their thanks to L. G. Wilson and V. C. Shore of these Laboratories who did the x-ray diffraction studies, and to the Defence Research Board for permission to publish.

Manuscript received Jan. 28, 1957. Paper issued as DRCL Report No. 231.

Any discussion of this paper will appear in a Discussion Section to be published in the December 1958 JOURNAL.

REFERENCES

1. K. Huber, *This Journal*, **100**, 376 (1953).
2. S. A. Rozentsveig, B. V. Ershler, E. L. Shtrum, M. M. Ostanina, *Trudy Soveshchaniya Elektrokhim. Akad. Nauk. S.S.S.R. Otdel. Khim. Nauk*, **1950**, 571 (1953).
3. R. Scholder and E. Staufenbiel, *Z. anorg. u. allgem. Chem.*, **247**, 259 (1941).
4. T. P. Dirkse, *This Journal*, **101**, 328 (1954); *ibid.*, **102**, 497 (1955).
5. C. A. Hogarth, *Proc. Phys. Soc.*, **B64**, 691 (1951).
6. A. Hickling and S. Hill, *Disc. Faraday Soc.*, **1947**, 236.

Technical Note



Sedimentation Volumes of a Phosphor Powder in Potassium Silicate and Potassium Silicate-Barium Acetate Settling Media

J. Fred. Hazel and Louis Fiorito

Department of Chemistry, University of Pennsylvania, Philadelphia, Pennsylvania

The preparation of cathode ray screens for black and white television receivers involves the sedimentation of a luminescent powder through an aqueous solution containing potassium silicate and barium ions. The silicate is adsorbed on the solid surfaces and as a result the negative charge on the particles and on the glass foundation is increased (1, 2). Rapid adhesion of the particles to each other and to the glass is obtained on addition of a soluble barium salt (2). This decreases the repulsion between the silicate covered surfaces by decreasing the charge. Polymerization of the silicate and binding of the surfaces follow spontaneously.

The settling procedure for producing cathode ray screens is remarkable from the point of view of the uniformity in thickness of the screen. This conclusion is suggested from the consideration that the displacement of a layer one particle thick could cause a variation in thickness of up to 50% in a screen that averages only a few particle diameters in thickness. Another factor affecting screen thickness, in addition to the particle diameter and the number of particles per unit area, is the density of packing of the particles in the screen. The present study on sedimentation volume was designed to yield information on this factor. It is known that the charge on mineral powders has an effect on their sedimentation volume (3). This is of interest since the charge on phosphor particles depends on the composition of the liquid through which the particles settle (1, 2).

Materials

Du Pont No. 1630 zinc sulfide-zinc cadmium sulfide phosphor was shaken with distilled water and allowed to settle, after which the liquid was decanted. Three washings were performed before the

wet slurry was poured onto a large watch glass and permitted to dry in a dark cabinet.

The potassium silicate solution (Kasil No. 22, Philadelphia Quartz Co.), containing approximately 8.6% alkali calculated as K_2O and 18.9% SiO_2 was a purified solution of $K_2O \cdot 3.45 SiO_2$.

Experimental

The sedimentation volumes were measured in 9 mm glass tubes. The tubes were made by cutting 20 cm lengths and sealing them at one end. A mark was etched at 1.00 ml on each tube and a linear scale was made with divisions of 0.1 ml. The scale divisions were 2.88 mm apart and readings could be estimated to 0.1 scale division, corresponding to 0.01 ml. The precision of the measurements was satisfactory after a standardized procedure was developed, the mean deviation being approximately 0.15 scale divisions.

The volume of a freshly prepared 1% or 10% stock solution of the silicate required to be added to water to bring the total volume to 10 ml and contain the desired concentration of $K_2O \cdot 3.45 SiO_2$, in parts per million (ppm), was calculated. The potassium silicate solution was pipetted into a dry 30 ml beaker, and the water into another beaker. The silicate was added all at once to the water, and transferred from one beaker to another to mix the diluted system thoroughly. A portion of the silicate solution immediately was added to 2.00 g of phosphor powder which had been placed in the tube. The volume of solution in the tube was approximately 5 ml. The tubes were shaken vigorously after addition of the silicate and placed in a rack in an upright position to permit the phosphor to settle. Readings were taken daily until none of the samples in a given series showed a decrease in sedi-

Table I. Sedimentation volumes of phosphor powder in potassium silicate solutions. Sedimentation Time: 19 Days

Potassium silicate, ppm	Sedimentation volume, ml	Potassium silicate, ppm	Sedimentation volume, ml
0	1.03	1,770	0.89
17	0.91	2,040	0.89
34	0.94	2,720	0.88
102	0.92	4,860	0.89
340	0.90	6,800	0.92
680	0.91*	13,600	1.03
1,360	0.85	20,400	1.04
1,720	0.89	34,000	1.08

* 9 day sedimentation period.

Table II. Sedimentation volumes of phosphor powder in potassium silicate-barium acetate mixtures

Potassium silicate, ppm	Barium acetate, ppm	Sedimentation volume, ml
0	275	1.02
1,720	275	0.98
1,770	275	0.98
6,800	275	1.06
20,400	275	1.13

mentation volume of more than 0.01 ml on successive readings. In the preparation of the systems containing barium acetate the volume of barium acetate solution required to produce a concentration of 275 ppm in the final system, was pipetted into the beaker containing the water. The potassium silicate was poured into the diluted barium acetate solution and the same procedure followed as before.

Results and Discussion

The sedimentation volumes of the phosphor given in Table I were obtained after a 19 day sedimentation period in potassium silicate solutions of increasing concentration. The reported values are not significantly different from those measured after 12 days: in only two cases did the readings differ as much as 0.02 ml.

Sedimentation volumes of the phosphor in potassium silicate-barium acetate mixtures are given in Table II. The values correspond to a sedimentation time of 19 days.

The data in Table I indicate that the sedimentation volume of phosphor particles decreases with increasing concentration of potassium silicate. The volume occupied by the particles passes through a minimum and then increases to a value above that in water alone. The change in sedimentation volume may be attributed to the change in zeta potential as the concentration of silicate is varied. It is suggested that as the negative potential of the particles is increased they repel each other more in settling. This permits the particles to pass by one another and pack together in a small volume. They do not stick to each other or coagulate and entrap a large amount of liquid in their packing, Fig. 1, as is the case when the zeta potential has a low value.

The silicate concentration is plotted against the zeta potential of the particles in the upper part of Fig. 2 and against the sedimentation volume of the particles in the lower part of the same figure. A

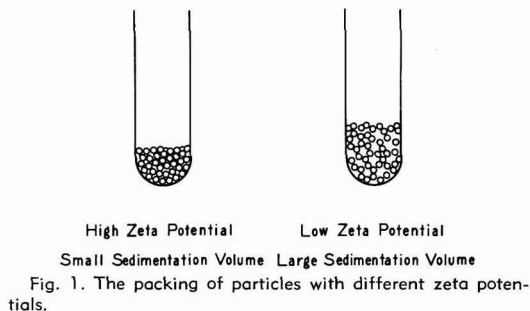


Fig. 1. The packing of particles with different zeta potentials.

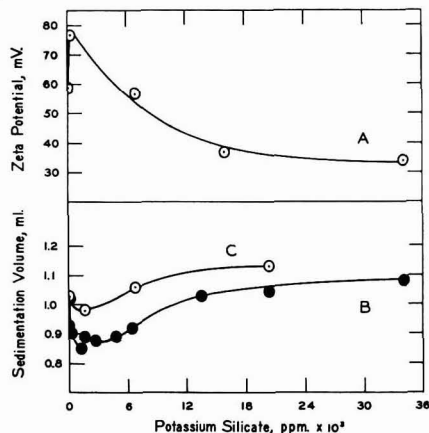


Fig. 2. Relationship of zeta potential to sedimentation volumes.

maximum in the zeta potential curve and a minimum in the sedimentation volume occur at low concentrations of silicate. Moreover, as the silicate concentration increases the zeta potential decreases and the sedimentation volume increases. That the maximum in the zeta potential curve occurs at a somewhat lower silicate concentration than the minimum in the sedimentation volume can be attributed to the fact that the former was determined by using a streaming potential diaphragm and a constant flow of silicate while the latter was determined in a static system.

The presence of barium acetate caused an increase in sedimentation volumes as shown in the bottom part of Fig. 2. The role of barium acetate in the preparation of cathode ray screens is to reduce the charge on the particles (2). The larger sedimentation volumes observed in all cases when barium acetate was employed, indicate that the charge on the particles was reduced under these conditions.

Manuscript received June 25, 1957. This paper was prepared for delivery before the Washington Meeting, May 12-16, 1957.

Any discussion of this paper will appear in a Discussion Section to be published in the December 1958 JOURNAL.

REFERENCES

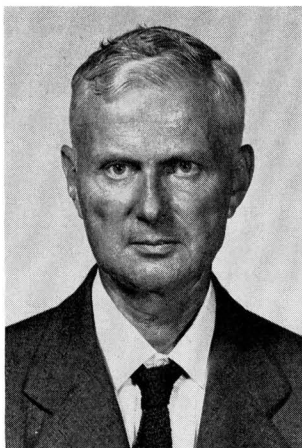
1. R. Edelberg and J. F. Hazel, *J. (and Trans.) Electrochem. Soc.*, **96**, 13 (1949).
2. J. F. Hazel and G. L. Schnable, *This Journal*, **100**, 65 (1953).
3. N. K. Adam, "The Physics and Chemistry of Surfaces," p. 202, Oxford University Press, London (1941).



Carl Wagner to Become Head of Max Planck Institute at Goettingen

Professor Carl Wagner of the Dept. of Metallurgy at Massachusetts Institute of Technology, well known for his fundamental researches in electrochemistry, will become Director of the Max Planck Institute for Physical Chemistry at Goettingen beginning February 1958. This position was held until recently by the late Professor K. F. Bonhoeffer.

Professor Wagner came to this country from the Technische Hochschule in Darmstadt in 1945. He previously received his Ph.D. degree in electrochemistry from the University of Leipzig, where his thesis was directed by Professor Max LeBlanc. After teaching and research at various German universities, he was appointed in 1934 to associate professor of physical chemistry at the Technische Hochschule of Darmstadt, succeeding to full professor in 1940, and Dean of the Faculty of Science in 1942. Immediately following the war, he joined the research staff at Fort Bliss, Texas, operating under the supervision of the Ordnance Research and Development Division of the U. S. Army. In



Carl Wagner

1948 he was invited to become visiting professor at M.I.T., and in 1955 was made full professor of metallurgy.

Professor Wagner is probably best known for his contributions to the ionic theory of oxidation and tarnish of metals. He has also contributed prominently to the fields of thermo-

dynamics and kinetics, catalysis, solid state, and cathodic protection. Together with some papers in pure mathematics, his publications total more than 160. He is coauthor of "Thermodynamik" with W. Schottky and H. Ulich published in 1929. He is also author of two extensive chapters in the "Handbuch der Metallphysik" on thermodynamics of metal systems and kinetics of metal reactions which was published in 1940.

In 1951 he was the first recipient of the Palladium Medal, awarded by the Society for his distinguished contributions to electrochemistry. In 1952 he received an honorary D.Sc. from the Technische Hochschule of Darmstadt, and earlier in 1957 he was granted the Willis R. Whitney Award of the National Association of Corrosion Engineers for his contributions to the science of corrosion.

At Goettingen, he will continue his researches in electrochemistry and in physical chemistry with the collaboration of one of the finest research staffs in pure science anywhere in the world.

New York Meeting, April 27 to May 1, 1958

The Spring Meeting of the Society will be held at the Hotel Statler, New York City, April 27 to May 1, 1958. This will be the 113th meeting of the Society and the 17th to be held in New York.

A full and interesting program of technical papers is planned, of particular interest to the Electric Insulation, Electronics, Electrothermics and Metallurgy, Industrial Electrolytic, and Theoretical Electrochemistry Divisions. In addition, a Richards Memorial Lecture will be presented.

Social events include a mixer on Monday evening, April 28, and the President's reception and banquet on Tuesday evening, April 29. The Society Luncheon, featuring a short

business meeting and an outstanding speaker, will take place on Tuesday noon.

A full program of activities for the ladies is being planned. Recognizing, however, that New York offers unparalleled opportunities for individual activities, from shopping in the world's finest stores to visiting museums and other places of interest, the Ladies' Committee is leaving sufficient free time.

It is hardly necessary to recount the attractions of the world's greatest city: there is something for everyone, whatever his tastes. New York is the home of the United Nations and the New York Yankees; the Metropolitan Museum of Art and Madison Square Garden. Hun-

dreds of restaurants offer cuisine of all types and nationalities; after dinner one has a choice of legitimate theater, first-run movies, concerts, night life either high or low. The Convention Committee believes that planned social activities for the registrants must be judiciously mixed with plenty of free time for the satisfaction of individual tastes, and the program is being designed on that basis.

Note to drama-lovers: getting seats for hit shows at the last minute is often difficult or impossible. If you are planning some theater-going it is best to write in to the box office as far ahead as possible. Some national magazines such as *The New Yorker* carry a list of current shows



© New York Convention & Visitors Bureau

An endless stream of vessels, one every 20 minutes around the clock, sails from the busy port of New York, passing the famous lady of the port.

and the addresses of the theaters. When you write for tickets, enclose your check for the exact amount and a self-addressed stamped envelope.

Further details will appear in the February *JOURNAL*, and the complete program, including general informa-

tion, technical sessions, and abstracts, will be published in the March issue.

Hotel reservation cards will be sent to members shortly. If writing on your own letterhead, be sure to mention The Electrochemical Society.

Highlights of the Board of Directors' Meeting

(Held October 6, 1957, Hotel Statler, Buffalo, N. Y.)

The Board of Directors held its regular meeting on October 6, 1957, prior to the opening of the Buffalo Convention.

The following gentlemen were appointed as Tellers of Election for 1958: Gerald Lux, Chairman; F. A. Lowenheim, E. B. Saubestre.

The President presented a request from I. R. Maxwell, Director of Pergamon Institute of London and New York, that the Society cooperate with them in getting Soviet- and Soviet-orbit-country articles translated into English, French, and German. It was voted that The Electrochemical Society cooperate with the Pergamon Institute in this endeavor. It is understood that the news items in the *JOURNAL* will be used to publicize these translations.

The following committee appointments were approved: Hans Thurnauer—Chairman, Sustaining Membership Committee; Harry R. Copson—Resolutions Committee; J. R. Musgrave and Abner Brenner—Acheson Award Committee; Charles L. Faust

—Chairman, Acheson Award Committee.

The Treasurer announced that the complete report of the audit will not be published in the *JOURNAL*; however, certification will be published.

The Washington Convention report was discussed in the light of the fact that considerable money had been made at this meeting, and it was voted to accept this report with thanks for a job well done.

Dr. F. A. Lowenheim, General Chairman of the forthcoming New York Meeting, discussed the preliminary budget for this meeting.

On the recommendation of the Ways and Means Committee, the Board approved an increase of \$1 in the registration fee for this meeting, if necessary.

The New York local committee was authorized to select a Richards Memorial Lecturer for the New York Meeting.

At the request of the New York local committee, the duplication of the registration lists at conventions

will be discontinued, to take effect after the Buffalo Meeting.

Dr. Arthur Middleton reported that the Indianapolis Section would be happy to accept the bid of the Society to hold a meeting in Indianapolis, and requested a spring meeting.

At the recommendation of the Ways and Means Committee, the Executive Secretary (currently designated Assistant Secretary) will become a regular member of the Council of Engineering Society Secretaries and will attend the regular meetings of this body at the expense of the Society; this expense is to become a budgeted item, and approval to attend each meeting shall be obtained from the Secretary.

The Ways and Means Committee presented instructions to be given members planning to hold technical sessions—which were prepared by a subcommittee headed by Dr. C. L. Faust—using as one portion the instructions formerly prepared by A. C. Haskell. It was voted that these instructions be approved.

It was voted that the new Bylaws will take effect April 1, 1958, provided the Constitution is approved by mail vote of the membership.

The Electrochemical Society will support the nomination of the Engineers Joint Council for appointment to the Board of the National Science Foundation as follows: T. Keith Glennan and Murrough P. O'Brien, with General L. E. Simon as an alternate.

The Board approved the Ways and Means Committee's recommendation that a reduced registration fee be permitted only on the last of registration.

At the request of the Editor, approval was given for the appointment of divisional co-editors, R. T. Foley and Andre de Bethune, for Corrosion and Theoretical, respectively.

JOURNAL statistics were presented which show that the principal hold-up is in review, and not in publication, once the papers are cleared.

The Board approved the following recommendations of the Publication Committee:

"1. Monographs should be primarily compilations of latest scientific progress.

"2. The Committee recommends the authorization of the monograph on 'The Structure of Electrolytes,' based on recent symposia by the Theoretical Division, with Walter Hamer as editor.

"3. Late news abstracts for the spring 1957 meeting of the Semiconductor Section of the Electronics

Division will be published. This is not to be considered a precedent for future action.

"4. It was agreed to accept the proposal of the Semiconductor Abstract Committee of the Electronics Division as follows:

"1. As of this date, May 15, 1957, it is recommended that further royalties from the 1953 and 1954 issues of the Semiconductor Abstracts be used to defray the deficit already incurred by the Society.

"2. In regard to the 1955 issue of the Abstracts (which will be sold at \$10 per copy), the estimated royalties of about \$800 within the next year shall be turned over to Battelle by the Society for partial defrayment of their costs for preparing future issues of the Abstracts.

"3. The arrangement indicated in (2) will continue to exist until such time as either (a) Battelle obtains a sponsor to pay for their costs, or (b) the royalties received by the Society and turned over to Battelle exceed the cost of preparation of the Abstracts by Battelle.

"4. Any royalties in excess of the Battelle cost will revert to the Society and, if a sponsor is obtained by Battelle, all royalties will revert to the Society.

"5. In lieu of the above proposed modifications to the agreement with Battelle by the Abstracts Committee and the Executive Committee of the Electronics Division, Battelle will not receive any free copies of the 1955 or subsequent issues of the Abstracts from the Society."

"5. It was agreed that publication of the Highlights of the Meeting of the Board of Directors should be continued. However, it was recommended that the News Editor review these Highlights prior to printing.

"6. On Friday morning, May 17, 1957, Norman Hackerman and H. B. Linford made the decision to approve the publication of a monograph based on the Niobium Sym-

posium to be edited by E. M. Sherwood."

Mr. F. W. Koerker, Chairman of the Membership Committee, reported that we have 2772 total members in all categories, as of September 3, 1957; of this total 2772, 66 represent Sustaining Member companies and 8 represent Patron Member companies, but there are also 59 Sustaining Member companies not represented by an Active Member in our total. Life, Emeritus, and Honorary Members account for 67 of the total, and Student and Associate Members account for 89 more. Delinquent members equal one half of the number last May, but there are still 73 such members. This is slightly higher than the 72 reported for 1954 and 66 reported for 1955. However, it was hoped that this figure could be lowered before the end of 1957.

In the report of the Council of Local Sections, it was noted that, including the three new local sections approved at the Washington Meeting, the total number of sections now stands at 18. This compares to 10 in 1947 and 13 in 1954 when the Council of Local Sections was instituted.

The President announced that the next meeting of the Board of Directors would be held on January 24, 1958, in New York City, at a place to be designated.

Robert K. Shannon,
Assistant Secretary

Division News

Corrosion Division

Annual Report

The Corrosion Division participated in a joint symposium with the Electrothermics and Metallurgy Division at the Spring Meeting of the Society in Washington, D. C. The symposium consisted of two

half-day sessions and was entitled "Role of Metal and Oxide Structure in Oxidation and Corrosion."

The regular annual meetings of the Division, consisting of four half-day sessions and a one-day joint symposium with the Electrodeposition Division on "Corrosion of Electrodeposited Metals" were held at the Fall Meeting in Buffalo.

The annual luncheon was held on October 8. At its close, the annual business meeting was convened by Chairman J. E. Draley. The Secretary-Treasurer reported the treasury balance as unchanged at \$21.68.

The Chairman pointed out that action of the Board of Directors made it mandatory that the Division revise Article VII of the Bylaws, dealing with the administration of royalties from the sale of monographs sponsored by the Division. Copies of the old Article VII and the proposed version were distributed. After discussion and rewording the revised article was adopted without dissent as given below, together with a small change in paragraph (f), item (1) of Article VIII.

Article VII

ADMINISTRATION OF MONOGRAPH FUNDS

(1) Royalties accruing from the sale of Division Monographs shall be administered, subject to approval by the Board of Directors of The Electrochemical Society, by a committee comprised of the following:

1. Chairman of the Division, who shall serve as chairman of this committee, or shall appoint a chairman from membership of the committee.

2. A member of the Board of Directors, to be appointed by the President of the Society.

3. Editors of Division Monographs; when there are more than three monographs, committee members shall be editors of those three monographs which have earned the

Manuscripts and Abstracts for Fall 1958 Meeting

Papers are now being solicited for the Fall Meeting of the Society, to be held at the Chateau Laurier in Ottawa, Canada, September 28, 29, 30, October 1, and 2, 1958. Technical sessions probably will be scheduled on Batteries, Corrosion, Electrodeposition (including symposia on "Electrodeposition on Uncommon Metals" and "Chemical and Electropolishing"), Electronics (Semiconductors), Electro-Organics, and Electrothermics and Metallurgy.

To be considered for this meeting, triplicate copies of abstracts (*not to exceed 75 words in length*) must be received at Society Headquarters, 1860 Broadway, New York 23, N. Y., *not later than June 1, 1958. Please indicate on abstract for which Division's symposium the paper is to be scheduled.* Complete manuscripts should be sent in triplicate to the Managing Editor of the JOURNAL at the same address.

* * *

The Spring 1959 Meeting will be held in Philadelphia, Pa., May 3, 4, 5, 6, and 7, 1959, at the Sheraton Hotel. Sessions will be announced in a later issue.

greatest amounts in royalties, based on available reports for the 12 months preceding election of officers of the Division.

Article VIII

(1) . . . Chairman's (duties) . . .

(f) To represent the Division on a Committee charged with administration of income from the sale of the Division Monographs, as provided for in Article VII.

On proposal of the nominating committee (J. V. Petrocelli, Chairman; F. W. Fink, H. Copson, and N. Hackerman) the following were unanimously elected officers of the Division for the coming year (1957-58):

Chairman—C. V. King
 Vice-Chairman—M. A. Streicher
 Secretary-Treasurer—R. T. Foley
 General Electric Co.
 Bldg. 37, Rm. 2083
 Schenectady, N. Y.

M. A. Streicher,
Past Secretary-Treasurer

Electrodeposition Division

At the business meeting of the Electrodeposition Division on October 8, 1957, it was decided that a symposium, "Electrodeposition on Uncommon Metals," would be planned for the fall of 1958. Chairman Bar-

nartt announced that Dr. Charles Faust and John Beach will head up this activity which will include plating on uncommon metals such as titanium, beryllium, zirconium, thorium, niobium, etc., and alloys such as Inconel, Kovar, etc.

"Chemical and Electropolishing" was selected as a second symposium for the 1958 meeting with Dr. D. Gardner Foulke responsible for soliciting papers. Anyone interested in contributing papers to either or both programs is urged to contact Dr. Faust at Battelle Memorial Institute in Columbus, Ohio, or Dr. Foulke at Hanson-Van Winkle-Munning Co., Matawan, N. J.

Other symposia suggested for the future include "Electrowinning and Electrorefining," a round table on "Corrosion Resistance of Electrodeposited Coatings," "Principles of Electrodeposition from Organic Solvents and Mechanisms of Electrode Reactions in Such Systems," "Coatings by Electrophoresis," and "Principles of Electrodeposition from Fused Salts."

Comments from members of the Division unable to attend the meeting on these or other subjects should be addressed to Dr. S. Barnartt, Research Labs., Westinghouse Electric Corp., Pittsburgh 35, Pa.

D. Gardner Foulke,
Secretary-Treasurer

national meeting in Indianapolis, if the Society approves. A brochure outlining facilities and inviting the Society was submitted at the recent Buffalo Meeting.

Dr. Herman C. Froelich of the General Electric Co., Nela Park, Cleveland, Ohio, then presented a paper entitled "The Promise of Electroluminescence." Dr. Froelich first covered the scientific and economic driving factors which have led to extensive research effort on the development of practical electroluminescent devices throughout the world. The relative potentialities of incandescent, fluorescent, and electroluminescent illumination were delineated and the current inadequacies of the latter type of lighting were discussed. The general basic construction of current electroluminescent devices was also explained.

Relationships of brightness to frequency and excitation potential were illustrated, as well as variation in color and efficiency with phosphor formulation. Some current theories of light production in electroluminescent devices were discussed. It was shown that none of the proposed mechanisms would explain the action of all electroluminescent materials under all conditions of excitation.

Dr. Froelich demonstrated some typical electroluminescent devices. He concluded that no publicly acceptable electroluminescent source of illumination is currently available; and that when such sources are ultimately developed, they probably would be based upon somewhat different structures from those reported currently.

Thomas C. O'Nan,
Secretary-Treasurer

Section News

Boston Section

The eighth meeting of the Boston Section was held on October 21, 1957, at the Officers' Club of the Watertown Arsenal. Dr. Ben Allen, Manager of the Melting Research Dept. of Corning Glass Works, spoke on "Pyroceram," the name for the group of new ceramic materials produced by the nucleation of glass mixtures. They have excellent mechanical strength, insulating properties, and thermal shock resistance. A lively question and discussion period followed the presentation.

At the January 22 meeting, Manson Benedict will describe the M. I. T. Nuclear Reactor.

Worden Waring,
Secretary-Treasurer

Chicago Section

The Chicago Section held its first meeting of the 1957-58 season at the Chicago Engineers Club on Friday, October 4. This meeting was the Section's Semiconductor and Physics Night. Dr. Jordan J. Markham of the Research Dept. of Zenith Radio

Corp. spoke on the subject "Color Centers in Crystals for Television."

Dr. Markham discussed experiments which he has performed in the study of color centers in alkali halide crystals. He discussed some of the fundamentals of color centers in alkali halides and developed the analogy between color centers and transistor phenomena.

As the concluding portion of his talk, Dr. Markham showed a color film which had been taken of the actual formation of color in an alkali halide crystal. The talk was followed by a lively question period, after which the group accorded him a rising vote of thanks and adjourned.

Jerome Kuderna, *Secretary*

Indianapolis Section

The Indianapolis Local Section of the Society held its Fall Technical Meeting on Tuesday, October 15, 1957, at the Student Union and Food Services Building of the Indiana University Medical Center in Indianapolis. A short business meeting was held at which it was decided that the local organization would undertake holding the Spring 1961

Washington-Baltimore Section

The first regular meeting of the 1957-58 year was held on October 3, 1957 at the National Bureau of Standards. The program included talks by Dr. Jerome Kruger and Dr. John K. Taylor, both of the National Bureau of Standards. Dr. Kruger spoke on "Oxidation of Copper Single Crystals in Oxygen-Saturated Water at Room Temperature." He described an investigation of corrosion in a copper, water, oxygen system. Cuprous oxide films were formed when the system was exposed to the atmosphere and cupric oxide films were formed in the absence of carbon dioxide. Pourbaix diagrams predict formation of these films on the basis of the existing pH. Dr. Taylor's topic was "Coulometric Titration—A Precision Electro-Ana-

lytical Technique." Accurate and rapid determinations of small or large amounts of material may be made with this device. The constant current type of coulometer offers more advantages. This is an absolute method with the following limitations: (a) there must be only one reaction; (b) the exact end point must be determined; (c) value of the Faraday.

David Schlain, *Secretary*

Personals

James P. Hoare has accepted a position as principal research engineer associate with the Ford Scientific Lab., Dearborn, Mich., where he will conduct an investigation of fundamental electrode processes. Formerly Dr. Hoare was a chemist in the Electrochemical Branch of the Chemistry Div., Naval Research Lab., Washington, D. C.

Robert Bakish, formerly with Sprague Electric Co., North Adams, Mass., has accepted a position with Ciba Ltd., Basle, Switzerland. Ciba recently organized a Rare Metals Div.; Dr. Bakish is in charge of the physical metallurgy section of that division.

Michael C. Carosella, previously Assistant to Manager of the Product and Process Development Dept., Electro Metallurgical Co., Niagara Falls, N. Y., has been advanced to Assistant Manager of the department.

Paul R. Kruesi, formerly of Chicago, Ill., is now in Chattanooga, Tenn., as Manager of the Manufacturing Div., Heavy Minerals Co.

Luther E. Vaaler recently joined National Carbon Co.'s Development Labs. in Niagara Falls, N. Y. He had been with Battelle Memorial Institute, Columbus, Ohio.

Bernard Jacobs recently became Vice-President and Director of the Research Div., General Transistor Corp., Jamaica, N. Y. Formerly he was connected with the Sperry Rand Corp., So. Norwalk, Conn.

Lipman S. Gerber, of Lakewood, N. J., retired electrical engineer, U. S. Army Ordnance, is now doing consulting on storage batteries and engineering problems.

Keith G. Blanton has left the Naval Ordnance Lab., Washington, D. C., to take a position as Process Engineer at the Semiconductor Products Div. Lab. of Motorola, Inc., in Phoenix, Ariz.

Hamburg Tang has taken a position as Chief Metallurgist at Alloys Unlimited, Inc., in Long Island City, N. Y. He had been with Alpha Metals, Inc.

E. R. Breining, formerly Electro-chemistry Supervisor, General Motors Research Staff, Detroit, Mich., is now Manager of the Gas Plating Lab., Commonwealth Engineering Co., Dayton, Ohio.

J. Vaid has left the C.E.C.R.I., Karaikudi, and rejoined the Indian Telephone Industries, Bangalore. He is at present in the National Physical Lab., New Delhi, on deputation in connection with the manufacture of condensers.

M. S. Thacker has been elected as an Honorary Fellow of the Institute of Telecommunication Engineers, India.

T. L. Rama Char, India, has been elected a member of the Electrochemical Society of Japan.

S. Ramaswamy, India, at present is on a business tour of Europe.

News Items

Nominations for 1958 Acheson Award

Charles L. Faust, Chairman of the Acheson Medal Award Committee, would like to receive suggestions for possible candidates for the next Acheson Medal Award, to be made in the fall of 1958.

The procedure to be followed by the membership, taken from the Rules Governing the Award of the Acheson Medal, is given below.

1. Nominations shall be accepted from the membership at large.

2. All nominations, whether made by a member of the Nominating Committee or by any other member of the Society, must be accompanied by a full record of qualifications of the nominee for the award. Such supporting documents from friends of the candidate or from his organization shall be in order.

3. The nominator must assume the responsibility for providing the Chairman of the Nominating Committee with nine copies of the supporting documents, one for each member.

Nominations must be sent to the Chairman not later than March 1 of the year in which the medal is awarded and nominations will be considered closed after that date.

All nominations of candidates for the medal shall be continued in force

for a period of two consecutive awards of the medal. Any unsuccessful candidate may be renominated in the usual manner for any subsequent Medal award.

Correspondence should be addressed to Charles L. Faust, Battelle Memorial Institute, 505 King Ave., Columbus 1, Ohio.

New Sustaining Members

The following recently became Sustaining Members of The Electrochemical Society: C & D Batteries, Inc., Conshohocken, Pa.; Federal Telecommunication Labs., Nutley, N. J.; Raytheon Manufacturing Co., Waltham, Mass.

1957 Annual Index

The Annual Index for Vol. 104 (1957) of the JOURNAL will appear in the February 1958 issue. Reprints of the Index can be obtained about the middle of March by writing to The Electrochemical Society, 1860 Broadway, New York 23, N. Y.

Chemical Institute of Canada Meeting Dates

The Chemical Institute of Canada has scheduled the following meetings for the first half of 1958.

Feb. 20—12th Divisional Conference, Protective Coatings Subject Division, Montreal, Que.

Feb. 21—12th Divisional Conference, Protective Coatings Subject Division, Montreal, Que.

April 20-23—Joint Conference, American Institute of Chemical Engineers and Chemical Engineering Subject Division, CIC, Montreal, Que.

May 12-14—8th Canadian High Polymer Forum, cosponsored by the CIC and the National Research Council, Macdonald College, Ste. Anne de Bellevue, Que.

May 26-28—41st Annual Conference and Exhibition, Royal York Hotel, Toronto, Ont.

Erratum

In the paper by D. A. Vermilyea entitled "Nucleation of Crystalline Ta₂O₅ During Field Crystallization" which appeared on pp. 542-546 of the September 1957 issue of the Journal, Vol. 104, No. 9, it was stated that crystalline regions similar to those observed on anodic Ta₂O₅ films had been observed on anodic aluminum oxide films by R. C. Spooner. The statement was not correct; no such observations have been made by Dr. Spooner.

Announcement from Publisher

"A Study of Cadmium-Tin and Zinc-Tin Alloy Electrodeposits," B. Cohen, Wright Air Development Center, Sept. 1954. Report PB 121808,* 44 pages, \$1.25.

Cadmium-tin electrodeposits were found superior to coatings of cadmium in both corrosion resistance and embrittling effects. The alloy systems evaluated were deposited from fluoborate solutions. The coating had very little embrittling effect on steel as compared to cadmium plated from a cyanide solution. It was easily soldered by the same techniques used for cadmium. Zinc-tin alloy coatings were inferior in all tests to those of both cadmium and cadmium-tin.

* Order from Office of Technical Services, U.S. Dept. of Commerce, Washington 25, D. C.

Book Reviews

Chemistry of Natural and Synthetic Rubbers, by Harry L. Fisher. Published by Reinhold Publishing Corp., New York, 1957. vi + 208 pages; \$12.50.

The author describes this as a "book of facts," and so it is in the sense that it offers a compendium of useful information on rubbers rather than a development of theoretical material. Subjects covered include history, industrial processes in manufacturing and modifying rubbers, structure and properties of both natural and synthetic rubbers, and reclamation.

Of interest to electrochemists is a short chapter on bonding of rubber to metal. This objective is served by use of appropriate bonding agents, which include modified rubbers, synthetic copolymer resins, and other adhesives. As an application example, the Colorado River waters flow to the turbine generators of the Hoover Dam through large steel tubes lined with rubber to prevent corrosion.

Electrolytic processes involving latex are briefly treated. These include concentration of latex by electrodecantation and manufacture of products having special shapes (e.g., gloves) by electrodeposition, the positive latex particles migrating toward the shaped anode.

Amos Turk

Quantitative Inorganic Analysis, by G. Charlot and Denise Bézier. Translated by R. C. Murray from

the 3rd French edition of 1955. Published by John Wiley & Sons, Inc., New York, 1957. x + 691 pages; \$15.00.

This translation of an established French text is a very comprehensive treatise of modern quantitative analysis. It is an excellent book for an advanced course, for graduate students preparing for comprehensive examinations, or as a reference for practicing analysts.

The volume is divided into two parts. Part I treats of the general methods of analysis, such as: the various kinds of titrimetry, gravimetry; separations by chromatography, distillation, and extraction; absorption and emission spectrophotometry; radioactivity in analysis; gas analysis; and sampling and precision of measurement. Of especial interest here are the nine chapters (84 pages) devoted to electrochemical methods: theory, separations, internal electrolysis, electrography, polarography, potentiometry, amperometry, coulometry, and conductimetry. Many typical graphs and polarization curves are shown. The treatment is somewhat different from that in American texts, but is clear and concise.

Part II takes up the determination of each of the elements, including

Advertiser's Index

Bell Telephone Laboratories, Inc.	3C
Enthone, Incorporated	Cover 4
Great Lakes Carbon Corporation	Cover 2
E. H. Sargent & Company.....	6C
Stackpole Carbon Company....	5C
Wyandotte Chemicals Corporation	12C

the rare earths, the rarer elements, carbon, nitrogen, and oxygen. The methods are modern and lean heavily on physicochemical instruments. Each element is treated under such headings as: general separations, specific methods, titrimetry, gravimetry, potentiometry, electrolysis, determination of traces, colorimetry, and special cases.

There are many references to American as well as European journals and texts as recent as 1953. The appendix contains tables of conversion factors (many only to three significant figures), specific gravities, atomic weights, a very complete general bibliography, subject index, and author index.

The printing and format are excellent.

Barnett Faiman

INORGANIC OR PHYSICAL CHEMISTS FOR FUSED SALT RESEARCH AND METALS & INTERMEDIATES RESEARCH

A proposed expansion of our Inorganic Research activity has created the need for chemists who are capable of helping initiate and expand a research program in these areas. The nature of the positions require chemists with considerable initiative and a Ph.D degree or with approximately equivalent experience. Experience may be in any area pertinent to fused salts or extractive and preparative metallurgy.

These are responsible positions offering:

- Broad area of interest.
- Considerable individual freedom.
- Modern research facilities.
- Excellent personnel policies.
- Fine living and recreational areas.

Send resume to: Manager, Personnel Planning

**WYANDOTTE CHEMICALS
CORPORATION**

Wyandotte, Michigan



The Electrochemical Society

INSTRUCTIONS TO AUTHORS OF PAPERS

Address all correspondence to the Editor,
JOURNAL OF THE ELECTROCHEMICAL SOCIETY,
1860 BROADWAY, NEW YORK 23, N. Y.

FORM

Manuscripts submitted for publication should be in triplicate to expedite review. They should be typewritten, double-spaced, with 2½-4 cm (1-1½ in.) margins.

Title should be brief, followed by the author's name and his business or university connection.

Abstract of about 100 words should state the scope of the paper and give a brief summary of results.

ILLUSTRATIONS

Drawings will be reduced to column width, 8.3 cm (3¼ in.), after reduction should have lettering at least 0.15 cm (1/16 in.) high. Original drawings in India ink on tracing cloth or white paper are preferred. Curves may be drawn on coordinate paper only if the paper is ruled in blue. All lettering must be of lettering-guide quality. See sample drawing on reverse page.

Photographs must be glossy prints and mounted flat.

Captions for all figures must be included on a separate sheet. Captions and figure numbers should not appear in the body of the figure.

General—Figures should be used only when necessary. Omit drawings or photographs of familiar equipment. Figures from other publications are to be used only when the publication is not readily available, and should always be accompanied with written permission for reprinting.

REFERENCES

Literature and patent references should be listed at the end of the paper on a separate sheet, in the order in which they are cited. They should be given in the style adopted by *Chemical Abstracts*. For example:

R. Freas, *Trans. Electrochem. Soc.*, **40**, 109 (1921).

H. T. S. Britton, "Hydrogen Ions," Vol. 1, p. 309, D. Van Nostrand Co., New York (1943).

H. F. Weiss (To Wood Conversion Co.), U. S. Pat. 1,695,445, Dec. 18, 1928.

UNITS OF MEASUREMENT

Metric units should be used throughout but, where desirable, English units may be given in parentheses.

Corrosion rates in the metric system should preferably be expressed as milligrams per square decimeter per day (mdd), and in the English system as inches penetration per year (ipy).

As regards algebraic signs of potentials, the standard electrode potential for $Zn \rightarrow Zn^{++} + 2e$ is negative; for $Cu \rightarrow Cu^{++} + 2e$, positive.

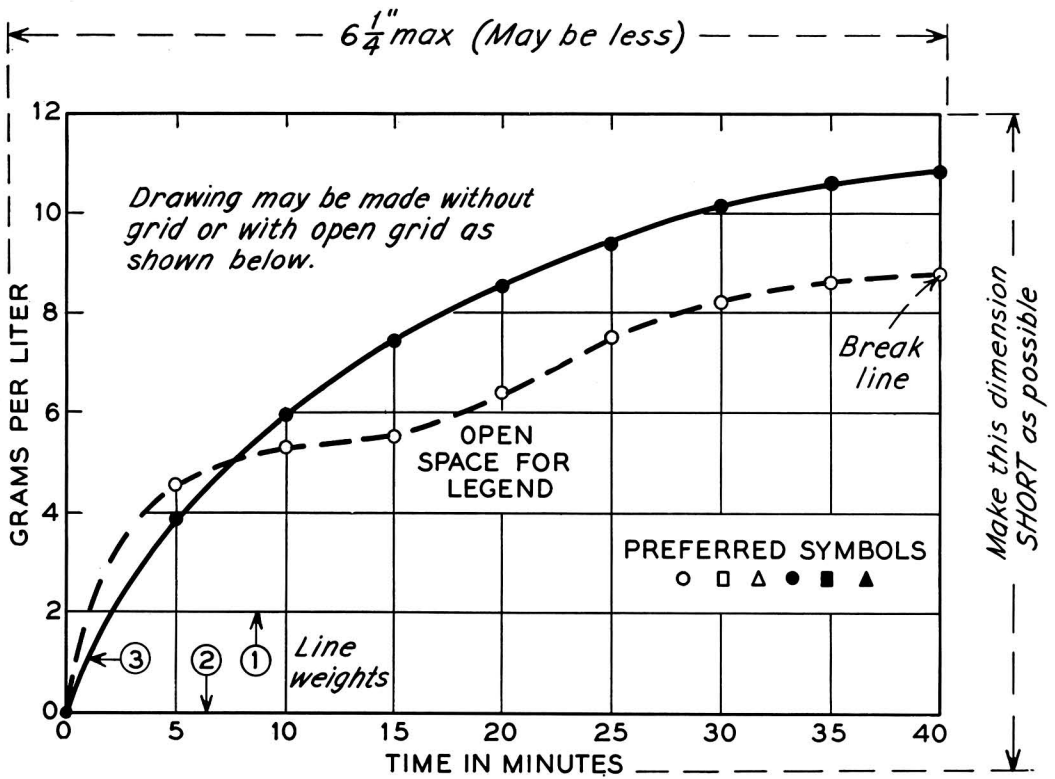
ABBREVIATIONS

GENERAL

Abbreviations should conform with the American Standards Association's list of "Abbreviations for Scientific and Engineering Terms."

Authors should be as brief as is consistent with clarity, and must omit all material which can be regarded as familiar to specialists in the particular field.

The use of proprietary names, trade-marks, and trade names should be avoided if possible. If used, these should be capitalized so that the owner's legal rights are not jeopardized.



Remarks: Line weight ② is used for borders and zero lines. When several curves are shown, each may be numbered and described in the caption. Lettering is approx. $\frac{1}{8}''$.

SAMPLE CURVE DRAWING FOR REDUCTION TO $\frac{1}{2}$ SIZE

The Electrochemical Society

Patron Members

Aluminum Co. of Canada, Ltd., Montreal, Que., Canada
International Nickel Co., Inc., New York, N. Y.
Union Carbide Corp.
Divisions:
Electro Metallurgical Co., New York, N. Y.
National Carbon Co., New York, N. Y.
Westinghouse Electric Corp., Pittsburgh, Pa.

Sustaining Members

Air Reduction Co., Inc., New York, N. Y.
Ajax Electro Metallurgical Corp., Philadelphia, Pa.
Allied Chemical & Dye Corp.
General Chemical Div., Morristown, N. J.
Solvay Process Div., Syracuse, N. Y. (3 memberships)
Alloy Steel Products Co., Inc., Linden, N. J.
Aluminum Co. of America, New Kensington, Pa.
American Machine & Foundry Co., Raleigh, N. C.
American Metal Co., Ltd., New York, N. Y.
American Platinum Works, Newark, N. J. (2 memberships)
American Potash & Chemical Corp., Los Angeles, Calif. (2 memberships)
American Zinc Co. of Illinois, East St. Louis, Ill.
American Zinc, Lead & Smelting Co., St. Louis, Mo.
American Zinc Oxide Co., Columbus, Ohio
Auto City Plating Co. Foundation, Detroit, Mich.
Bart Manufacturing Co., Bellville, N. J.
Bell Telephone Laboratories, Inc., New York, N. Y. (2 memberships)
Bethlehem Steel Co., Bethlehem, Pa. (2 memberships)
Boeing Airplane Co., Seattle, Wash.
Burgess Battery Co., Freeport, Ill. (4 memberships)
C & D Batteries, Inc., Conshohocken, Pa.
Canadian Industries Ltd., Montreal, Que., Canada
Carborundum Co., Niagara Falls, N. Y.
Chrysler Corp., Detroit, Mich.
Columbia-Southern Chemical Corp., Pittsburgh, Pa.
Consolidated Mining & Smelting Co. of Canada, Ltd., Trail, B. C., Canada (2 memberships)
Corning Glass Works, Corning, N. Y.
Cramet, Inc., Chattanooga, Tenn.
Crane Co., Chicago, Ill.
Diamond Alkali Co., Painesville, Ohio (2 memberships)
Dow Chemical Co., Midland, Mich.
Wilbur B. Driver Co., Newark, N. J. (2 memberships)
E. I. du Pont de Nemours & Co., Inc., Wilmington, Del.
Eagle-Picher Co., Chemical Div., Joplin, Mo.
Eaton Manufacturing Co., Stamping Div., Cleveland, Ohio
Electric Auto-Lite Co., Toledo, Ohio
Electric Storage Battery Co., Philadelphia, Pa.
The Eppley Laboratory, Inc., Newport, R. I. (2 memberships)
Federal Telecommunication Labs., Nutley, N. J.
Food Machinery & Chemical Corp.
Becco Chemical Div., Buffalo, N. Y.
Westvaco Chlor-Alkali Div., South Charleston, W. Va.
Ford Motor Co., Dearborn, Mich.
General Electric Co., Schenectady, N. Y.
Chemistry & Chemical Engineering
Component, General Engineering Lab.
Chemistry Research Dept.
Metallurgy & Ceramics Research Dept.

General Motors Corp.
Brown-Lipe-Chapin Div., Syracuse, N. Y. (2 memberships)
Guide Lamp Div., Anderson, Ind.
Research Laboratories Div., Detroit, Mich.
Gillette Safety Razor Co., Boston, Mass.
Gould-National Batteries, Inc., Depew, N. Y.
Graham, Crowley & Associates, Inc., Chicago, Ill.
Great Lakes Carbon Corp., New York, N. Y.
Hanson-Van Winkle-Munning Co., Matawan, N. J. (3 memberships)
Harshaw Chemical Co., Cleveland, Ohio (2 memberships)
Hercules Powder Co., Wilmington, Del.
Hooker Electrochemical Co., Niagara Falls, N. Y. (3 memberships)
Houdaille-Hershey Corp., Detroit, Mich.
International Minerals & Chemical Corp., Chicago, Ill.
Jones & Laughlin Steel Corp., Pittsburgh, Pa.
Kaiser Aluminum & Chemical Corp.
Chemical Research Dept., Permanente, Calif.
Div. of Metallurgical Research, Spokane, Wash.
P. R. Mallory & Co., Indianapolis, Ind.
McGean Chemical Co., Cleveland, Ohio
Merck & Co., Inc., Rahway, N. J.
Metal & Thermit Corp., Detroit, Mich.
Minnesota Mining & Mfg. Co., St. Paul, Minn.
Monsanto Chemical Co., St. Louis, Mo.
National Cash Register Co., Dayton, Ohio
National Lead Co., New York, N. Y.
National Research Corp., Cambridge, Mass.
Norton Co., Worcester, Mass.
Olin Mathieson Chemical Corp., Niagara Falls, N. Y.
Aviation Div. (2 memberships)
Industrial Chemicals Div. (2 memberships)
Pennsalt Chemicals Corp., Philadelphia, Pa.
Philips Laboratories, Inc., Irvington-on-Hudson, N. Y.
Poor & Co.
Promat Div., Waukegan, Ill.
Potash Co. of America, Carlsbad, N. Mex.
Radio Corp. of America, Harrison, N. J.
Ray-O-Vac Co., Madison, Wis.
Raytheon Manufacturing Co., Waltham, Mass.
Reynolds Metals Co., Richmond, Va.
Shawinigan Chemicals Ltd., Montreal, Que., Canada
Speer Carbon Co.
International Graphite & Electrode Div., St. Marys, Pa. (2 memberships)
Sprague Electric Co., North Adams, Mass.
Stackpole Carbon Co., St. Marys, Pa. (2 memberships)
Stauffer Chemical Co., Henderson, Nev., and New York, N. Y. (2 memberships)
Sylvania Electric Products Inc., Bayside, N. Y. (2 memberships)
Sarkes Tarzian, Inc., Bloomington, Ind.
Tennessee Products & Chemical Corp., Nashville, Tenn.
Texas Instruments, Inc., Dallas Texas
Titanium Metals Corp. of America, Henderson, Nev.
Udylite Corp., Detroit, Mich. (4 memberships)
Vanadium Corp. of America, New York, N. Y.
Victor Chemical Works, Chicago, Ill.
Wagner Brothers, Inc., Detroit, Mich.
Weirton Steel Co., Weirton, W. Va.
Western Electric Co., Inc., Chicago, Ill.
Wyandotte Chemicals Corp., Wyandotte, Mich.
Yardney Electric Corp., New York, N. Y.



ENTHONE

Which of ENTHONE's metal-finishing developments do you need?

- ENSTRIP METAL STRIPPERS**—Products for quickly and economically stripping defective plated coatings, coatings from plating racks, excess solder, silver brazing metal and metal smuts, without attacking base metals in any way.
- ENAMEL STRIPPERS**—A wide variety of strippers are maintained "in stock". In addition, Enthone will be glad to study your requirements and develop the precise stripper you need to meet your requirements.
- "ALUMON"**—A product of highest-purity chemicals for preparing aluminum for plating. Used successfully for over 13 years by hundreds of manufacturers, Alumon is economical and easy to use.
- EBONOL® METAL BLACKENERS**—Products for blackening copper, brass and other copper alloys; iron and steel; zinc plate and zinc castings.
- RUST REMOVERS**—A complete line of chemicals for the removal of rust and scale. Both alkaline and acid compounds are available.
- CLEANERS & DEGREASERS**—New alkaline and emulsion-type cleaners for removing grease, oil, and solid dirt from metals.
- RUSTPROOFING COMPOUNDS**—Rustproofing oils, waxes and chemical compounds for protecting steel against rust in salt spray, high humidity and outdoors.
- ZINC & CADMIUM CONVERSION COATINGS**—Enthox® salts produce iridescent, gold colored chromate coatings with high salt-spray resistance. Very simple and economical to use.

Remember — your metal finishing problem is our business! Since Enthone has been studying these problems, and developing their solutions, for 20 years, chances are we have the answer to your problem in stock. On the other hand, if yours is an unusual requirement, we will be glad to study your needs and develop the precise chemical for the purpose. Just send us a letter, outlining the problem or process—and enclose a sample of the metal concerned, if possible.

Write to Dept. J-1.

DISTRIBUTION AND SERVICE THROUGHOUT THE UNITED STATES, CANADA, MEXICO, BRAZIL AND EUROPE

PRODUCTS OF *Enthone* THE SCIENTIFIC SOLUTION OF METAL FINISHING PROBLEMS

ENTHONE

ENTHONE

INCORPORATED

442 ELM STREET, NEW HAVEN 11, CONN.

Metal Finishing Processes • Electroplating Chemicals

SUBSIDIARY OF AMERICAN SMELTING AND REFINING COMPANY